Implementing a Dutch building energy simulation tool

Energy model testing for Rijssen-Holten

MSc Geomatics

Gabriela Koster

TU Delft

Implementing a Dutch building energy simulation tool

Energy model testing for Rijssen-Holten

by

Gabriela Koster

to obtain the degree of Master of Science
in Geomatics
at Delft University of Technology,

Student number:	4596870	
Project duration:	November 1, 2023 – June 20, 2024	
Thesis committee:	C. León-Sánchez	TU Delft, first supervisor
	Dr. G. Agugiaro	TU Delft, second supervisor
	M. Mosteiro Romero	TU Delft, co-reader

TU Delft

Abstract

Lowering energy demand in buildings is high on the political agenda considering household energy consumption accounts for 22% of the total final energy usage in the Netherlands. Tools that can run these types of simulations for an entire city are required for effective policy design to lower energy consumption within the built environment. This thesis explores how to build such a tool that allows for space heating demand to be computed that follows the NTA 8800 norm. Therefore, the main research question is: "To what extent can a heat demand model be developed that adapts and implements the NTA 8800 to be coupled with CityGML-based semantic 3D city models?". The thesis uses a mixed-method research approach of qualitative concept mapping and quantitative modelling to build a space heating demand model for urban analysis. The final product is a Python-based model with database interactions, compatible with CityGML-based semantic 3D city models, following the NTA 8800 computation methods.

Initial testing on two buildings highlighted areas for model development, including the underestimating of ventilation losses and the omission of windows and doors in transmission estimates. Improved window quality could result in significant energy savings, according to the solar gain analysis. The model's capacity to mimic anticipated trends in space heating demand was verified using benchmark data, although it deviated from previous consumption patterns, indicating the need for additional research. The model was tested for Rijssen-Holten and produced rapid results within 5 minutes. Despite limitations due to data availability and model assumptions, the thesis model underscores the utility of Geomatics in urban energy management and the results can help design energy policy design for sustainable development.

Keywords: *Heat Demand, NTA 8800, Semantic 3D city models, Built Environment, Netherlands*

Contents

List of Figures

List of Tables

1

Introduction

1.1. Background

Addressing energy demand in buildings is currently high on the political agenda for national and municipal governments worldwide. This is particularly the case for the Netherlands, where household energy consumption accounts for an estimated 22% of total final energy usage, of which the majority goes to space heating (van den Brom, 2020). Assessing a building's energy demand can be simulated with the help of building energy simulation (BES) tools. These tools are essential to the architectural design process because they provide information on patterns of energy usage, help determine which renovations are most cost-effective, and calculate the payback periods of energy-saving solutions (van den Brom, 2020). But the state of BES tools today poses a distinct difficulty, especially when it comes to city-level analysis, which calls for a new strategy to handle the delicate balance between scalability, detail and accuracy in energy demand modelling.

1.2. Problem definition

Although detailed information and established tools are available for single-building analysis, the complexity and computation escalate at the urban level (Agugiaro, 2016). This becomes problematic for municipalities that try to predict and create localized solutions that successfully reduce the demand for heating in residential buildings for entire cities. Challenges arise from several factors such as the interplay between changing climatic conditions, evolving building standards, and diverse resident behaviours, which make standardized predictions difficult. In addition, collecting high-quality building-level data for entire neighbourhoods or cities also becomes a hindering factor for municipalities to be able to run these types of analyses. Moreover, Dutch buildings are required as of January 1, 2021, to comply with the *Bijna Energie Neutrale Gebouwen* (BENG) standard, which translates to "Almost Energy Neutral Building" (Bodelier and Herfkens, 2021) [1]. BENG is grounded in the principles outlined in the NTA 8800 norm, which

[1]The Building Decree includes the three BENG criteria:

- BENG1: This criterion estimates the maximum energy demand a building has expressed in kWh/m² year.

stands for *Nederlands Technische Afspraak*, translated to the "Dutch Technical Agreement" — a comprehensive method for energy performance assessment. Furthermore, research has shown that existing BES tools compute theoretical demand values that often deviate significantly from actual consumption values (Majcen et al., 2013; van den Brom, 2020), suggesting that there are limitations with the current approach to how BES tools are being developed.

1.3. Relevance

In response to this challenge, the proposed solution is the development of a BES tool for city-scale analysis tailored to the Dutch context. This tool would provide a more accurate and scalable method of predicting heating demand at the municipal level. It would be based on the NTA 8800 norm and leverage the power of semantic 3D city models. Predicting energy usage might be achieved by integrating semantic 3D models, which include comprehensive information about the urban environment. In short, the goal is to ensure that the tool can compute energy usage for an entire city while maintaining the granularity of individual buildings as the smallest unit. This new approach aims to give municipalities a reliable, scalable, and accurate tool for energy simulations, bridging the gap between detailed dynamic models and oversimplified national-scale tools. This will allow for more informed and efficient decision-making in the pursuit of energy efficiency and ultimately contribute to the reduction of the environmental footprint of the Dutch building stock.

1.4. Objective

This research sets out to implement a method for computing theoretical heat demand estimates that adheres to the NTA 8800 principles and is compatible with semantic 3D city models to enhance city-scale energy analysis. The specific objectives include:

- Reviewing the NTA 8800 norm to understand the required data inputs necessary for energy performance computation to ensure compliance with BENG principles and suitability for the Dutch built environment
- Assessing the semantic 3D city model capabilities in terms of storage and enrichment for energy performance calculations
- Establish the data requirements from the NTA 8800 norm and what a semantic 3D city model can store, bridging the identified gaps with additional datasets or assumptions
- Implementing a heat demand model for the built environment for city-scale analysis, suitable for semantic 3D city models
- Validating the model's result accuracy
- Following the Findable, Accessible, Interoperable, and Reusable (FAIR) science principles

- BENG2: This standard computes the annual primary fossil energy consumption within a building, also in kWh/m² year.
- BENG3: This norm emphasises the value of renewable energy integration by imposing a minimum requirement for the share of renewable energy sources in the building's energy mix.

1.5. Reader's guide

The thesis proposal is structured in the following seven sections:

- **Section 2** outlines the core concepts of the research through theoretical frameworks and provides an overview of the state of the art.
- **Section 3** elaborates on the mixed method research design approach and the corresponding research questions and introduces the study area.
- **Section 4** explains the relevant concepts for computing the theoretical heat demand according to the NTA 8800 principles and outlines the relevant data requirements.
- **Section 5** covers how the model is implemented.
- **Section 6** assesses the model estimates with another tool results, statistical consumption patterns and energy performance indicators.
- **Section 7** discusses the research implications, limitations, and future research possibilities.
- **Section 8** concludes the thesis.

2

Literature review

The research process is guided by a review of scholarly material to present the fundamental concepts outlined in the thesis. This section is split into two sections: section 2.1 and section 2.2. In section 2.1, subsection 2.1.1 provides an overview of the different urban building energy modelling approaches to provide the context of the existing modelling approaches used in the field. Then, subsection 2.1.2 introduces what a semantic 3D city model is and how to represent a city model through the data model CityGML in subsection 2.1.3, which also explains the main module used in this thesis, the building module, and level of detail. In addition, subsection 2.1.4 describes the Energy ADE data model, an extension to CityGML that allows for energy modelling, compatible with semantic 3D city models. Lastly, the entity relational model concept is explained, to later on be used to aid with the model implementation chapter. For section 2.2, a brief overview is provided of related work explaining the two main energy model types and elaborates on the details of the NTA 8800 method in subsection 2.2.2. Lastly, an overview of the existing simulation tools in the field in subsection 2.2.4 is provided.

2.1. Theoretical framework

2.1.1. Urban building energy modelling

Urban building energy modelling (UBEM) is becoming more important as areas are urbanizing at a fast pace and the question of reducing energy consumption becomes more urgent. As a response to the situation, several spatial decision-making tools emerged (e.g. *CitySim Pro*, *Simstadt* etc.) However, UBEM is still difficult for a variety of reasons. One reason is that it is difficult to obtain the high level of detail (LoD) data needed for the analysis. Another reason is that there are also high computational costs tied to the analysis scale combined with high-level data. In addition, setting up these models requires many generalizations and assumptions, creating many uncertainties with the simulation results. Another limitation of UBEM is the modelling of occupant behaviour. Several studies point out that occupancy behaviour is the reason theoretical estimates deviate from actual consumption values (Majcen et al., 2013; van den Brom, 2020). These reasons add complexity to urban-scale modelling.

Despite that, UBEM can have valuable insight into energy modelling. UBEM is made possible by the development of geometric and geo-data modelling capabilities, enhanced accessibility, and higher quality of spatial and non-spatial data (Allegrini et al., 2015). Several studies outline different UBEM approaches (Allegrini et al., 2015; Conti et al., 2020; De Rosa et al., 2014; Swan and Ugursal, 2009), however, this thesis focuses on the classification definition of UBEM approaches; top-down and bottom-up, according to Swan and Ugursal (2009). Further development of Swan and Ugursal's (2009) research resulted in a quadrant classification (Langevin et al., 2020) (see Figure 2.1) that encompasses the distinction of transparency (e.g., black box and white box) inside top-down and bottom-up UBEMs techniques. The goal was to eliminate the hierarchical structure and replace it with a more flexible and adaptable framework that would allow for the addition of new techniques and support layers (such as occupant behaviour, environmental factors, etc.) as well as dimensions outside of the quadrants (such as system boundaries, spatiotemporal resolution, detailed dynamics, and model uncertainty) (Langevin et al., 2020). An overview of Swan and Ugursal's (2009) expanded UBEM classification is given in Table 2.1, which also includes a summary of each approach's pertinent advantages and disadvantages as well as an example of a matching modelling technique. Yet, the main distinction this thesis focuses on is top-down and bottom-up.

In top-down, the total energy demand of the building stock is computed on a national scale. Top-down models frequently use therefore variables such as macroeconomic data (such as GDP, employment rates, and price indices), weather patterns, rates of home building and demolition, estimates of appliance ownership, and the number of residential units (Swan and Ugursal, 2009). The residential sector, in this case, is viewed as a single energy entity, which does not differentiate energy use based on specific end-uses (e.g. space heating or lighting) (Swan and Ugursal, 2009). Because it doesn't require specific technical data for each building, this method is helpful for general estimations across wide regions (Ferrando et al., 2020; Langevin et al., 2020; Swan and Ugursal, 2009). This approach's primary advantage is its ability to include indicator patterns in the study with minimal requirement for input data. Nevertheless, they are unable to forecast future trends as they only employ historical indicators and frequently present aggregated data as results rather than precise spatial or temporal detail (Ferrando et al., 2020). Therefore, when testing levers to lower energy usage at the building level is the goal, this technique is a bit restrictive.

Conversely, bottom-up models can account for the energy consumption of particular end-uses, individual houses, or groups of houses and are then extended to represent the area or nation depending on the representative weight of the modelled sample (Swan and Ugursal, 2009). Bottom-up models make it possible to calculate end-use consumption in a more detailed way. It looks at certain purposes inside single-family homes or residential complexes (Langevin et al., 2020; Swan and Ugursal, 2009). It can provide a more realistic image of how much energy is used for particular activities and appliances by concentrating on the specifics. After that, these precise estimations are combined to provide an overview of the energy usage for a greater region or maybe the entire country (Langevin et al., 2020; Swan and Ugursal, 2009). The modelling technique (T. Hong et al., 2016) is sufficiently flexible to identify the best mix of policies and renovation actions for building stocks.

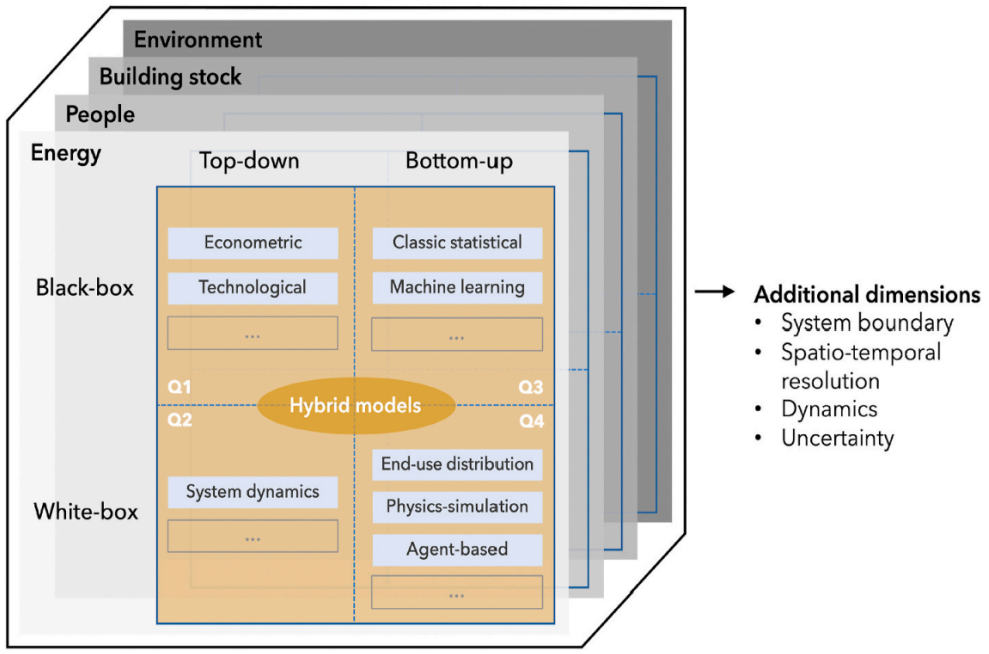

Figure 2.1: Overview of the UBEM approaches, originally outlined by Swan and Ugursal (2009) and extended by Langevin et al. (2020)

Classification	Description	Advantage	Disadvantage	Modelling technique example
Top-down (Black-box)	It determines the building's overall energy consumption	Easy and computationally manageable	Frequently incapable of demonstrating the implications of particular technologies	Econometric and Technological
Top-down (White-box)	It can depict physical causation on an aggregate level	It can demonstrate how intricate building stock energy usage is	It is unable to connect building level activities to the overall energy usage of buildings	System dynamics
Bottom-up (Black-box)	It allocates certain energy end uses to building-level energy usage	It can reveal important relationships between energy-related end uses	However, unable to articulate important processes influencing energy end uses in a meaningful manner	Classic statistical and Machine learning
Bottom-up (White-box)	It can replicate physical connections at the building level	It may accurately depict significant factors influencing building energy end-use	It is computationally demanding and necessitates large amounts of data	End-use distribution, Agent-based and Physics-simulation

Table 2.1: Overview of the UBEM approaches, advantages, disadvantages and techniques described by Langevin et al. (2020)

2.1.2. Semantic 3D city models

A 3D city model is described as "*a digital representation, with three-dimensional geometries, of the common objects in an urban environment, with buildings usually being the most prominent objects*" (Ledoux, 2021, p. 1). The structure of city models can vary depending on the acquisition methods used (Ledoux, 2021). A semantic 3D city model, on the other hand, is considered a city data model in which the pertinent objects stored, have characteristics assigned to them and are labelled with the respective meaning (Ledoux, 2021). To be clear, a semantic 3D city model goes further than the physical representation of geometries by giving urban objects contextual and functional meaning (Kolbe & Donaubauer, 2021). For example, a building object can store information about the construction materials used on each surface and contains surface classifications for the walls, floors, and roofs.

Semantic 3D city models can be stored according to standards, and CityGML is the unique and most relevant one in the international open standards domain (more on CityGML in subsection 2.1.3). These models can have different encodings in CityGML, such as CityGML and CityJSON, which are based on the XML and JSON formats, respectively. Semantic 3D city models can also be processed and stored in a geographic database management system (DBMS). An example of such DBMS is the *3DCityDB*, which is defined as "*an Open Source software suite allowing to import, manage, analyze, visualize, and export virtual 3D city models according to the CityGML standard, supporting both versions 2.0 and 1.0*" (Yao et al., 2018, p. 2). For this thesis, a key focus is placed on the CityGML data model with database encoding.

2.1.3. CityGML

CityGML can be used to represent semantic 3D city models. CityGML is an open standardized data model internationally issued by the Open Geospatial Consortium (OGC) since 2008 (Gröger et al., 2012). CityGML is implemented as a Geography Markup Language (GML) application schema that allows for the exchange format to store 3D city models (Gröger et al., 2012). CityGML supports multiple LoD 3D geometry, topology, semantics and appearance and it is extendable to other application domains (Gröger et al., 2012), making it particularly useful for urban planning, architectural design or environmental simulations. The current version of the standard is 3.0 (Open Geospatial Consortium, 2023). However, this thesis focuses on version 2.0 since it is compatible for extension with other data model features (more on this in subsection 2.1.4).

2.1.3.1.Core and building modules

CityGML 2.0 has various modules available for declaring to define in detail objects that exist in a city. The main ones are: *Core*, *Generics*, *Appearances* and the thematic modules. In *Core*, there is *CityGML Core*, which creates the foundation for more specialized thematic modules that cover a range of urban environment facets.

In thematic, there are *Bridge*, *Building*, *CityFurniture*, *CityObjectGroup*, *LandUse*, *Relief*, *Transportation*, *Tunnel*, *Vegetation* and *Waterbody* (Gröger et al., 2012). *CityObject* serves as the basis class for all thematic modules, and it is defined in the *Core* module together with fundamental data types (Gröger et al., 2012).

The *Building* module is of particular importance in this study. Figure 2.2 provides a UML excerpt overview of how a building is modelled in CityGML. The abstract class *Building* is delineated, which consists of the features *Building* and *BuildingPart*. This distinction of *Building* and *BuildingPart* within the *Building* class allows for scenarios such as two buildings e.g. a house and a garden shed on a land plot to be classified as building parts but both adhere to as one building feature.

A key aspect of the *Building* module is the application of modelling semantic classification of the boundary surfaces of the building. These surfaces can be classified as either *WallSurface*, *RoofSurface*, and *GroundSurface*, and other integral components of the building's structure. The *BoundarySurface* module allows for these surfaces to be modelled by a *MultiSurfaces* geometry, defined with its respective LoD. Furthermore, the module facilitates other architectural element representations such as Windows and doors through the *Opening* feature.

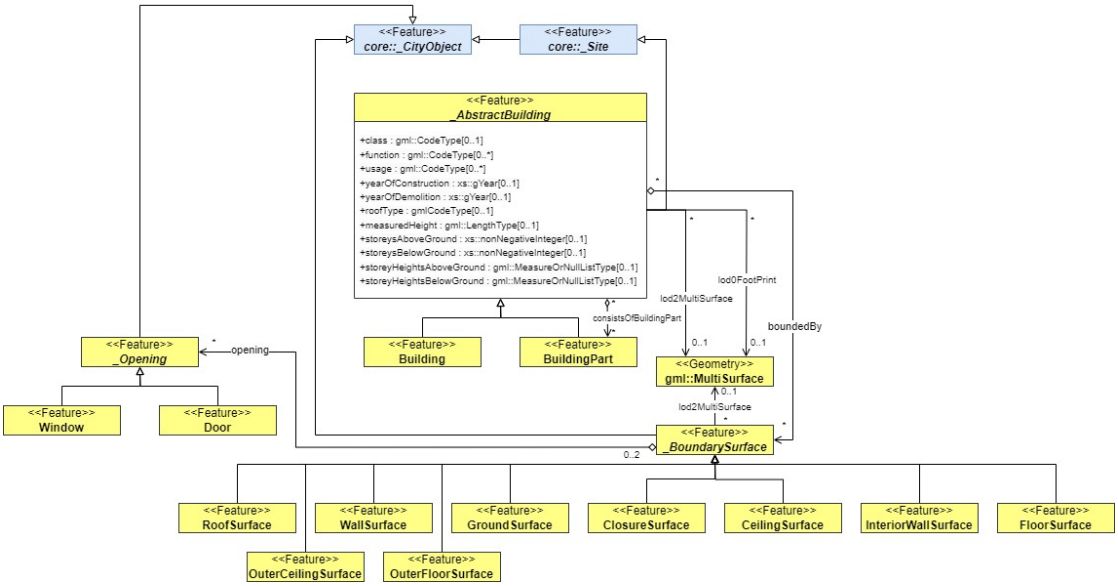

Figure 2.2: Excerpt of the building module (Gröger et al., 2012)

2.1.3.2.Level of detail

A key characteristic in CityGML is that the same object can be represented in different LoDs at once (Gröger et al., 2012). It is also possible to merge or combine two different CityGML datasets with the same object but different LoDs (Gröger et al., 2012). This feature can become useful when trying to enrich a semantic 3D city model, when higher LoDs CityGML datasets become available. In essence, there are five LoD levels (e.g. LoD0, LoD1, LoD2, LoD3 and LoD4) that buildings can be represented by. LoD0 buildings refer to either a building footprint or rooftop representation, and LoD1 buildings are shown as blocks (Gröger et al., 2012). LoD2 buildings are *Solids* or *MultiSurfaces* that also incorporate thematic surfaces such as e.g. walls and incorporate the specific roof geometry, and LoD3 buildings are similar to LoD2 but now also include windows and doors (Gröger et al., 2012). LoD4 buildings include levels of information such as LoD3 and also rooms, stairs, and furniture (Gröger et al., 2012). Figure 2.3 visualize displays the LoD 0-4 representation of buildings explained before (Biljecki et al., 2016). Despite having LoD4 data

storage capabilities available in CityGML, most 3D city models do not go up to LoD4. Most 3D city models do not have information such as the number of rooms or furniture types there are in each building, which is attributed to LoD4, the most detailed LoD.

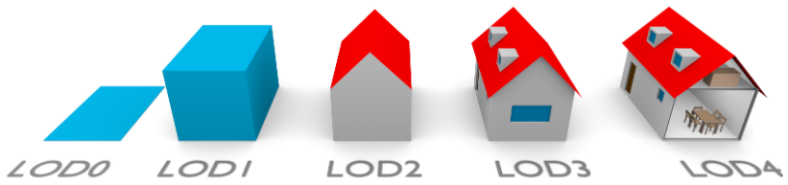

Figure 2.3: Overview of the different LoDs. Figure from Biljecki et al. (2016)

2.1.4. Energy application domain extension

In CityGML, *Generic Attributes* and *Generic CityObjects* provide a flexible means of extending the standard model without changing its fundamental schema. When certain applications require data that the regular CityGML model does not natively handle, this functionality can be helpful. *Generic* attributes can be useful to use for example when you want to tag a building with historical significance without fundamentally changing the CityGML structure. *Generic CityObjects* can be helpful when you want to present urban features that are included in the CityGML's established object classes (e.g. fountains). So in short, CityGML can be extended by *Generic Attributes* and *Generic CityObjects*, however, that is not the only one. Another add-on example is Energy Application Domain Extension (ADE).

CityGML is extendable by the Energy ADE, which allows for storing and managing energy-related information for buildings (Agugiaro et al., 2018; Benner, 2018). Energy ADE improves CityGML by providing comprehensive data regarding the thermal characteristics of structures, installations, and energy systems. In essence, Energy ADE is an extension package for CityGML to enrich city models, and Figure 2.4 shows the 6 new packages added to the CityGML model through the Energy ADE. The packages only extend to *CityGML Core* and *Building* modules (Agugiaro et al., 2018; Benner, 2018). The 6 packages are *Energy ADE Core*, *Supporting Classes*, *Occupant Behavior*, *Material and Construction*, *Energy Systems* and *Building Physics*. To provide a brief explanation of the packages (Agugiaro et al., 2018; Benner, 2018):

- The *Energy ADE Core* module includes abstract base classes for the four primary theme modules, as well as a variety of generic data types, enumerations, and codelists.
- The *Supporting Classes* module contains classes to classify time series, weather data, and schedules
- The *Occupant Behavior* module facilitates the modelling of energy-related behaviours among occupants.
- The *Material and Construction* module allows for the physical properties of the building materials to be modelled.
- The *Energy Systems* module allows for the representation of a building's energy conversion system, distribution system, and storage system.
- The *Building Physics* module enables the ability for single- or multizone building energy simulations.

Despite this development in CityGML energy modelling, the Energy ADE has a complex structure. To simplify the Energy ADE while still maintaining its relevancy with energy modelling, the Karlsruhe Institute of Technology has developed a simplified version known as the KIT profile. This version eliminates specific modules and classes from the original data model, resulting in a more user-friendly subset (Leon-Sanchez et al., 2021). The key distinctions between the original Energy ADE and the KIT profile are the elimination of the *Energy Systems* module, and the simplification of the *Supporting Classes* module.

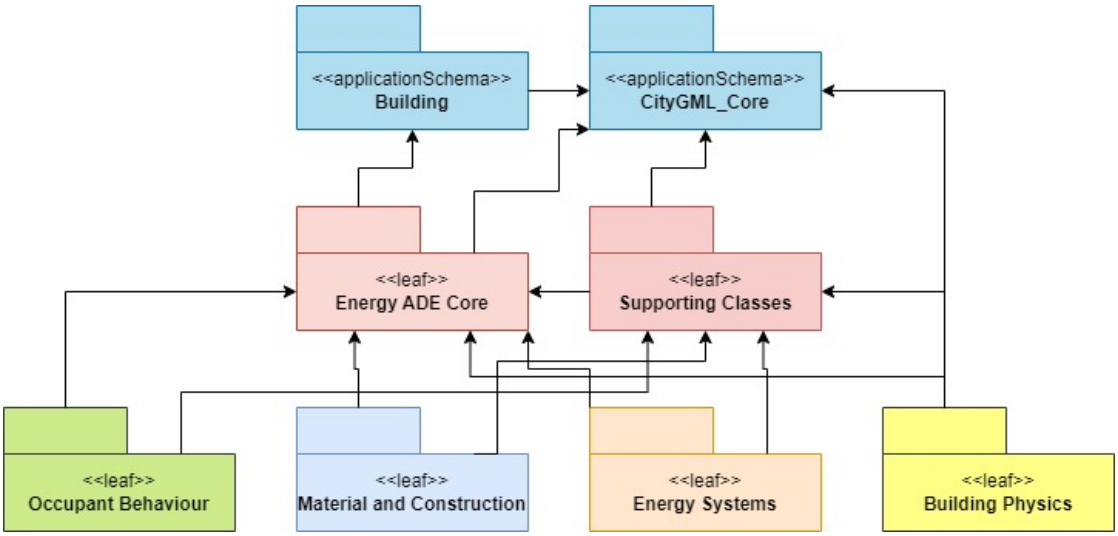

Figure 2.4: Overview of the Energy ADE packages (Agugiaro et al., 2018; Benner, 2018)

2.1.5. Entity relational model

Since this thesis plans to use the CityGML data model with database encoding, the conceptual framework of an entity relational model (ERM) is used in the thesis to aid the implementation of the building energy model. For reference, an ERM diagram is best created during the conceptual design phase of the database process (see Figure 2.5). The ERM provides a conceptual framework for creating relational databases that can handle and retain massive amounts of data. This attribute can be particularly useful for energy consumption modelling that often deals with Big Data. This is the case in this thesis as it is planned to make use of semantic 3D city models stored in databases to avoid complications occurring during data retrieval and processing that can occur with XML and JSON files.

To elaborate on what ERM is, ERM was originally proposed as a conceptual modelling approach for database design by Peter Chen in 1976 (Saiedian, 1997). The ERM provides a simple graphical approach to logical database architecture by purposefully leaving out information concerning efficiency and storage, which are dealt with during the physical design phase (Saiedian, 1997). ERM solves the issues typically occurring with logical database architecture design. Conventional design techniques immediately translate real-world data into a database schema designed for a particular database management system (DBMS), frequently constrained by issues with access, retrieval, and update performance as well as data structure constraints (Saiedian, 1997). By using an ERM diagram to create an enterprise schema or view, the ERM approach adds an intermediate step (Saiedian, 1997). This conceptual design avoids getting mired down in technical

details, accurately representing real-world things and connections. A DBMS-specific user schema is subsequently developed from this conceptual schema, allowing for a more structured and straightforward design approach (Saiedian, 1997). This increases the basic design's manageability and flexibility to accommodate other DBMSs as needed and hence has made ERM a staple in the conceptual database design phase and requirement analysis due to its simplicity(Saiedian, 1997).

ERM has three core concepts to consider when creating the diagrams; entity types, attributes, and relationship types. Entities refer to the defined tables that contain the data/information (Watt, 2014). In the real world, an entity is an object that can be distinguished from other objects and has its independent existence (Watt, 2014). It can either be an actual physical thing (e.g. building) or an item having a conceptual presence (e.g. heat demand). A collection of attributes characterizes each entity (e.g., Building = (year, typology, etc.). Every attribute has a name, is connected to an entity, and falls within a certain set of allowed values (Watt, 2014). Relationships are the associations or interactions between entities, that link relevant data from tables to one another (Watt, 2014).

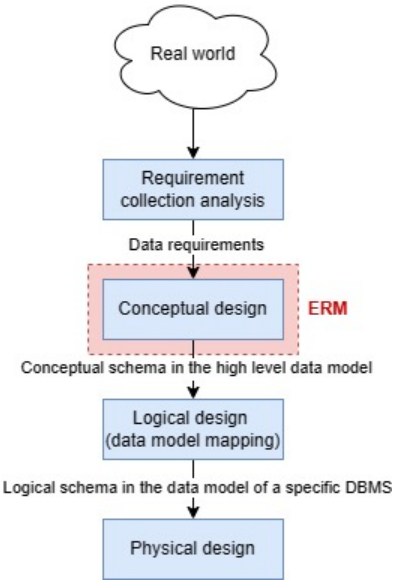

Figure 2.5: Overview of the database design process phases (Watt, 2014), adapted to highlight where the ERM diagram occurs

2.2. State of the art

After reviewing the concepts defined above, this thesis intends to follow the bottom-up approach that works with CityGML version 2.0 together with Energy ADE and uses database encoding. In the next section, a focus is placed on the state of the art of energy models. To put it simply, an energy model is a set of computer-generated computations that offer data on the expected energy usage of a building and its systems. An energy model is an essential tool that can help designers or policymakers understand how to manage energy consumption within the building. To further understand an energy model tool, a distinction should be clarified between energy model types. Specifically, for thermal building models, there is a difference between statistical (hybrid) building models and dynamic building models (transient heat transfer). In the next

sections, the differences between the two are explained.

2.2.1. Statistical (hybrid) building models

Statistical (hybrid) building models employ the energy balance method. According to Conti et al. (2000), the energy balance method is predicated on a quasi-stationary monthly computation of the building's useful heat gains and heat loss. The computation utilizes the monthly averages for the outside temperature and solar radiation. It also accounts for heat gain from people, objects, lights, and equipment, as well as the building's ability to store heat (Conti et al., 2020). Figure 2.6 provides a representation of the energy flows typically considered in the energy balance method. Figure 2.6 also shows the conversion of energy from utility companies extracting the raw materials (primary energy) which get processed and transported to residential homes where the final energy can be consumed. This is also part of the energy balance method but outside the scope of the thesis research.

According to De Rosa et al. (2024), long-term calculations using steady-state models are typically utilized for scenario studies and early construction design, usually ignoring the inertia effect (or taking certain correction factors into account). The degree-days approach is a quick and easy way to do quick calculations to get an estimate of how much energy a structure uses (De Rosa et al., 2014). Their underlying premise is that, in the long run, energy usage will always be proportionate to the difference in temperature between the inside and outside (De Rosa et al., 2014).

The data requirements typically needed for the energy balance method include (Agugiaro, 2016):

- Building geometry data (thermal boundaries, etc.) retrievable through semantic 3D city model
- Building physics data (U-values, g-values, etc.) retrievable through libraries of parameters grouped according to the building archetype
- Building usage data (average internal gains, set-point temperatures, etc.) which can be retrievable from norm standard

The energy balance method is a norm-based method used for calculating energy performance calculation, which varies across countries due to national standards. Each country adopts its own guidelines of computation and fixed values appropriate for the country's situation. For instance, Germany employs the DIN 18599 standard (Monien et al., 2017) which uses different average temperature values in comparison to Italy which uses the UNI-TS 11300 standard (Agugiaro, 2016) with their corresponding temperature values. For this thesis, the NTA 8800 norm is consulted, which is the official method in the Netherlands (NEN, 2024).

2.2.2. NTA 8800

Based on the European Union (EU)'s Energy Performance of Buildings Directive (EPBD), NTA 8800 seeks to provide a transparent and policy-free technique for determining the energy performance of buildings (NEN, 2024). The NTA 8800 employs one determination method, using norms and values from the Dutch NEN 8800, so that it can be used for assessing the energy performance of building stock for Dutch building regulation. The determination method has a fixed degree of accuracy that can be used for calculations of existing and new buildings (NEN,

2024). The norm offers fixed values (e.g. building usage data) to be used when the data is not available or becomes time-consuming to compute (NEN, 2024). Calculations are performed on a monthly basis e.g. average monthly values are used for computation (NEN, 2024). Certain components of modelling such as building parts, installation and climate variables are generalized to utilization factors (NEN, 2024). The fixed values can be substituted for higher-quality values if available. The NTA 8800 was published in July 2021 and is considered a precursor to the requirements of BENG on January 1, 2021. There are four versions of the NTA 8800 (2021, 2022, 2023, 2024) released. This thesis considers the principles explained in the latest version 2024. Some important terms from the NTA 8800 norm (NEN, 2024) to consider:

- Use function: The category of the building (e.g. residential or commercial)
- Thermal zone: Building or group of building parts for which energy performance is calculated (see Figure 2.7 for an example of the thermal zone classification of a building).
- Calculation zone: Portion of a building that may be considered as one unit to calculate energy requirements for heating.
- Usable area: Area of the room or a group of spaces - for example:
  - Use area of the thermal zone: The total area of use of the thermal zone is determined as the sum of the areas of use of all calculation zones in the building or building section over which the energy performance is determined
  - Usable area of the calculation zone: The usable area of a calculation zone is determined as the sum of the usable areas of all (groups of) non-common areas and the (groups of) common areas lying within the calculation zone

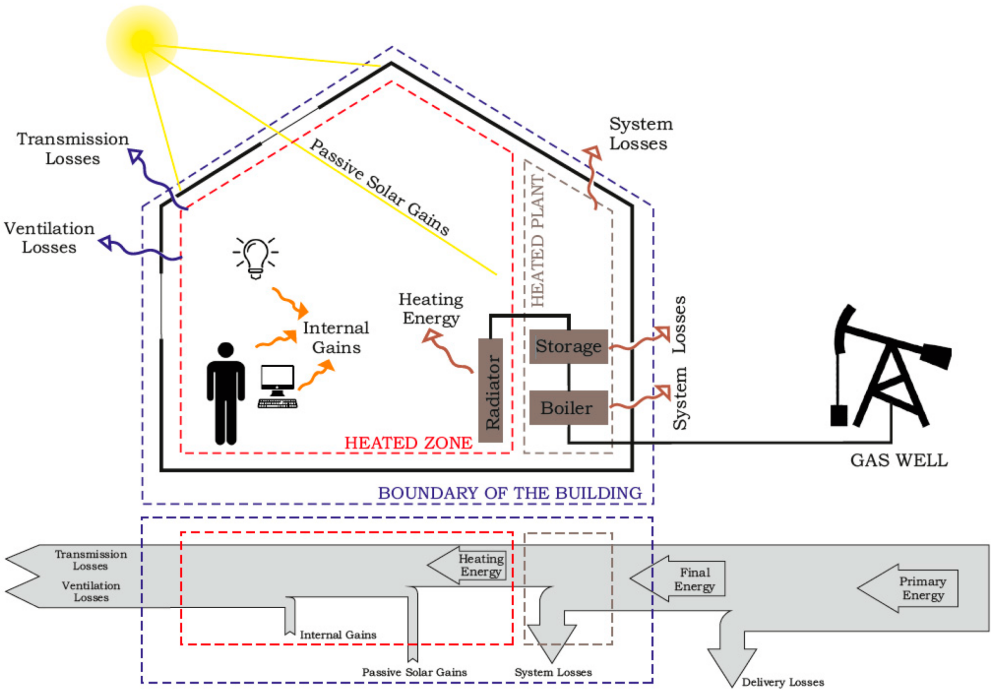

Figure 2.6: Simplified overview of the thermal energy balance of a building and the primary energy conversion to final energy (Borowski et al., 2020)

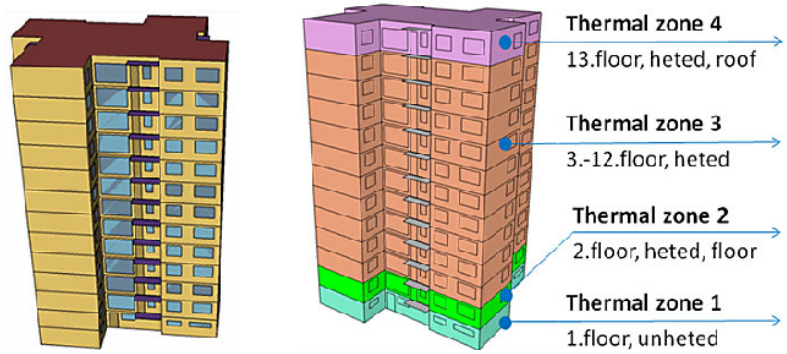

Figure 2.7: Example of a thermal zone classification of an apartment model (Kmeťková et al., 2018)

2.2.3. Dynamic building model

Dynamic building models (transient heat transfer) are an alternative method to energy balance modelling. These are physical models, which present more detailed results since more factors in buildings, such as occupant behaviour, household composition, and climate patterns are modelled with more details. These models also, therefore, require more high-level detailed data sets as inputs. Dynamic models typically also operate on daily or hourly values instead of monthly estimates like in the energy balance method, in which the computation time ends up taking longer. There are several tools available that use the dynamic modelling method: *CitySim Pro*, *EnergyPlus*, and *TRNSYS*. There is always a trade-off to be made between computational costs and the quality of input data. Dynamic models are typically preferred when the input data is available. When modelling on a city-scale level, data availability can become scarce and hence the energy balance method is more suitable and considered as the modelling method in this thesis.

2.2.4. Building energy simulation tools

An example of an energy model is a building energy simulation (BES) tool. BES tools are developed to model building performances, for example, determining the energy demand of a building. They can be used to model strategies to lower the energy consumption in the building stock. Although numerous tools can do complex energy models, they often require extensive, precise data and substantial computation time. Which tool to use will depend on the model's purpose of study. To help with this, 20 distinct BES tools were evaluated by Allegrini et al. (2015), who categorized each BES tool into four detail levels: not included (1), link to another program (2), simplified program (3) or detailed model (4) over 17 energy modelling category results. Figure 2.8 summarizes the important findings of the BES assessment as reported by the author and provides an overview of the various BES tool's detail level and modelling capability, which helps determine the trade-offs between various tools to evaluate which tool to use depending on the study use case.

Of the 20 tools specified in the Allegrini et al. (2015) paper, a closed look is taken at the two tools; *EnergyPlus* and *TRNSYS*, which scored highly on the detailed model category on multiple sections, indicative of being a sophisticated model for energy modelling. *EnergyPlus* is a dynamic building-level modelling tool (Allegrini et al., 2015). It can be used to simulate district networks, renewable technologies, longwave radiation exchange, and external air movement (Allegrini

et al., 2015). Some key strengths of *EnergyPlus* include the capability of extensive detailed energy analysis for various building phases, integration with other CAD tools such as SketchUp through plugins, and a strong technical foundation valued for its empirical validation and precise capabilities (Attia et al., 2009; Crawley et al., 2008). Some downsides for the *EnergyPlus* tool is the high learning curve for users due to its complexity and text-based interface and its limited early design phase capabilities (Attia et al., 2009; Crawley et al., 2008). Although, *DesignBuilder*, a new interface for *EnergyPlus* that is more suited for the conceptual design phase, has been around for a few years (Garg et al., 2020). In short, *EnergyPlus* is a significant tool for in-depth energy analysis for the later design stage of buildings.

Then, there is *TRNSYS*, which is also considered a dynamic building-level modelling tool but this one can simulate thermal and electrical energy systems (Allegrini et al., 2015; Crawley et al., 2008; Monien et al., 2017). It was created to simulate solar water heating systems (Allegrini et al., 2015). One of its strengths is that it offers flexibility in configuring heating, ventilation, and air conditioning (HVAC) systems and also is capable of simulating a wide range of discrete HVAC components (Crawley et al., 2008). However, similarly to *EnergyPlus*, *TRNSYS* has a high learning curve due to its complexity and lack of graphical interface and is also limited in its early design phase capabilities (Crawley et al., 2008). So it is also more suitable for the later design stage, specifically ideal for simulating various types of renewable energy technologies (Crawley et al., 2008).

Comparing both tools, it can be concluded that both offer detailed analysis capabilities that do require some higher level technical expertise since both lack a user-friendly graphical interface or have a limited one; *DesignBuilder*. Both are more suitable for the later stages of design, while *TRNSYS* stands out for renewable energy system simulations and *EnergyPlus* for more comprehensive building and environmental systems simulations. Both tools require detailed data input and can have labour-intensive computation times just at the building level alone, making these programs not appropriate for modelling broad energy flows at the district or city level (Allegrini et al., 2015).

For modelling city-scale level, it is better to use the BES tool such as *CitySim Pro*, *City Energy Analyst* or *SimStadt*, which offer this capability. *CitySim Pro* is developed in C++ by the Swiss Federal Institute of Technology Lausanne (CitySimPro, 2023; Sola et al., 2020), designed to facilitate sustainable urban planning decision-making (Allegrini et al., 2015; CitySimPro, 2023; Ferrando et al., 2020; Robinson et al., 2009). It is composed of a radiation model for shortwave radiation to detect solar gains on facades and roofs, and a basic resistor-capacitor thermal model to simulate the energy performance of the building stock (Allegrini et al., 2015; Ferrando et al., 2020; Robinson et al., 2009). It takes into consideration the exchange of longwave radiation and shortwave radiation (Allegrini et al., 2015). *CitySim Pro* considers subspaces in buildings and links them through wall conductance (Ferrando et al., 2020). To account for tenant behaviour uncertainty inside the buildings, a stochastic model of occupant behaviour is provided (Allegrini et al., 2015; Salim et al., 2020). *CitySim Pro* allows the user to import 3D city models through CityGML files or other formats (Mutani et al., 2018) and compute calculations in an hourly unit (Leon-Sanchez et al., 2021).

Then, there is *City Energy Analyst*, an open-source energy simulation tool developed by Eid-

genössische Technische Hochschule (ETH) Zürich in 2013, which can perform multidisciplinary energy analysis from a building's energy demand to estimated CO_2 emissions and perform economic analysis (Bottino-Leone et al., 2024; Future Cities Laboratory Global, 2024; The CEA Team, 2024). *City Energy Analyst* was created as an addition to the ArcGIS v10.3, using Python v2.7 (Fonseca et al., 2016). The tool operates using 7 databases (e.g. urban data, weather data, sensor data, distribution data, archetypes data, technology data and performance targets data) and 6 calculation modules (Fonseca et al., 2016). The energy demand output is computed in an hourly unit (The CEA Team, 2024).

The previously explored BES tools were examples of dynamic building models, however, there are also tools that employ the energy balance method, one being *SimStadt*. *SimStadt* was created in Java at HFT Stuttgart to assist decision-makers in the energy sector by executing energy simulations (Ferrando et al., 2020; Monien et al., 2017; SimStadt, 2023). *SimStadt* calculates the monthly energy demand of buildings using a steady-state technique based on the German standard DIN V 18599 (Monien et al., 2017; SimStadt, 2023). It supports the fast creation and evaluation of energy scenarios for urban planning using refurbishment rates and time horizons (Ferrando et al., 2020). The program takes 3D city models through CityGML files as input data but also uses pre-built libraries to model climate patterns or building physics (Ferrando et al., 2020; Leon-Sanchez et al., 2021; Monien et al., 2017). It can facilitate solar potential analysis with the help of online databases (Ferrando et al., 2020). It was designed for large-scale analysis, making it less suitable for building-level assessment. To compare, all three tools are suitable for urban-scale modelling, with *CitySim Pro* offering more detailed thermal modelling capabilities in hourly time horizons, *City Energy Analyst* offering more multidisciplinary analysis capabilities, and *SimStadt* allowing for more scenario creation capabilities in monthly time horizons.

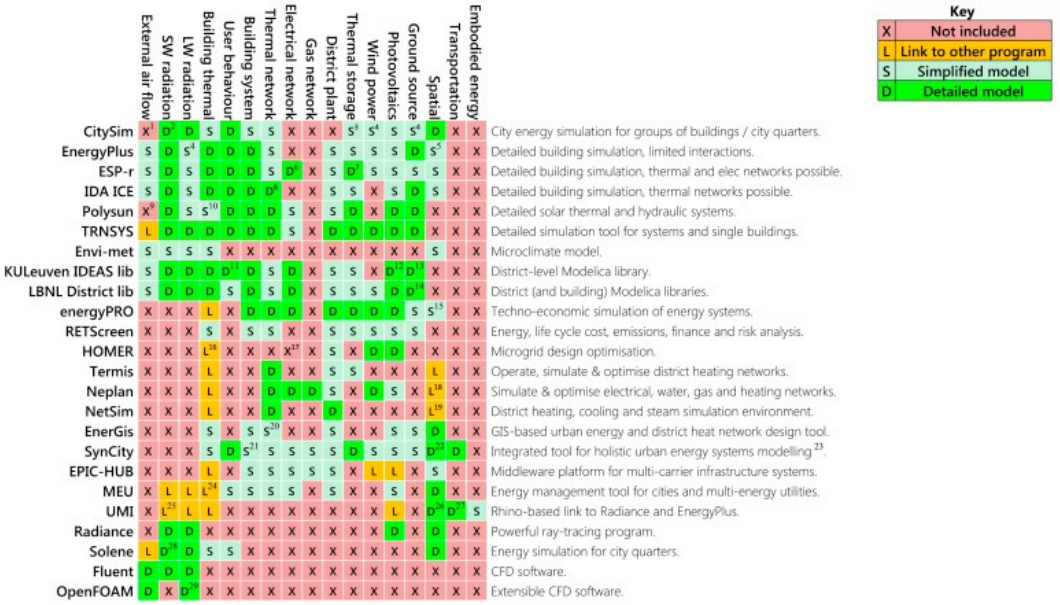

Figure 2.8: Overview assessment of the various BES tools by Allegrini et al. (2015)

3

Research questions and approach

3.1. Research questions

There is limited academic research regarding energy demand modelling using semantic 3D city models for the built environment in compliance with the NTA 8800 norm in the Netherlands. Therefore, the main research question is formulated as:

To what extent can a heat demand model be developed that adapts and implements the NTA 8800 to be coupled with CityGML-based semantic 3D city models?

The overarching research question is divided into the following sub-questions:

1. What are the key parameters and data inputs required by the NTA 8800 norm for calculating the theoretical heat demand of buildings, and what is the availability of such data?
2. How effective is CityGML coupled with the Energy ADE in handling the data required for NTA 8800 heat demand calculations for energy modelling and how can such a model that computes the heat demand for a semantic 3D city model be implemented?
3. To what extent can the computed heat demand values be validated?

3.2. Research framework

The research process is depicted in Figure 3.1. The first step includes conducting a literature review on the NTA 8800 norm on heat demand modelling and developing a mind map of all the relevant parameters necessary for modelling heat demand according to the norm. This sheds light on the data requirements for computing the heat demand of a building and provides a checklist of data input that can, later on, be used to data map the required input and possible storage within the CityGML and the Energy ADE framework and devise a possible database implementation to facilitate the heat demand computation. The second step is applying the lessons learned from the first step into a working heat demand model with as input data, a semantic 3D city model. This step requires implementing the theoretical formulas into a Python script model. The third step consists of comparing the heat demand estimates with another

energy simulation tool, statistical consumption patterns and energy performance benchmark values to potentially validate the developed model.

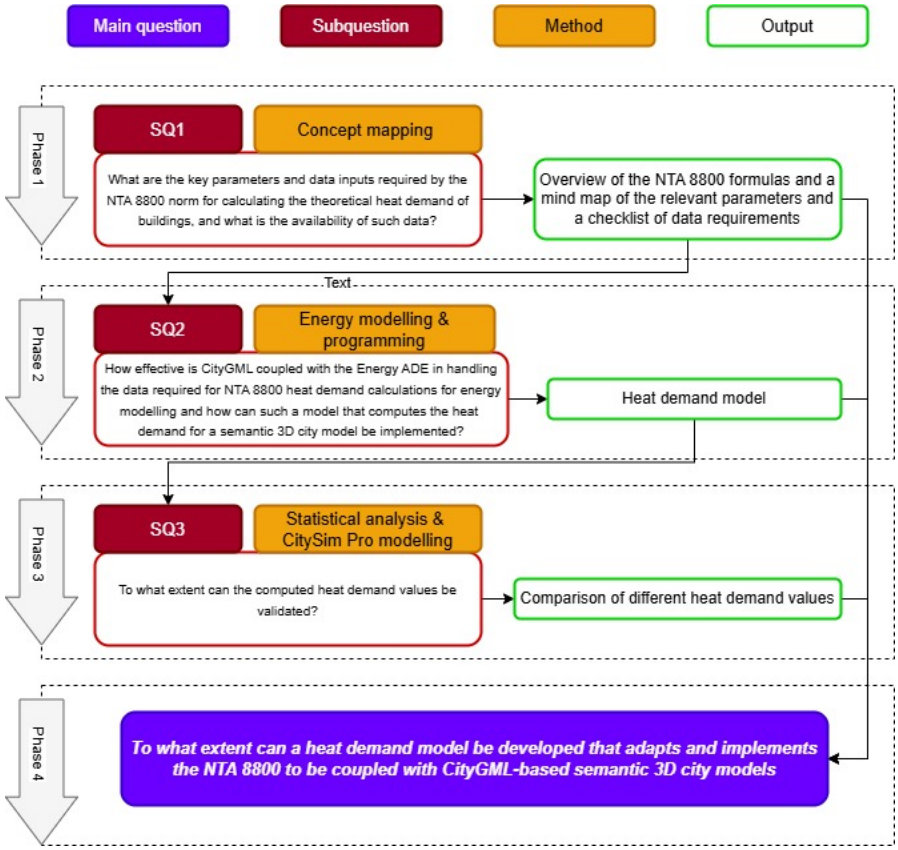

Figure 3.1: The research process

The thesis employs a scientific concurrent descriptive mixed-method research approach following the principles according to Bhattacherjee (2012) and Creswell and Clark (2017). To answer the *what*, *where*, and *when* types of research questions, descriptive research focuses on making meticulous observations and thorough documentation of the phenomena of interest based on repeatable and accurate observations (Bhattacherjee, 2012). Converging quantitative and qualitative research methods to provide a comprehensive assessment of the research problem is known as a concurrent mixed methods approach (Creswell & Clark, 2017).

3.3. Study area: Rijssen-Holten

Rijssen-Holten was chosen as the study area for this thesis. The reason why Rijssen-Holten was chosen as the thesis study area was due to data availability and level of data enrichment. A project was started in Rijssen-Holten initially to collect detailed information about the building stock in this area, which was later on picked up by TUDelft 3D geoinformation group to further enrich the dataset and store it in a semantic 3D city model in the 3DBAG (Leon-Sanchez et al., 2021). The semantic 3D city model of Rijssen-Holten is openly available on GitHub and has been academically verified and published in Leon-Sanchez et al. (2021) paper. It is the most enriched version available of the 3DBAG dataset to date. The dataset comes in LoD 2. More details about

the semantic 3D city model are outlined in subsection 4.4.1.

To give some geographical context about the study area, the municipality Rijssen-Holten is located in Overijssel, the Netherlands and contains around 15,005 buildings of which this thesis specifically looks at the buildings in Rijssen of Rijssen-Holten (see Figure 3.2). Rijssen-Holten has around 37,000 inhabitants (Leon-Sanchez et al., 2021). For geographical mapping purposes, Rijssen-Holten resides in the UTM zone 31N (Morton, n.d.)

Figure 3.2: Overview of the study area Rijssen-Holten, the Netherlands and the CityGML building subset

4

What are the key parameters and data inputs required by the NTA 8800 norm for calculating the theoretical heat demand of buildings, and what is the availability of such data?

To answer the first sub-question, the method of concept mapping is employed after reading the NTA 8800 norm. Concept mapping is a method to visually represent information. It can be in the form of charts, tables, flowcharts, Venn Diagrams, timelines, or decision trees. This method is included as the qualitative research component of the mixed-method approach applied after reading the NTA 8800 and noting down all the relevant formulas, variables, and assumptions. The final output is a mind map overview of the relevant components necessary for heat demand modelling (see section 4.2), which is useful for the second research phase where the mind map is used to implement a working Python script model. The mind map is also transformed into a data requirement checklist and outlines the potential data area sources the data is collected.

4.1. NTA 8800 calculation method for heat demand

The NTA 8800 determination method is deployed for this thesis. As mentioned in subsection 2.2.2, the NTA 8800 calculations are based on the steady-state energy balance method (NEN, 2024), which simply refers to the balance of heat losses and gains within the building. Heat demand is formulated as the monthly energy requirement for heating in the NTA 8800, chapter 7, which is

computed as:

- If $\gamma_{H;zi;mi} \leq 0$ and $Q_{H;gn;zi;mi} > 0$:

$$Q_{H;nd;zi;mi} = 0 \tag{4.1}$$

- If $\gamma_{H;zi;mi} > 2.0$:

$$Q_{H;nd;zi;mi} = 0 \tag{4.2}$$

- In other cases:

$$Q_{H;nd;zi;mi} = Q_{H;ht;zi;mi} - (\eta_{H;gn;zi;mi} \cdot Q_{H;gn;zi;mi}) \tag{4.3}$$

Where for each calculation zone zi and each month mi:

- $Q_{H;nd;zi;mi}$ is the monthly energy requirement for heating for the calculation zone zi and month mi in kWh.
- $\gamma_{H;zi;mi}$ is the dimensionless heat balance ratio for heating, see subsection 4.1.4
- $Q_{H;ht;zi;mi}$ is the total heat transfer for heating in kWh, determined according to subsection 4.1.1
- $\eta_{H;gn;zi;mi}$ is the dimensionless utilization factor for the heat gain, see subsection 4.1.4
- $Q_{H;gn;zi;mi}$ is the total heat gain for heating in kWh, determined according to subsection 4.1.2

4.1.1. Total heat transfer for heating

For each calculation zone and each month, the total heat transfer for heating $Q_{H;ht;zi;mi}$, in kWh, is calculated using the following formula:

$$Q_{H;ht;zi;mi} = Q_{H;tr;zi;mi} + Q_{H;ve;zi;mi} \tag{4.4}$$

Where, for each calculation zone zi and month mi:

- $Q_{H;ht;zi;mi}$ is the total heat transfer for heating in kWh
- $Q_{H;tr;zi;mi}$ is the total heat transfer through transmission for heating in kWh, determined according to subsubsection 4.1.1.1
- $Q_{H;ve;zi;mi}$ is the total heat transfer through ventilation for heating in kWh, determined according to subsubsection 4.1.1.2

4.1.1.1.Heat transfer through transmission

The heat transfer by transmission involves summing the heat transfer coefficients over individual constructions. The result is then multiplied by the temperature difference between the calculation temperature in the zone and the outdoor temperature for the respective month, and by the duration of that month. For each calculation zone and each month, the heat transfer through transmission $Q_{H;tr;zi;mi}$, in kWh, is calculated using the following formula[1]:

$$\begin{aligned} Q_{\mathrm{H;tr;zi;mi}} = \Big(& H_{\mathrm{H:tr(excl.gf);zi;mi}} \cdot \left(\theta_{\mathrm{int;calc;H;zi;mi}} - \theta_{\mathrm{e;avg;mi}}\right) \\ & + H_{\mathrm{g;an;zi,mi}} \cdot \left(\theta_{\mathrm{int;calc;H;zi;mi}} - \theta_{\mathrm{e;avg;mi}}\right) \Big) \cdot 0.001 \cdot t_{\mathrm{mi}} \end{aligned} \tag{4.5}$$

[1]The "0.001" in the equation represents the conversion factor necessary to convert Wh to kWh. This conversion coefficient appears in other formulas as well and implies the same meaning.

In which:

$$H_{\text{H;tr(excl.gf;mi);zi;mi}} = H_{\text{H;D;zi;mi}} + H_{\text{H;U;zi;mi}} + H_{\text{H;A;zi;mi}} + H_{\text{H;p;zi}} \tag{4.6}$$

Where, for each calculation zone zi and month mi:

- $Q_{\text{H;tr;zi;mi}}$ is the total heat transfer by transmission for heating in kWh
- $H_{\text{H;tr(excl.gf;mi);zi;mi}}$ is the total heat transfer coefficient by transmission for heating, with the exception of the ground floor, in W/K
- $H_{\text{H;D;zi;mi}}$ is the direct heat transfer coefficient between the heated space and the outside air in W/K, determined according to paragraph 4.1.1.1.2
- $H_{\text{H;U;zi;mi}}$ is the heat transfer coefficient via adjacent unheated spaces in W/K, determined according to paragraph 4.1.1.1.3
- $H_{\text{H;A;zi;mi}}$ is the heat transfer coefficient via adjacent heated spaces in W/K, determined according to paragraph 4.1.1.1.4
- $H_{\text{H;p;zi}}$ is the heat transfer coefficient of zone zi through vertical pipes in W/K, determined according to paragraph 4.1.1.1.5
- $\theta_{\text{int;calc;H;zi;mi}}$ is the calculation temperature of the calculation zone for heating in °C, determined according to subsubsection 4.1.3.1
- $\theta_{\text{e;avg;mi}}$ is the average outdoor temperature in month mi in °C, determined according to Table 4.7
- $H_{\text{g;an;zi,mi}}$ is the heat transfer coefficient for building elements in thermal contact with the ground, including floors poured directly on the ground, self-supporting floors and cellars, based on the annual temperature difference in W/K, determined according to paragraph 4.1.1.1.1
- t_{mi} is the calculation length of the month in h, determined according to Table 4.7

The heat exchange through transmission between adjacent calculation zones is not considered. For floating structures, transmission to water is considered equivalent to transmission to outdoor air. It's noted that at certain times or even throughout an entire month (e.g., summer), the temperature in the calculation zone may be higher than the calculation temperature for heating. Despite this, calculating heat loss relative to the calculation temperature is still valid because any differences with the actual average temperature (including dynamic effects) are accounted for in the utilization factor for heat gain. The (monthly average) outdoor temperature at the exterior of the construction, as seen from the calculation zone, is crucial. If this temperature is higher than the calculation temperature in the calculation zone, the heat loss is negative. This is why the European norms use the neutral term "heat transfer" instead of "heat loss".

4.1.1.1.1 Heat transfer coefficient for building elements in thermal contact with the ground

For each calculation zone and each year, the heat transfer coefficient for building elements in thermal contact with the ground $H_{\text{g;an;zi,mi}}$ (in chapter 7 of the NTA 8800) or H_g (in chapter 8 of the NTA 8800), in W/K, is computed with the following formula:

$$H_g = A_{\text{fl}} \cdot U_{\text{fl}} + \sum_j (\ell_j \cdot \psi_{\text{gr};j}) \tag{4.7}$$

Where:

- A_{fl} is the surface area of the floor directly on the ground, above a crawl space, or above an unheated space in m^2
- U_{fl} is the heat transfer coefficient of the floor surface, above a crawl space, or above an unheated space in $W/(m^2K)$, e.g thermal transmittance
- ℓ_j is the length of the linear thermal bridge of the (interior) floor perimeter, j, in m, e.g. the length size of the surface sides
- $\psi_g r; j$ is the linear heat transfer coefficient of part j of the (interior) floor perimeter to the ground, in W/(mK), e.g. thermal transmittance

H_g is computed for two situations:

1. Surfaces directly on the ground
2. Surfaces above crawl spaces, or unheated basements

The flat-rate allowance method of the linear thermal bridges is also possible, making the output stationary heat transfer coefficient through the ground surfaces, $H_{g;for}$, in W/K:

$$H_{g;for} = A_{\text{fl}} \cdot U_{\text{fl}} + 0.5 \cdot P \tag{4.8}$$

Where:

- P is the length of the perimeter in m

If a building has storeys below the ground floor, e.g. floor level -3 like in a parking lot or a cellar, the $H_{g;for}$ needs to be computed using the formula:

$$H_{\text{g;for}} = A_{\text{fl}} \cdot U_{\text{fl}} + 0.5 \cdot P + \sum A_{;T;bw} \cdot (U_{bw;j} + \Delta U_{for}) \tag{4.9}$$

Where:

- $A_{T;bw}$ is the total projected area of the basement walls in m^2
- $U_{bw;j}$ is the stationary heat transfer coefficient of the area below ground level wall part j in $W/(m^2K)$, e.g thermal transmittance

It is important to note that at the time of this thesis documentation, the semantic 3D city model used in this thesis did not contain information regarding storey levels below the ground or about the linear thermal bridge transmittance factor, due to the limitations of the data availability. The semantic 3D city model, however, can store this type of information in the CityGML data model. So even though this is a limitation of this thesis, this is not to say that this will not be available in future versions. However, due to this limitation, only equation 4.8 can be implemented.

If the storeys below the ground floor are not heated, the $H_{g;for}$ still needs to be computed and not be confused with $H_{\text{H;U;zi;mi}}$ (see paragraph 4.1.1.1.3).

4.1.1.1.2 Direct heat transfer coefficient between the heated space and the outside air

The NTA 8800 initially outlines the following formula to compute the direct heat transfer coefficient between the heated space and the outside air $H_{\text{H;D;zi;mi}}$ (in chapter 7 of the NTA 8800) or H_{D} (in chapter 8 of the NTA 8800) in W/K:

$$H_D = \sum_i (A_{T,i} \cdot U_{G,i}) + \sum_k (\ell_k \cdot \psi_k) + \sum_j \chi_j \tag{4.10}$$

Where:

- $A_{T,i}$ is the projected surface area of the opaque element i of the external separation construction in m^2, simply put the building surface (e.g. walls and roofs). It is important to note that the NTA 8800 specifically mentions that this surface, $A_{T,i}$ does not include the window or door surface in Appendix K.1.2 of the NTA 8800
- $U_{C,i}$ is the heat transfer coefficient of the flat element i of the external separation construction in $W/(m^2K)$, e.g thermal transmittance
- ℓ_k is the length of the linear thermal bridge, k, in m, e.g. the length size of the surface sides
- ψ_k is the linear heat loss coefficient of the thermal bridge, k, in W/(mK), e.g. thermal transmittance
- χ_j is the heat loss coefficient of the point thermal bridge, j, in W/K, e.g thermal transmittance

The NTA 8800 outlines methods and equations that can be used to determine $A_{T,i}$, $U_{C,i}$, ℓ_k, ψ_k and χ_j. However, the NTA 8800 formulation for the computation of χ_j requires information regarding the building material type composition of the surface, specifically the construction material (e.g. brick, wood, metal) and weight. Given that the thesis is using a semantic 3D city model that does allow for the storage of material type information, but at the time of this thesis data collection, there was no viable building material type dataset available to store into the semantic 3D city model. Due to the limitation of material data availability, it is difficult to compute this equation and hence I chose to not implement this formula. This is not to say that this type of information will not be available in the future and hence this equation can be implemented in future versions.

Fortunately, the NTA 8800 also outlines an alternative simplified formula, flat-rate allowance for linear thermal bridges, that can be deployed when the linear thermal bridges information is not readily available to the user. Therefore, for each calculation zone and each month, the direct heat transfer coefficient between the heated space and the external environment $H_{\mathrm{H;D;zi;mi}}$ (in chapter 7 of the NTA 8800) or $H_{\mathrm{D,for}}$ (in chapter 8 of the NTA 8800), in W/K, is computed with the following formula:

$$H_{D,for} = \sum_i \left(A_{T,j} \cdot (U_{C,j} + \Delta U_{for})\right) \tag{4.11}$$

In which:

$$\Delta U_{for} = \max\left\{0;\, 0.1 - 0.025 \cdot \left(\frac{\sum_i (A_{T,ntr;i} \cdot U_{C,ntr;i})}{\sum_i A_{T,ntr;i}} - 0.4\right)\right\} \tag{4.12}$$

Where:

- $A_{T,ntr;i}$ is the projected surface area of the non-transparent element i, not being a floor above a crawl space or directly on the ground or a roof in m^2
- $U_{C,ntr;i}$ is the heat transfer coefficient of the non-transparent element i, not being a floor above a crawl space or directly on the ground or a roof in $W/(m^2K)$

The flat-rate compensation of linear thermal bridges may only be applied when done for the whole building; heat loss coefficient calculation with mixing of flat-rate and non-flat-rate calculation methods is not allowed. All surfaces, except for floors above crawl spaces or directly on the ground or roof, are included.

Average U-value of the non-transparent external separating constructions, not being a floor above a crawl space or directly on the ground or a roof in one unit [W/(m^{2}K)]	**ΔU_{for} [W/(m^{2}K)]**
0.8	0.00
0.6	0.05
0.4	0.10

Table 4.1: Example values for standardized addition for the calculation of linear thermal bridges (NEN, 2024)

The calculation of direct heat transfer coefficient does not include:

- Separation surfaces between the heated space and adjacent unheated spaces
- Separation surfaces between the heated space and adjacent heated spaces
- linear thermal bridges that form a separation between separating surfaces and the ground (or water)

4.1.1.1.3 Heat transfer coefficient via adjacent unheated spaces

The NTA 8800 mentions that for the heat transfer coefficient via adjacent unheated spaces, $H_{H;U;zi;mi}$, can be assumed to be 0 (NEN, 2024). Therefore, for each calculation zone and each month, the heat transfer coefficient via adjacent unheated spaces $H_{H;U;zi;mi}$ or $H_{U,for}$, in W/K, is considered:

$$H_{U,for} = 0 \tag{4.13}$$

This is a simplified generalisation outlined by the norm to use for the heat transfer coefficient via adjacent unheated spaces and is considered a modelling limitation.

4.1.1.1.4 Heat transfer coefficient via adjacent heated spaces

The NTA 8800 mentions that the heat transfer coefficient via adjacent heated spaces, $H_{H;A;zi;mi}$ (in chapter 7 of the NTA 8800) or $H_{A;mi}$ (in chapter 8 of the NTA 8800), in W/K, is neglected and therefore:

$$H_{A;mi} = 0 \tag{4.14}$$

This is a simplified generalisation outlined by the norm to use for the heat transfer coefficient via adjacent heated spaces and is considered a modelling limitation.

4.1.1.1.5 Heat transfer coefficient through vertical pipes

For each calculation zone, the heat transfer coefficient through vertical pipes $H_{H;p;zi}$, is computed using the following formula:

$$H_{H;p;zi} = \sum_{j} N_{storeys;j} \cdot H_{H;p;spec;j} \tag{4.15}$$

Where for each calculation zone zi:

- $H_{H;p;zi}$ is the heat transfer coefficient of zone zi through vertical pipes in W/K
- j is the number of vertical pipes in the calculation area
- $N_{storeys;j}$ is the number of storeys of the calculation zone in which vertical pipe j is located, e.g. the number of storeys the building has

- $H_{\text{H;p;spec;j}}$ is the heat transfer coefficient per building layer for vertical pipe j, determined according to Table 4.2 in W/K

Even though a semantic 3D city model can store information about the vertical pipes, information about the vertical pipes of the building stock was not available during the thesis process. Therefore, in order to compute this heat transfer coefficient through vertical pipes, I made an assumption that depends on the building's HVAC system specification, which was available. The assumption I made is that if a building had the heating system VR or H107 boiler, I assumed the building would have the uninsulated pipe value from Table 4.2, while if the building has an electric heat pump, I assumed the insulated pipe value from Table 4.2. This assumption was made based on the premise that buildings with electric heat pumps typically are recommended to increase their building insulation before installing them (Association of the European Heating Industry, 2024). However, I acknowledge that this assumption is a limitation of the model implementation.

Type of pipe	**$H_{\text{H;p;spec;j}}$ in W/K**
Uninsulated vertical pipe through thermal shell	1.8
Insulated vertical pipe through thermal shell	0.5
No penetrations through thermal shell	0

Table 4.2: Heat transfer coefficient via vertical pipes per building layer (NEN, 2024)

4.1.1.2.Heat transfer through ventilation

The heat transfer through ventilation in a calculation zone is determined by the amount of infiltration and ventilation air entering the calculation zone. The heat exchange due to ventilation between adjacent calculation zones is not taken into account. For each calculation zone and each month, the total heat transfer through ventilation $Q_{\text{H;ve;zi;mi}}$, in kWh, is calculated with the following formula:

$$Q_{\text{H;ve;zi;mi}} = H_{\text{H;ve;zi;mi}} \cdot \left(\theta_{\text{int;calc;H;zi}} - \theta_{\text{e;avg;mi}}\right) \cdot 0.001 \cdot t_{\text{mi}} \tag{4.16}$$

Where for each calculation zone zi and month mi:

- $Q_{\text{H;ve;zi,mi}}$ is the total heat transfer by ventilation for heating in kWh
- $H_{\text{H;ve;zi,mi}}$ is the total heat transfer coefficient through ventilation for heating in W/K, determined according to paragraph 4.1.1.2.1
- $\theta_{\text{int;calc;H;zi}}$ is the calculation temperature of the calculation zone for heating in°C, determined according to subsubsection 4.1.3.1
- $\theta_{\text{e;avg;mi}}$ is the average outdoor temperature in month mi in °C, determined according to Table 4.7
- t_{mi} is the calculation length of the month in h, determined according to Table 4.7

4.1.1.2.1 Heat transfer coefficient for ventilation

For each calculation zone and each month, the total heat transfer coefficient through ventilation for heating, $H_{\text{H;ve;zi;mi}}$, in W/K, is calculated with the following formula:

$$H_{\text{H;ve;zi;mi}} = \rho_{\text{A}} \cdot c_{\text{A}} \cdot \sum_{k} \left(q_{\text{v;k;H;zi;mi}} \cdot b_{\text{v;k;H;zi;mi}} \cdot f_{\text{v;dyn;k;zi;mi}}\right)/3600 \tag{4.17}$$

Where for each calculation zone zi and month mi:

- $H_{\text{H;ve;zi;mi}}$ is the total heat transfer coefficient by ventilation for heating in W/K
- $\rho_{\text{A}} \cdot c_{\text{A}}$ is the heat capacity of air per volume in $J/(m^3 \cdot K)$ with:
  - ρ_{A} is the density of air, which equates to $1.205 kg/m^3$ (NEN, 2024)
  - c_{A} is the heat capacity of air, which equates to $1005 J/kgK$ (NEN, 2024)
- $b_{\text{v;k;H;zi;mi}}$ is the supply temperature correction factor for air volume flow k, determined according to paragraph 4.1.1.2.1.2, assumed to be 1
- $f_{\text{v;dyn;k;zi;mi}}$ is the dynamic correction factor for air volume flow k, with $f_{\text{v;dyn;k;zi;mi}} = 1$ (NEN, 2024). This implies that the dynamic effects on air volume flow such as changes in pressure or temperature are not taken into account in this computation as it is set to 1.
- $q_{\text{v;k;H;zi;mi}}$ is the air volume flow k, in m^3/h, determined in paragraph 4.1.1.2.1.1

4.1.1.2.1.1 Air volume flow

For modelling the heat transfer coefficient for ventilation, the effective air volumetric flows, $qv;k;H;zi,mi$ (in chapter 7 of the NTA 8800) or q_v (in chapter 8 of the NTA 8800) need to be established. Chapter 11 of the NTA 8800 outlines that the effective air volumetric flows are determined using a simplified airflow model. This calculation is done at the building level, not at the building function, for simplification.

In a simplified explanation, according to the NTA 8800, the airflow model for determining the effective air volume flow q_v, in m^3/h, is determined based on the pressure difference across the opening, the flow exponent, and the air permeability coefficient of the opening:

$$q_v = C \cdot \Delta p^n \tag{4.18}$$

Where:

- q_v is the effective air volume flow, in m^3/h, assumed as 50 m^3/h (Yoshino et al., 2004)
- C or C_{path} is the air permeability coefficient of the opening, in $\text{m}^3/\text{h(Pa)}^n$
- Δp is the pressure difference across the airflow, in Pa, and is set to the differential of 10 Pa since this is the norm value in the Netherlands (Bramiana et al., 2016).
- n is the flow exponent of the opening

The NTA 8800 chapter 11 continues explaining a detailed method of computing the air permeability per ventilation system type, which unfortunately requires detailed information on the building stock which is not available per building level for entire neighbourhoods or as building typology level characterisation.

The Dutch Building Code only mentions that the permitted total air flow rate of residential including toilet and bathroom must not be bigger than 0.2 m^3/h (Bramiana et al., 2016; Ministerie van Binnenlandse Zaken en Koninkrijksrelaties, 2011). Therefore, literature estimations on the effective air volumetric flow were consulted and set as fixed values in the model implementation.

The Netherlands use the norm w10, which is the specific leakage rate at 10 Pa difference (Bramiana et al., 2016). The average specific leakage rate at 10 Pa of all Dutch dwellings was measured

and turned out to be on average 0.55 $dm^3/s \cdot (m)^2$and the airtightness measured in buildings over different construction year groups; pre-1992, 1992-2002, 2003-2001 and post-2021 equated to 3.09 $dm^3/s \cdot (m)^2$ (pre-1992), 0.50 $dm^3/s \cdot (m)^2$ (1992-2002), 0.17 $dm^3/s \cdot (m)^2$ (2003-2001), and 0.52 $dm^3/s \cdot (m)^2$ (post-2021) (Bramiana et al., 2016). However, it should be noted that the values recorded were not statistically significant (Bramiana et al., 2016).

Another paper identified that the average minimum effective air volume flow lies between 25-75 m^3/h (Yoshino et al., 2004), and hence the average value 50 m^3/h is used for the model implementation for each building. I acknowledge that this is a model limitation since this causes each building to have similar ventilation losses.

4.1.1.2.1.2 Supply temperature correction factor

The supply temperature correction factor, $b_{v;k;H;mi}$, for air volume flow k and month mi for heating is computed with the following formula:

$$b_{v;k;H;mi} = \frac{\left(\theta_{int;set;H;stc;mi} - \theta_{sup;k;H;mi}\right)}{\left(\theta_{int;set;H;stc;mi} - \theta_{e;avg;mi}\right)} \tag{4.19}$$

Where for each month mi:

- $b_{v;k;H;mi}$ is the supply temperature correction factor for airflow k for heating.
- $\theta_{int;set;H;stc;zi;mi}$ is the set-point temperature for the thermally conditioned zones of the adjacent calculation zone zi for heating in °C, as determined in Table 4.8
- $\theta_{sup;k;H;mi}$ is the supply temperature of airflow k for heating in °C
- $\theta_{e;avg;mi}$ is the average outside temperature per month in °C, as determined in Table 4.7

The supply temperature correction factor deviates from 1 when the temperature of the air supplied to the calculation zone, $\theta_{sup;k;H;mi}$, is not equal to the outdoor temperature, $\theta_{e;avg;mi}$. For example, if the outside airflow comes directly and is not heated, then the following condition applies:

$$\theta_{sup;k;H;mi} = \theta_{e;avg;mi} \tag{4.20}$$

Since I do not have a detailed dataset of the ventilation system conditions of the building stock, I am assuming the outside air entering the building is not preheated, so $b_{v;k;H;mi}$ stays 1.

4.1.2. Total heat gain for heating

For each calculation zone and each month, the total heat gain for heating $Q_{H;gn;zi;mi}$, in kWh, is calculated using the following formula:

$$Q_{H;gn;zi;mi} = Q_{H;int;zi;mi} + Q_{H;sol;zi;mi} \tag{4.21}$$

Where, for each calculation zone zi and month mi:

- $Q_{H;gn;zi;mi}$ is the total heat gain for heating, in kWh
- $Q_{H;int;zi;mi}$ is the total internal heat gain for heating, in kWh, determined according to subsubsection 4.1.2.1
- $Q_{H;sol;zi;mi}$ is the total solar heat gain for heating, in kWh, determined according to subsubsection 4.1.2.2

4.1.2.1.Internal heat gain for heating

Internal heat gain refers to the contribution to the heat balance from internal sources other than the deliberate supply of heat or cooling for space heating, space cooling or domestic hot water (DHW) preparation. Only the internal heat gain in the calculation zone itself is included in the calculation. In adjacent unheated spaces, the internal heat gain is disregarded. Cold heat production from e.g. air conditioning is, therefore, considered as a negative internal heat gain input.

4.1.2.1.1 Residential building

For each calculation zone and each month, the internal heat gain, $Q_{H;int;zi;mi}$ or $Q_{H;int;dir;zi;mi}$, is computed using the following formula:

$$Q_{\text{H;int;dir;zi;mi}} = 180 \cdot N_{\text{woon;zi}} \cdot N_{\text{P;woon;zi}} \cdot 0.001 \cdot t_{\text{mi}} \tag{4.22}$$

The NTA 8800 also outlines the conditionals to determine the number of residents per calculation zone per residential building $N_{\text{P;woon;zi}}$, which is based on the average usable area per dwelling:

$$\frac{A_{\text{g;zi}}}{N_{\text{woon;zi}}} \leq 30m^2 : N_{\text{P;woon;zi}} = 1 \tag{4.23}$$

$$30m^2 < \frac{A_{\text{g;zi}}}{N_{\text{woon;zi}}} \leq 100m^2 : N_{\text{P;woon;zi}} = 2.28 - \frac{1.28}{70} \cdot \left(100 - \frac{A_{\text{g;zi}}}{N_{\text{woon;zi}}}\right) \tag{4.24}$$

$$\frac{A_{\text{g;zi}}}{N_{\text{woon;zi}}} > 100m^2 : N_{\text{P;woon;zi}} = 1.28 + 0.01 \cdot \frac{A_{\text{g;zi}}}{N_{\text{woon;zi}}} \tag{4.25}$$

Where:

- $Q_{\text{H;int;dir;zi;mi}}$ is the internal heat gain in calculation zone zi for heating, in kWh
- $N_{\text{woon;zi}}$ is the number of residential units in calculation zone zi
- $N_{\text{P;woon;zi}}$ is the average number of residents per calculation zone per residential building
- $A_{\text{g;zi}}$ is the usable area of the considered calculation zone in m^2
- t_{mi} is the calculation length of the month in h, determined according to Table 4.7

This computation includes both internal heat production by persons and equipment.

4.1.2.1.2 Non-Residential building

For each calculation zone and each month, the internal gain for heating for non-residential buildings, $Q_{H;int;zi;mi}$ or $Q_{H;int;dir;zi;mi}$, in kWh, is calculated with the following formula:

$$\begin{aligned} Q_{\text{H;int;dir;zi}} = (&\Phi_{\text{H;int;oc;zi;mi}} + \Phi_{\text{H;int;A;zi;mi}} + \Phi_{\text{H;int;L;zi;mi}} + \Phi_{\text{H;int;W;zi;mi}} \\ &+ \Phi_{\text{H;int;V;zi;mi}} + \Phi_{\text{H;int;proc;zi;mi}}) \cdot 0.001 \cdot t_{\text{mi}} \end{aligned} \tag{4.26}$$

Where, for calculation zone zi and month mi:

- $Q_{\text{H;int;dir;zi}}$ is the internal heat gain for heating in kWh
- $\Phi_{\text{H;int;Oc;zi;mi}}$ is the heat flow as a result of heat production by persons for heating in W, determined according to paragraph 4.1.2.1.2.1
- $\Phi_{\text{H;int;A;zi;mi}}$ is the heat flow due to heat production by equipment for heating in W, determined according to paragraph 4.1.2.1.2.2

- $\Phi_{H;int;L;zi;mi}$ is the heat flow through recoverable losses from lighting for heating in W, determined according to paragraph 4.1.2.1.2.3
- $\Phi_{H;int;W;zi;mi}$ is the heat flow through recoverable losses of the DHW system for heating in W, determined according to paragraph 4.1.2.1.2.4
- $\Phi_{H;int;V;zi;mi}$ is the heat flow through recoverable losses of the ventilation system in W, determined according to paragraph 4.1.2.1.2.5
- $\Phi_{H;int;proc;zi;mi}$ is the heat flow through recoverable losses from or to processes and goods for heating in W, determined according to paragraph 4.1.2.1.2.6
- t_{mi} is the calculation length of the month in h, determined according to Table 4.7

4.1.2.1.2.1 Heat flow through people

For each calculation zone, the heat flow through people, $\Phi_{int;Oc;zi}$, in W, is calculated with the following formula:

$$\Phi_{int;Oc;zi} = q_{Oc;usi} \cdot f_{\tau;usi} \cdot A_{g;zi} \tag{4.27}$$

Where:

- $\Phi_{int;Oc;zi}$ is the heat flow of the heat production by persons in the considered calculation zone, in W
- $q_{Oc;usi}$ is the specific internal heat production by persons in W/m^2, according to Table 4.3
- $f_{\tau;usi}$ is the correction factor for the occupancy time, according to Table 4.3. The correction factor in this case is an adjustment based on the occupancy time and accounts for the fact that people are not present in the calculation zone all the time, and hence, the heat production by people varies over time. The magnitude of the correction factor is based on the building function, e.g. a hospital has a higher correction factor than a meeting facility.
- $A_{g;zi}$ is the usable area of the calculation zone in m^2.

Use function of a building(part)	$\mathbf{q_{Oc}}$ **in W/m²**	$\mathbf{f_{\tau;usi}}$
Childcare facilities	10	0.30
Other meeting facility	10	0.15
Prison	3	0.80
Health care with sleeping space	5	0.80
Other healthcare facility	5	0.30
Offices	5	0.30
Lodging	3	0.40
Educational	10	0.30
Sports	3	0.30
Business	3	0.40

Table 4.3: Specific internal heat production by people q_{Oc} (NEN, 2024)

4.1.2.1.2.2 Heat flow through equipment

For each calculation zone, the heat flow through equipment, $\Phi_{int;A;zi}$, in W, is calculated with the following formula:

$$\Phi_{int;A;zi} = q_{A;usi} \cdot A_{g;zi} \tag{4.28}$$

Where:

- $\Phi_{int;A;zi}$ is the heat flow due to heat production by equipment in W
- $q_{A;usi}$ is the specific internal heat production due to the average power of equipment in W/m^2, according to the Table 4.4
- $A_{g;zi}$ is the usable area of the calculation zone in m^2

Use function of a building(part)	$\mathbf{q_A}$ **in** $\mathbf{W/m^2}$
Childcare facilities	1
Other meeting facility	1
Prison	2
Health care with sleeping space	4
Other healthcare facility	3
Offices	2
Lodging	4
Educational	2
Sports	1
Business	3

Table 4.4: Specific internal heat production by equipment q_A (NEN, 2024)

4.1.2.1.2.3 Heat flow through recoverable losses from lighting

For each calculation zone, the heat flow through recoverable losses from lighting, $\Phi_{int;L;zi}$, in W, is calculated with the following formula:

$$\Phi_{int;L;zi} = \frac{f_L \cdot W_t \cdot 1000}{t_{an}} \tag{4.29}$$

Where:

- $\Phi_{int;L;zi}$ is the heat flux through recoverable losses from lighting in W
- f_L is the dimensionless reduction factor whose value is:
  - 0.3 if the total installed power (Pn) is determined for lighting
  - 0.5 if at least 70% of the luminaires, weighted by the total installed power (P_n), is extracted
  - 1.0 in other cases
- W_t is the energy consumption for lighting to provide the necessary lighting levels per year in kWh. Here, a literature assumption is used to model it as a fixed value of 46.94 kWh/m²/year (W. Y. Hong & Rahmat, 2022) times the usable area of the building since the NTA 8800 refers to using formulas from chapter 14 lighting, which is outside the thesis scope of space heat demand. The downside of this approach is that I am using one value for each building, which is a major limitation since it can vary based on building type or construction year of occupant behaviour
- t_{an} is the calculation value for the total length of the year in h

4.1.2.1.2.4 Heat flow through recoverable losses of the DHW system

For each calculation zone and each month, the heat flow through recoverable losses of the hot tap water system, $\Phi_{\text{int;WA;zi;mi}}$, in W, is calculated with the following formula:

$$\Phi_{\text{int;WA;zi;mi}} = \frac{\sum_{si} Q_{\text{W;ls;rbl;si;zi;mi}} \cdot 1000}{t_{\text{mi}}} \tag{4.30}$$

Where:

- $\Phi_{\text{int;WA;zi;mi}}$ is the heat flow through recoverable losses from or to the DHW system in W
- $Q_{\text{W;ls;rbl;si;zi;mi}}$ is the recoverable loss of DHW system si in kWh. Here, a computation assumption is used to model it as a fixed value of 7718.4 kWh/year based on literature values (Hamburg et al., 2021) (see recoverable loss of DHW system computation explanation below), since the NTA 8800 refers to using formulas from chapter 13 DHW system, which is outside the thesis scope of space heat demand. The downside of this approach is that I am using one value for each building, which is a major limitation since it can vary based on building type or construction year of occupant behaviour
- t_{mi} is the calculation length of the month in h, determined according to Table 4.7

Recoverable loss of DHW system computation

This is computed using the values outlined in the Hamburg et al. (2021) study:

$$\text{Pipe heat loss with 40 mm insulation (basements)} : 10.8 \text{ W/m}$$
$$\text{Pipe heat loss with 40 mm insulation (shafts)} : 5.1 \text{ W/m}$$

The average pipe lengths (from the reference building):

$$l_{\text{basement}} \approx 200 \text{ m}$$
$$l_{\text{shaft}} \approx 100 \text{ m}$$

The estimated total heat loss:

$$\begin{aligned} Q_{\text{total}} &= (l_{\text{basement}} \times 10.8 \text{ W/m}) + (l_{\text{shaft}} \times 5.1 \text{ W/m}) \\ &= (200 \text{ m} \times 10.8 \text{ W/m}) + (100 \text{ m} \times 5.1 \text{ W/m}) \\ &= 2160 \text{ W} + 510 \text{ W} \\ &= 2670 \text{ W} \end{aligned}$$

Considering 33% of pipe heat losses can be utilized as internal heat gain:

$$\begin{aligned} Q_{\text{recoverable}} &= 0.33 \times Q_{\text{total}} \\ &= 0.33 \times 2670 \text{ W} \\ &= 881.1 \text{ W} \end{aligned}$$

Convert to yearly values (since there are 8760 hours in a year):

$$\begin{aligned} Q_{\text{yearly}} &= Q_{\text{recoverable}} \times 8760 \text{ hours/year} \\ &= 881.1 \text{ W} \times 8760 \text{ hours/year} \times 0.001 \\ &\approx 7718.4 \text{ kWh/year} \end{aligned}$$

4.1.2.1.2.5 Heat flow through recoverable losses from the ventilation system

The recoverable losses of the ventilation system, $\Phi_{H;int;V;zi;mi}$, are set to zero (NEN, 2024). This is a simplification that can be considered a limitation.

4.1.2.1.2.6 Heat flow through processes and goods

The recoverable losses due to processes and goods, $\Phi_{H;int;proc;zi;mi}$, are set to zero (NEN, 2024). This is a simplification that can be considered a limitation.

4.1.2.2.Solar heat gain for heating

The heat gain from prominent solar radiation (solar heat gain) is the contribution to the building's heat balance as a result of the solar radiation present on site, the orientation of the receiving surfaces, permanent and movable shading, and the solar transmittance, solar absorption and heat transfer properties of the receiving surfaces. The determination method also includes a correction

for shading due to external obstacles belonging to the own plot. In addition, a correction is applied for skyward radiation.

4.1.2.2.1 Total heat gain due to incident solar radiation

For each calculation zone and each month, the solar gain for heating, $Q_{\text{H;sol;zi;mi}}$, in kWh, is calculated with the following formula:

$$Q_{\text{H;sol;zi;mi}} = Q_{\text{H;sol;dir;zi;mi}} \tag{4.31}$$

Where, for each calculation zone zi and each month mi:

- $Q_{\text{H;sol;zi;mi}}$ is the monthly solar heat gain of the calculation zone zi, in kWh
- $Q_{\text{H;sol;dir;zi;mi}}$ is the monthly solar heat gain of the calculation zone itself, as determined in paragraph 4.1.2.2.1.1, in kWh

4.1.2.2.1.1 Solar heat gain elements

For the calculation zone itself for each month, the solar gain for heating, $Q_{\text{H;sol;dir;zi;mi}}$, in kWh, is calculated using the following formula:

$$Q_{\text{H;sol;dir;zi;mi}} = \sum_{k} Q_{\text{H;sol;wi,k;mi}} + \sum_{k} Q_{\text{H;sol;op,k;mi}} \tag{4.32}$$

Where, for each element k and each month mi:

- $Q_{\text{H;sol;dir;zi;mi}}$ is the monthly solar gain of the calculation zone for heating in kWh
- $Q_{\text{H;sol;wi,k;mi}}$ is the monthly solar heat gain through transparent element wi, k, for heating in kWh, as determined in paragraph 4.1.2.2.1.1.1A
- $Q_{\text{H;sol;op,k;mi}}$ is the monthly solar heat gain by non-transparent element op, k, for heating in kWh, as determined in paragraph 4.1.2.2.1.1.1B

4.1.2.2.1.1.1A Transparent surfaces

The heat flux due to incident solar radiation through transparent parts of the building envelope (hereinafter called windows) wi for heating, $Q_{\text{H;sol;wi,k;mi}}$, in kWh, is calculated for each element k with the following formula:

$$Q_{\text{H;sol;wi,k;mi}} = g_{\text{gl;wi,k;H;mi}} \cdot A_{\text{wi,k}} \cdot (1 - F_{\text{fr;wi,k}}) \cdot F_{\text{sh;obst;wi,k;mi}} \cdot I_{\text{sol;wi,k;mi}} \cdot 0.001 \cdot t_{\text{mi}} - Q_{\text{sky;wi,k;mi}} \tag{4.33}$$

Where, for each window wi and month mi:

- $Q_{\text{H;sol;wi,k;mi}}$ is the solar heat gain through transparent element wi, k for heating in kWh
- $g_{gl;wi;k;H;mi}$ is the dimensionless average effective total solar energy transmittance of the window w_i, per month m_i, for heating, determined according to paragraph 4.1.2.2.1.1.1A.1, where for all glazing the calculation method for non-diffusing glazing is applied.
- $A_{\text{wi,k}}$ is the area of window wi, k, in m^2, which is computed using a window to facade ratio of 30% (Dang, 2023; Technische Universiteit Delft, n.d.; Yang et al., 2020) on the wall and roof surfaces. This is a modelling assumption limitation used due to lack of data on windows for the Dutch building stock.

- $F_{\text{fr;wi,k}}$ is the frame fraction of window wi, k, the ratio of the projected frame area to the total projected area of the glazed portion of window wi, k, determined according to paragraph 4.1.2.2.1.1.1A.2
- $F_{\text{sh;obst;wi,k;mi}}$ is the dimensionless shading reduction factor for external impediments of window wi, k, determined according to Table B.1-B.8, implying the percentage of hindering/shadowing effects there is on the total solar radiation on surface due to obscuring objects nearby
- $I_{\text{sol;wi,k;mi}}$ is the monthly average total incident solar radiation per m^2 area of window wi, k, at a given angle of inclination β_{wi} and orientation γ_{wi} in W/m^2, determined according to Table B.9-B.13
- $Q_{\text{sky;wi,k;mi}}$ is the monthly extra heat flow due to heat radiation to the sky from window wi, k, determined according to paragraph 4.1.2.2.1.1.2, in kWh
- t_{mi} is the calculation length of the month in h, determined according to Table 4.7

4.1.2.2.1.1.1A.1 Sun accession factor: Windows with non-diffusing glazing

Considering there is no universal dataset regarding the thermal properties of the window conditions of all the Dutch building stock (e.g. the g-value, the frame length, or material or if there are curtains or blinds), this thesis opts to only implement the sun accession factor for windows with non-diffusing glazing since implementing the other conditions outlined in the NTA 8800 requires making significant assumptions of the window conditions of the building stock. Alternatively, different window types (e.g. different g-values) can be simulated into the model and the same operation can be tested to see the effect of different window types on the heat demand. This parameter then can serve as a sensitivity analysis on heat demand (see subsection 5.3.3 for the results).

The total solar accession factor depends on the angle of incidence (height and azimuth) of the incident solar radiation. The (time-weighted average) value required for the calculations is somewhat lower than the solar accession factor for radiation perpendicular to the glazing, $g_{\text{gl;n}}$. The total solar gain factor (corrected for the angle of incidence) is calculated according to the following formula:

$$g_{\text{gl;wi}} = F_{\text{w}} \cdot g_{\text{gl;n;wi}} \tag{4.34}$$

Where:

- $g_{\text{gl;wi}}$ is the total solar factor (corrected for the angle of incidence)
- F_{w} is the correction factor for non-scattering glazing, for which the following numerical value holds: $F_{\text{w}} = 0.90$ (NEN, 2024). This correction factor accounts for the impacts of materials used for windows that let light through with little to no diffusion or scattering.
- $g_{\text{gl;n;wi}}$ is the sun factor with perpendicular incidence of solar radiation, determined according to Table 4.5

The numerical value for $g_{\text{gl;n;wi}}$ must be rounded down to a multiple of 0.05.

Type	$g_{gl;n}$
Only glass	0.85
Double glass	0.75
Double glass with spectral (low) selective and low emissive coating (HR++)	0.60
Triple glazing without or with one spectrally (low) selective and low emissivity coating	0.50
Triple glass with two spectrally (low) selective and low emissivity coatings	0.40
Single glass with single glass front window or rear window without coating	0.75

Table 4.5: Standard values for the total solar factor at perpendicular incidence, $g_{gl;n}$, for common types of glazing (NEN, 2024)

4.1.2.2.1.1.1A.2 Frame fraction

The area of the glazing can be determined with the geometric data or window dimensions (Method A) or can be derived from a fixed frame fraction (Method B). The same choice must be made for all windows in a building and since the measurements of the fraction of frame is not readily available information from a data source, method B is chosen.

Method B

If the frame fraction is unknown when determining the transmission losses, e.g. because fixed values for the heat transfer coefficient are used, the following numerical value must be used for the frame fraction: $F_{fr;wi} = 0.25$ (NEN, 2024).

4.1.2.2.1.1.1B Non-transparent surfaces

The heat flux due to incident solar radiation through a non-transparent structure $op;k$, for heating, $Q_{H;sol;op,k;mi}$, in kWh, in month mi, is calculated for each element k with the following formula:

$$Q_{\text{H;sol;op,k;mi}} = \alpha_{\text{sol}} \cdot R_{\text{se}} \cdot U_{\text{c;op,k}} \cdot A_{\text{c;op,k}} \cdot F_{\text{sh;obst;op,k;mi}} \cdot I_{\text{sol;op,k;mi}} \cdot 0.001 \cdot t_{\text{mi}} - Q_{\text{sky;op,k;mi}} \quad (4.35)$$

Where, for every non-transparent construction k and every month mi:

- $Q_{\text{H;sol;op,k;mi}}$ is the solar heat gain by non-transparent element op, k, for heating in kWh
- α_{sol} is the dimensionless absorption coefficient for solar radiation of the outer surface of the non-transparent structure, generally set to 0.6 (NEN, 2024)
- R_{se} is the heat transfer resistance on the outside in m^2K/W, as determined according to Table 4.6
- $U_{\text{c;op,k}}$ is the heat transfer coefficient of non-transparent element op, k, in $W/(m^2 \cdot K)$
- $A_{\text{c;op,k}}$ is the projected area of non-transparent element op, k, in m^2
- $F_{\text{sh;obst;op,k;mi}}$ is the dimensionless shading reduction factor for external impediments of non-transparent element op, k, determined according to Table B.1-B.8, implying the percentage of hindering/shadowing effects there is on the total solar radiation on surface due to obscuring objects nearby
- $I_{\text{sol;op,k;mi}}$ is the monthly average total incident solar radiation per m^2 area of non-transparent element op, k, at a given angle of inclination β_{op} and orientation γ_{op} in W/m^2, determined according to Table B.9-B.13

- $Q_{\text{sky;op,k;mi}}$ is the monthly extra heat flow due to heat radiation to the sky from non-transparent element op, k, determined according to paragraph 4.1.2.2.1.1.2, in kWh
- t_{mi} is the calculation length of the month in h, determined according to Table 4.7

4.1.2.2.1.1.2 Heat radiation to the sky

The monthly extra heat flow due to thermal radiation to the sky, $Q_{\text{sky;mi}}$, for a specific building envelope element k, in the month mi, in kWh, is calculated with the following formula:

$$Q_{\text{sky;k;mi}} = 0.001 \cdot F_{\text{sky;k}} \cdot R_{\text{se;k}} \cdot U_{\text{c;k}} \cdot A_{\text{c;k}} \cdot h_{\text{lr;e;k}} \cdot \Delta\theta_{\text{sky;mi}} \cdot t_{\text{mi}} \tag{4.36}$$

Where, for each element k and for each month mi:

- $Q_{\text{sky;k;mi}}$ is the extra heat flow due to heat radiation from building envelope element k to the sky, in kWh
- $F_{\text{sky;k}}$ is the visibility factor between building envelope element k and the sky, determined according to paragraph 4.1.2.2.1.1.3
- $R_{\text{se;k}}$ is the heat transfer resistance on the outside of element k in m^2K/W, as determined according to Table 4.6
- $U_{\text{c;k}}$ is the heat transfer coefficient of element k in $W/(m^2 \cdot K)$
- $A_{\text{c;k}}$ is the projected area of element k in m^2
- $h_{\text{lr;e;k}}$ is the heat transfer coefficient for long-wave radiation on the outside of the structure, for which the following numerical value applies: $h_{\text{lr;e}} = 4.14W/(m^2 \cdot K)$ (NEN, 2024)
- $\Delta\theta_{\text{sky;mi}}$ is the average difference between the apparent sky temperature and the outside temperature, for which the following numerical value applies: $\Delta\theta_{\text{sky;mi}} = 11K$ (NEN, 2024)
- t_{mi} is the calculation length of the month in h, determined according to Table 4.7

4.1.2.2.1.1.3 Form Factor

This component refers to the visibility factor between building envelope element and the sky. For the form factor between the structure k and the sky $F_{\text{sky;k}}$ (NEN, 2024):

- $F_{sky} = 1$ for a horizontal structure, the angle of inclination from the horizontal of which is less than or equal to 5°C
- $F_{sky} = 0.75$ for inclined structures with an angle of inclination from the horizontal less than or equal to 75°, but greater than 5°C
- $F_{sky} = 0.5$ for a vertical structure with an angle of inclination from the horizontal greater than 75°C
- $F_{sky} = 0$ for external partition structures adjacent to the outside that lean over (facing the ground)
- $F_{sky} = 0$ for partition constructions between a calculation zone and an adjacent unheated sunspace.

4.1.2.2.1.1.4 Heat transfer resistance on the outside

The heat transfer resistance is determined in Table 4.6.

Heat transfer resistance	Direction of heat flow		
	Up	Horizontal	Down
R_{si}	0.10	0.13	0.17
R_{se}	0.04	0.04	0.04

Table 4.6: Heat transfer resistances at different heat flow directions (NEN, 2024)

4.1.3. Temperatures

To compute the space heating demand, the parameter temperature is an important component, especially the variable $\theta_{\text{int;calc;H;mi}}$, in °C, is necessary to perform the previous computations. In this section, an explanation is provided of how to compute the $\theta_{\text{int;calc;H;mi}}$, in °C, according to the NTA 8800.

4.1.3.1.Calculation temperature for heating

The calculation temperature in the calculation zone for heating, $\theta_{\text{int;calc;H;mi}}$, °C, is calculated with the following formula:

$$\theta_{\text{int;calc;H;mi}} = \alpha_{\text{H;red;zi;mi}} \cdot (\theta_{\text{int;set;H;zi}} - \theta_{\text{e;avg;mi}}) + \theta_{\text{e;avg;mi}} \tag{4.37}$$

Where, for each calculation zone zi and month mi:

- $\theta_{\text{int;calc;H;mi}}$ is the calculation temperature of the calculation zone for heating, in °C
- $\alpha_{\text{H;red;zi;mi}}$ is the reduction factor for discontinuous heating, for simplification, this is set to 1 because I don't have information about the discontinuous heating system behaviour of the building stock.
- $\theta_{\text{int;set;H;zi}}$ is the set point temperature for heating in °C, determined according to subsubsection 4.1.3.2
- $\theta_{\text{e;avg;mi}}$ is the monthly average outdoor temperature in °C, as determined in Table 4.7

Month	t_{mi} **in h**	$\theta_{\text{e;avg;mi}}$ **in** °C
January	744	2.61
February	672	4.82
March	744	5.91
April	720	9.32
May	744	14.73
June	720	16.12
July	744	18.05
August	744	18.48
September	720	15.63
October	744	10.40
November	720	7.99
December	744	4.00

Table 4.7: Calculation length of the month and average monthly outdoor temperature (NEN, 2024)

4.1.3.2.Set point temperature

Determine the set point temperature of the calculation zone for the heat demand calculation $\theta_{\text{int;set;H;zi}}$ for each usage function according to the formula below:

$$\theta_{\text{int;set;H;zi;mi}} = \theta_{\text{int;set;H;stc;zi}} - \Delta\theta_{\text{int;set;H;zi;mi}} \tag{4.38}$$

Where:

- $\theta_{\text{int;set;H;zi;mi}}$ is the set point temperature of the calculation zone for the heat demand calculation in °C
- $\theta_{\text{int;set;H;stc;zi}}$ is the set point temperature of the calculation zone for heating for the thermally conditioned zones in °C, determined according to Table 4.8
- $\Delta\theta_{\text{int;set;H;zi;mi}}$ is the set point temperature for temperature levelling within a building, between rooms with different assumed uses for the heat demand calculation, in °C. This is assumed to be $\Delta\theta_{int;set;H;zi,mi} = 0$, which is allowed for all usage functions (NEN, 2024) besides residential units. Residential units typically have to be computed but requires data not available for the Rijssen-Holten dataset, which I acknowledge is a limitation of the implementation.

Use function of a building(part)	$\theta_{int;set;H;stc;zi}$ **(°C)**	$\theta_{int;set;C;stc;zi}$ **(°C)**
Childcare facility	21	24
Other meeting facility	21	24
Prison	21	24
Health care with sleeping space	22	24
Other healthcare facility	21	24
Offices	21	24
Lodging	21	24
Educational	21	24
Sports	16	24
Business	21	24
Residential	20	24

Table 4.8: Set point temperature for thermally conditioned zones (NEN, 2024)

4.1.4. Utilisation factor

The dimensionless utilization factor for heat gain, $\eta_{\text{H,gn}}$, is a function of the heat balance ratio for heating, $\gamma_{\text{H;zi;mi}}$, and a numerical parameter, $\alpha_{\text{H;zi;mi}}$, which depends on the inertia of the building. The utilization factor is calculated for each zone and each month using the following formulas:

$$\text{if} \quad \gamma_{\text{H;zi;mi}} > 0 \,\text{and} \quad \gamma_{\text{H;zi;mi}} \neq 1: \qquad \eta_{\text{H;gn;zi;mi}} = \frac{1 - (\gamma_{\text{H;zi;mi}})^{a_{\text{H;zi;mi}}}}{1 - (\gamma_{\text{H;zi;mi}})^{(a_{\text{H;zi;mi}}+1)}} \tag{4.39}$$

$$\text{if} \quad \gamma_{\text{H;zi;mi}} = 1: \quad \eta_{\text{H;gn;zi;mi}} = \frac{a_{\text{H;zi;mi}}}{a_{\text{H;zi;mi}} + 1} \tag{4.40}$$

$$\text{if} \quad \gamma_{\text{H;zi;mi}} \leq 0 \quad \text{and} \quad Q_{\text{H;gn;zi;mi}} > 0: \quad \eta_{\text{H;gn;zi;mi}} = 1/\gamma_{\text{H;zi;mi}} \tag{4.41}$$

$$\text{if} \quad \gamma_{\text{H;zi;mi}} \leq 0 \quad \text{and} \quad Q_{\text{H;gn;zi;mi}} \leq 0: \quad \eta_{\text{H;gn;zi;mi}} = 1 \tag{4.42}$$

In which:

$$\gamma_{\mathrm{H;zi;mi}} = \frac{Q_{\mathrm{H;gn;zi;mi}}}{Q_{\mathrm{H;ht;zi;mi}}} \tag{4.43}$$

Where:

- $\eta_{\mathrm{H;gn;zi;mi}}$ is the dimensionless utilization factor for heat gain
- $\gamma_{\mathrm{H;zi;mi}}$ is the dimensionless heat balance ratio for heating
- $\alpha_{\mathrm{H;zi;mi}}$ is the dimensionless numerical parameter, determined according to equation 4.44
- $Q_{\mathrm{H;ht;zi;mi}}$ is the total heat transfer for heating, determined according to subsection 4.1.1, in kWh
- $Q_{\mathrm{H;gn;zi;mi}}$ is the total heat gain for heating, determined according to subsection 4.1.2, in kWh.

The dimensionless numerical parameter $\alpha_{\mathrm{H;zi;mi}}$ is calculated by the following formula:

$$\alpha_{\mathrm{H;zi;mi}} = \alpha_{\mathrm{H;0}} + \frac{\tau_{\mathrm{H;zi;mi}}}{\tau_{\mathrm{H;0}}} \tag{4.44}$$

Where:

- $\alpha_{\mathrm{H;0}}$ is the dimensionless numerical reference parameter, which has the following number value: $a_{\mathrm{H;0}} = 1.0$ (NEN, 2024)
- $\tau_{\mathrm{H;zi;mi}}$ is the time constant of the heat requirement, in h, determined according to Equation 4.45
- $\tau_{\mathrm{H;0}}$ is the reference time constant, for which the following number value holds: $\tau_{\mathrm{H;0}} = 15$, in h (NEN, 2024)

$$\tau_{H;zi;mi} = \frac{C_{m;int;eff;zi}/3600}{H_{H;tr(excl.gf.mi);zi;mi} + H_{g;zi} + H_{H;ve;zi;mi}} \tag{4.45}$$

Where:

- $\tau_{H;zi;mi}$ is the time constant of calculation zone zi for respectively the heating requirement, in hours.
- $C_{m;int;eff;zi}$ is the effective internal thermal capacity of the calculation zone, computed according to subsubsection 4.1.4.1, in J/K.
- $H_{H;tr(excl.gf.mi);zi;mi}$ is the total heat transfer coefficient by transmission for heating, determined according to subsubsection 4.1.1.1
- $H_{H;g;zi}$ is the total heat transfer coefficient by transmission through the ground floor, as defined in paragraph 4.1.1.1.1, in W/K.
- $H_{H;ve;zi;mi}$ is the total heat transfer coefficient by ventilation for month mi, computed according to paragraph 4.1.1.2.1, in W/K.

4.1.4.1.Effective internal heat capacity

The effective internal heat capacity of the calculation area (air, furniture and building elements) represents the total heat capacity seen from the inside, which can be determined by:

$$C_{\mathrm{m;int;eff;zi}} = D_{\mathrm{m;int;eff;zi}} \cdot 1000 \cdot a_{\mathrm{g;zi}} \tag{4.46}$$

Where:

- $C_{m;int;eff;zi}$ is the effective internal heat capacity of the calculation zone, in J/K
- $D_{m;int;eff;zi}$ is the specific internal heat capacity of the calculation zone, which for residential buildings is assumed to be 180 kJ/m^2K and for non-residential buildings 250 kJ/m^2K using the NTA 8800 tables in chapter 7 (NEN, 2024)
- $a_{g;zi}$ is the usable area of calculation zone zi

4.2. Output: NTA 8800 Mind map

To answer the initial aspect of what the key parameters are to compute heat demand, the following mind maps are for display. Figure 4.2 outlines how heat demand is modelled according to the NTA 8800 norm. In essence, the NTA 8800 heat demand formulation consists of the components: recoverable energy losses, total heat transfer for heating, total heat gain for heating, and utilisation factor for heat gain (see Figure 4.1). These components can be further broken down for total heat transfer into transmission (see Figure 4.3) and ventilation (see Figure 4.4) and for total heat gain into solar gain (see Figure 4.5) and internal gain (see Figure 4.6) as outlined in section 4.1. For each component, a close-up is provided below and the final mind map with all four components is visible in Figure 4.2. For an enlarged version of the mind maps, see Appendix A.

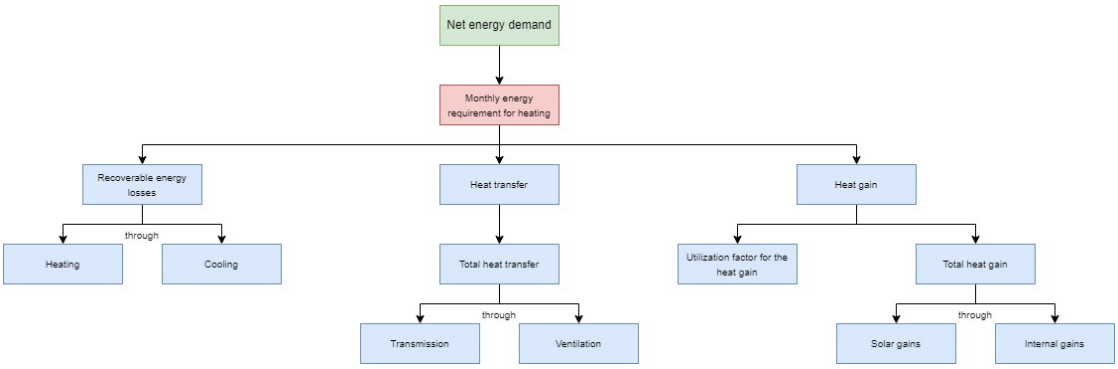

Figure 4.1: Close-up of the main heat demand components

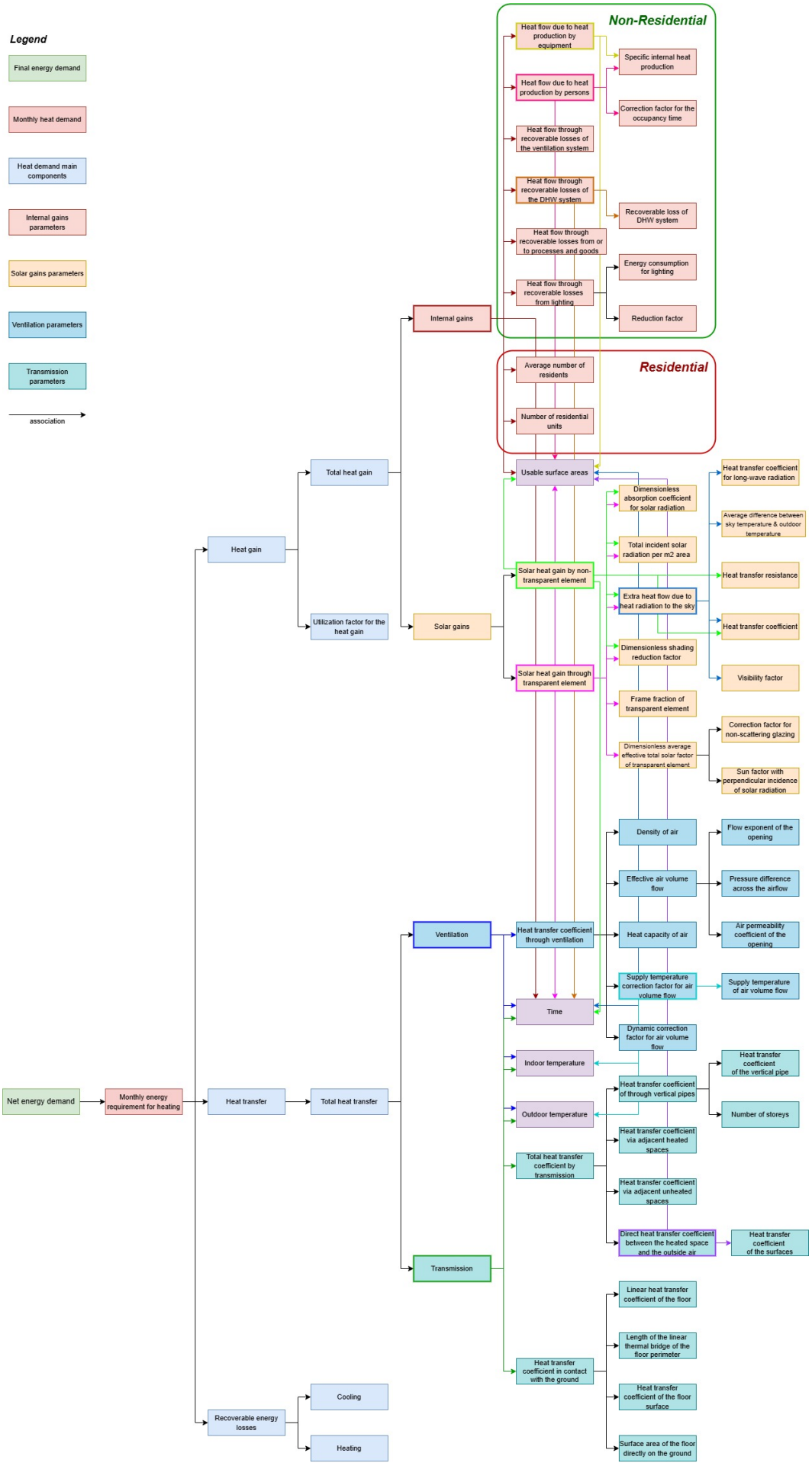

Figure 4.2: Overview of the mind map for heat demand modelling

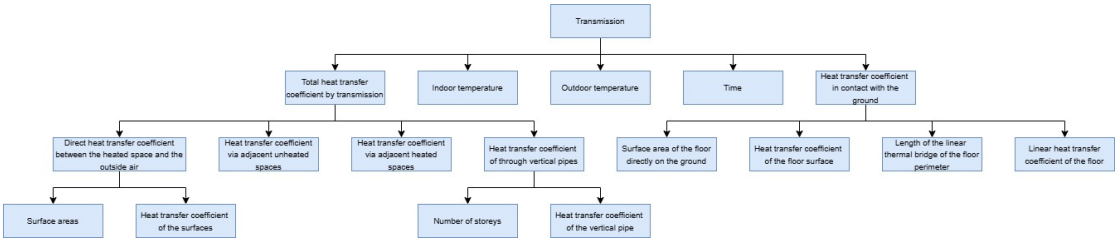

Figure 4.3: A close-up of transmission

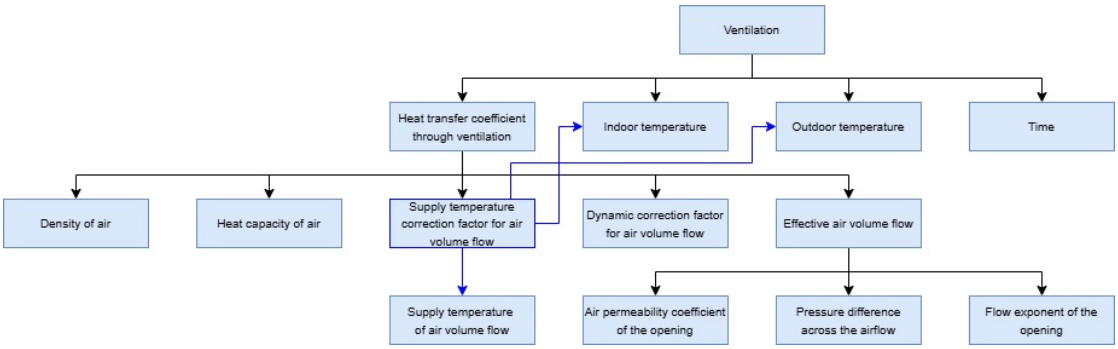

Figure 4.4: A close-up of ventilation

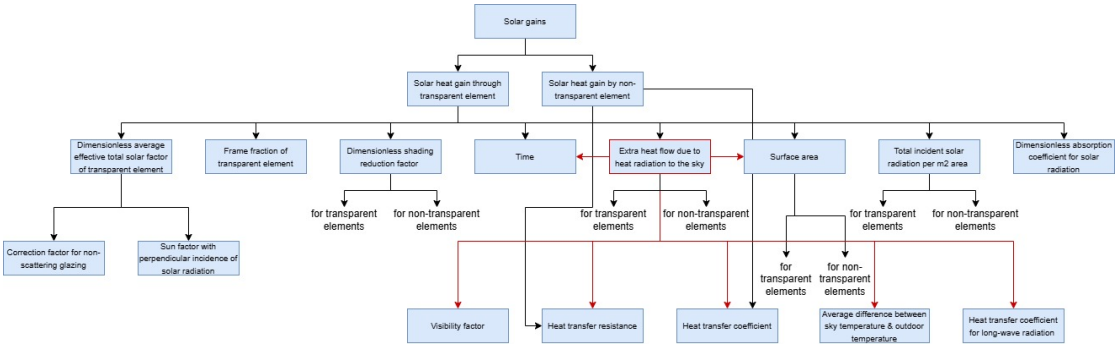

Figure 4.5: A close-up of solar heat gain

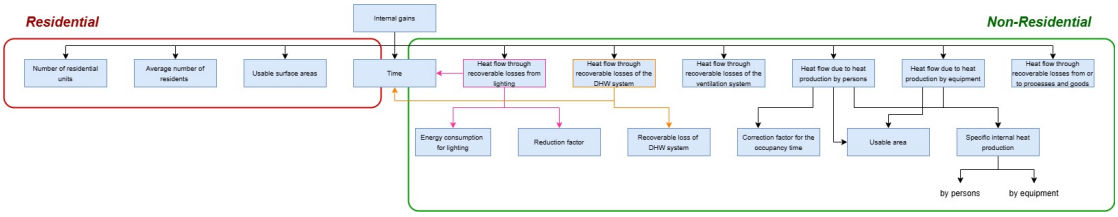

Figure 4.6: A close-up of internal heat gain

4.3. Data requirement and data availability

To help out with the model implementation, an overview of the model parameters is outlined in Table 4.9 to provide a checklist for data collection and also answers the second part of the sub-question.

Category	Parameter	Symbol	Data Availability
Transmission	Total heat transfer for transmission	$Q_{H;tr;zi;mi}$	Yes, computed
	Heat transfer coeff. excluding ground floor	$H_{H;tr(excl.gf;mi);zi;mi}$	Yes, computed
	Calculation temperature of the calculation zone	$\theta_{\text{int;calc;H;zi;mi}}$	Yes, computed
	Average outdoor temperature	$\theta_{\text{e;avg;mi}}$	Yes, Table 4.7
	Time length of month	t_{mi}	Yes, Table 4.7
	Heat transfer coeff. via ground contact	$H_{g;an;zi,mi}$	Yes, computed
	Surface area of the floor directly on the ground	A_{fl}	Yes, from 3DBAG
	Heat transfer coeff. of the floor surface	U_{fl}	Yes, from Voorbeeldwoning
	Direct heat transfer coeff.	H_D	Yes, computed
	Surface areas of the separation constructions	$A_{T,i}$	Yes, from 3DBAG
	Heat transfer coeff. of the separation constructions	$U_{C,i}$	Yes, from Voorbeeldwoning
	Heat transfer coeff. via unheated spaces	$H_{U,for}$	Yes, assumption is 0 by NTA 8800
	Heat transfer coeff. via heated spaces	$H_{A;mi}$	Yes, assumption is 0 by NTA 8800
	Heat transfer coeff. through vertical pipes	$H_{H;p;zi}$	Yes, computed
	Number of storeys	$N_{storeys;j}$	Yes, from 3DBAG
	Heat transfer coeff. of the vertical pipe	$H_{H;p;spec;j}$	Yes, Table 4.2 and also based on heating system type assumption (from Voorbeeldwoning)
Ventilation	Total heat transfer through	$Q_{H;ve;zi;mi}$	Yes, computed
	Total heat transfer coefficient through ventilation	$H_{H;ve;zi;mi}$	Yes, computed
	Calculation temperature of the calculation zone	$\theta_{\text{int;calc;H;zi;mi}}$	Yes, computed
	Average outdoor temperature	$\theta_{\text{e;avg;mi}}$	Yes, Table 4.7
	Time length of month	t_{mi}	Yes, Table 4.7
	Density of air	ρ_A	Yes, fixed value of 1.205 from NTA 8800
	Heat capacity of air	c_A	Yes, fixed value of 1005 from NTA 8800
	Supply temperature correction factor for air volume flow	$b_{v;k;H;zi;mi}$	Yes, computed
	Dynamic correction factor for air volume flow	$f_{v;dyn;k;zi;mi}$	Yes, assumption is 1 by NTA 8800
	Effective air volume flow	$q_{v;k;H;zi;mi}$	**No**, literature assumption of 50 is used as substitute (Yoshino et al., 2004)
Internal heat gain	Internal heat gain for heating	$Q_{H;int;dir;zi;mi}$	Yes, computed
	Number of residential units	$N_{woon;zi}$	Yes, from 3DBAG
	Average number of residents	$N_{P;woon;zi}$	Yes, based on $A_{g;zi}$ and $N_{woon;zi}$ from 3DBAG
	Usable surface areas	$A_{g;zi}$	Yes, from 3DBAG
	Time length of month	t_{mi}	Yes, Table 4.7
	Heat flow due to heat production by persons	$\Phi_{H;int;Oc;zi;mi}$	Yes, computed based on specific internal heat production, correction factor, and area and requires building function from 3DBAG
	Heat flow due to heat production by equipment	$\Phi_{H;int;A;zi;mi}$	Yes, computed based on specific internal heat production and area and requires building function from 3DBAG
	Heat flow through recoverable losses from lighting	$\Phi_{H;int;L;zi;mi}$	Partially, computed based on f_L and W_t. W_t requires a literature assumption

Table 4.9 continued from previous page

Category	Component	Symbol	Data Availability
	Heat flow through recoverable losses of the DHW system	$\Phi_{H;int;W;zi;mi}$	Partially, computed based on DHW system losses. DHW system losses requires a literature assumption
	Heat flow through recoverable losses of the ventilation system	$\Phi_{H;int;V;zi;mi}$	Yes, assumption is 0 by NTA 8800
	Heat flow through recoverable losses from or to processes and goods	$\Phi_{H;int;proc;zi;mi}$	Yes, assumption is 0 by NTA 8800
	Specific internal heat production by persons	$q_{Oc;usi}$	Yes, from Table 4.3 based on non-residential building use function from 3DBAG
	Correction factor for the occupancy time	$f_{\tau;usi}$	Yes, from Table 4.3 based on non-residential building use function from 3DBAG
	Specific internal heat production by equipment	$q_{A;usi}$	Yes, from Table 4.4 based on non-residential building use function from 3DBAG
	Recoverable loss of DHW system	$Q_{\mathrm{W;ls;rbl;si;zi;mi}}$	**No**, W_t requires a literature assumption of 46.94 times the usable area (W. Y. Hong & Rahmat, 2022)
	Energy consumption for lighting	W_{t}	**No**, DHW system losses requires a computed assumption of 7718.4 (Hamburg et al., 2021)
	Dimensionless reduction factor	f_{L}	Yes, fixed value assumed to be 1 by NTA 8800
	Time length of year	t_{an}	Yes, Table 4.7
Solar heat gain	Solar heat gain for heating	$Q_{H;sol;dir;zi;mi}$	Yes, computed
	Solar gain through windows	$Q_{H;sol;wi,k;mi}$	Yes, computed
	Effective total solar energy transmittance	$g_{gl;wi,k;H;mi}$	Yes, computed
	Window area	$A_{wi,k}$	**No**, window-to-facade assumption ratio of 30% is used on 3DBAG wall surfaces (Yang et al., 2020)
	Frame fraction	$F_{fr;wi,k}$	Yes, fixed value of 0.25 from NTA 8800
	Shading reduction factor	$F_{sh;obst;wi,k;mi}$	Yes, Table B.1-B.8
	Incident solar radiation	$I_{sol;wi,k;mi}$	Yes, Table B.9-B.13
	Time length of month	t_{mi}	Yes, Table 4.7
	Extra heat flow due to sky radiation	$Q_{sky;wi,k;mi}$	Yes, computed
	Solar gain through opaque surfaces	$Q_{H;sol;op,k;mi}$	Yes, computed
	Absorption coefficient	α_{sol}	Yes, fixed value of 0.6 from NTA 8800
	Heat transfer resistance outside	R_{se}	Yes, fixed value of 0.04 from NTA 8800
	Heat transfer coefficient	$U_{c;op,k}$	Yes, from Voorbeeldwoning
	Opaque surface area	$A_{c;op,k}$	Yes, from 3DBAG

Table 4.9 continued from previous page

Category	Component	Symbol	Data Availability
	Shading reduction factor	$F_{sh;obst;op,k;mi}$	Yes, assumed to be 1 by NTA 8800
	Incident solar radiation	$I_{sol;op,k;mi}$	Yes, Table B.9-B.13
	Extra heat flow due to sky radiation	$Q_{sky;op,k;mi}$	Yes, computed
	Average difference between the apparent sky temperature and the outside temperature	$\Delta\theta_{\text{sky;mi}}$	Yes, fixed value $\Delta\theta_{\text{sky;mi}} = 11K$ from NTA 8800
	Heat transfer coefficient for long-wave radiation	$h_{\text{lr;e;k}}$	Yes, fixed value $h_{\text{lr;e;k}}$= $4.14W/(m^2 \cdot K)$ from NTA 8800
	Form Factor	$F_{sky;k}$	Yes, conditional based on surface inclination from 3DBAG (had to be computed beforehand)

Table 4.9: Data requirement overview: Parameters needed to model heat demand

4.4. Data collection

The parameters required for performing heat demand modelling are classified into three groups:

- Building geometries
- Building attributes
- Weather information

4.4.1. Semantic 3D city model

The building stock's geometry and physical characteristics can be stored in a semantic 3D city model. A dataset in the CityGML format was gathered which contained the building geometry. For data collection, CityGML buildings of Rijssen-Holten were obtained through the TU Delft 3D geoinformation group (León-Sánchez et al., 2022b). The number of buildings accessible for the thesis in this dataset of Rijssen-Holten is shown in Figure 4.7. The dataset, which is based on the 3DBAG, is only accessible to the city of Rijssen-Holten. Table 4.10 provides an overview of the available data attributes of the building stock for Rijssen-Holten. Unfortunately, this dataset does not contain any physical thermal properties of the buildings. For the energy simulations, more specific building physical attributes—such as U-values and g-vales—need to be included in the dataset.

Figure 4.7: CityGML building dataset displayed in FME

Attribute	Description
Building ID	The pand identification from the BAG
Building type	Classification of the building
Building function(s)	The BAG use function of the building
Number of storeys	Number of floors (and below the building, if available)
Ground surface area	Ground surface area, in m^2
Gross volume	Gross volume (based on the LoD2 thematic surfaces), in m^3
Azimuth angle	Azimuth angle, in decimal degrees, measured counter-clockwise from North
Orientation	Orientation, expressed as one of N, NE, E, SE, S, SW, W, NW values
Inclination angle	Inclination angle, in decimal degrees, measured from the horizontal plane upwards
Normal vector	Normal vector to the thematic surface, expressed using its 3 components (nx, ny, nz)
Area of thematic surface	Area of the thematic surface, in m^2

Table 4.10: Overview of the building attributes available in the Rijssen-Holten semantic 3D city model (León-Sánchez et al., 2022a). The attributes; no of storeys, building function, and building type, were manually collected and are not readily available in the 3DBAG (León-Sánchez et al., 2022a).

By utilizing building typology characterisation, it is possible to incorporate generalisable building attribute information into the semantic 3D city model. Thankfully, the building type classifi-

cation and construction year are available in the CityGML building file (León-Sánchez et al., 2022a). With those two details, a building typology characterisation can be produced. The Voorbeeldwoning 2022 was used to gather the thermal characteristics of each building typology (Ministerie van Binnenlandse Zaken en Koninkrijksrelaties, 2023). Since the goal was to model the current conditions as closely as possible, Voorbeeldwoning 2022 scenario *Current* attributes were gathered and used for the energy simulation (see Table C.6 for an entire overview of each building typology's thermal attributes). The building features in *Current* is computed based on the WoON Energie 2018 survey data that is currently available for the Dutch building stock (Ministerie van Binnenlandse Zaken en Koninkrijksrelaties, 2023). Building physics data characteristics were gathered for the building typologies from the *Current* scenario, and they can be further extracted and entered into a database to carry out the required computations.

4.4.2. Weather features

The NTA 8800 offers several tables to represent the weather conditions of the Netherlands, necessary to perform the computations. Appendix B provides an overview of these tables and the temperature tables are described in subsection 4.1.3.

5

How effective is CityGML coupled with the Energy ADE in handling the data required for NTA 8800 heat demand calculations for energy modelling and how can such a model that computes the heat demand for a semantic 3D city model be implemented?

The quantitative research component of the mixed-method approach includes implementing heat demand principles as described in the qualitative research component into a model that uses as input semantic 3D city models. Before the model is implemented, with the help of the mind maps, which serve as the data requirement baseline for the model implementation, another additional diagram is created before programming to see which key data inputs are needed for heat demand modelling that can be implemented for semantic 3D city models using CityGML 2.0 and the Energy ADE V1 data model. The second diagram created is in the form of a UML diagram to map out the data requirements and possible management through CityGML 2.0 and Energy ADE V1 using the database design process framework. Specifically with the steps of conceptual design and logical design, can the data mapping be assessed to see the feasibility of the NTA 8800 heat demand computation implementation with CityGML 2.0 and Energy ADE V1. Therefore, after the conceptual design phase, a better overview is provided of how the data

is going to be handled, and thus, the model computation implementation is explored in the next section. In this section, an overview of the relevant Python libraries used and pseudo code implementation is provided. The intended outcome in this phase is to develop a model that allows any user to calculate the total heat demand of each building within a semantic 3D city model dataset using the NTA 8800 energy balance method. For this phase, the Python-developed script was tested initially for two buildings and later on an entire semantic 3D city model for the case study area Rijssen-Holten.

5.1. Database design process

To answer the sub-question on how effective CityGML 2.0 with Energy ADE V1 is with handling the data requirements to compute the NTA 8800 heat demand and how to implement the expected model, a data mapping approach was employed using as guidelines, the steps previously outlined in subsection 2.1.5 of the database design process. This approach is primarily used since CityGML is a data model that allows data to be encoded in database schemas, which after some initial attempts of modifying XML datasets and realizing the complexity of such operations, the database encoding simplifies retrieval and modification operations needed to compute the heat demand. It was decided based on this benefit to develop a model with database interactions to manage the data handling aspect with semantic 3D city models. Hence, data mapping assessment is conducted alongside the database design process principles, which follows the following steps (see Figure 2.5):

1. Requirement collection and analysis
2. Conceptual design
3. Logical design
4. Database implementation

5.1.1. Requirement collection and analysis

The first step is outlining the main data requirements, which a complete overview can be found in Table 4.9. The database requirement for this thesis is as follows; the semantic 3D city model is organised into building objects. Each building has a unique building ID, year of construction, building type classification, building function classification, height and usable area. The building also contains a thermal zone and the number of surfaces, surface types, surface area, inclination and orientation, and surface perimeter. A building equates to one heat transmission value, one ventilation value, one internal gain value and some possible solar gain computation, to compute the final space heating demand. Each building has to obtain thermal-specific properties for computation such as the U-values for each surface type, and the building's ventilation and heating system type.

The main operation this thesis focuses on is the computation of the space heating demand. This part is operated in the Python model script, creating a database-script interaction. The computation of the space heating demand is split up into four components; heat transmission, ventilation, internal gain value and solar gain, where the monthly computation values can be examined per component for each building by checking the building ID.

5.1.2. Conceptual design: Rough database design

However, to implement such a model, the necessary data input needs to be outlined and determined how it is stored to facilitate the Python-based computations that are also compatible with CityGML 2.0 and Energy ADE V1. To do so, an entity relationship diagram is developed to propose a conceptual design of the model operation, see Figure 5.1. Based on the requirements, I believe 6 entity types are sufficient to meet the desired outcome. One of the entities would be called "Building", which would be based on building ID. Each building has multiple heating demand computations (monthly computations). The entity would store the following attributes:

- Building ID (Primary Key)
- Year
- Building type
- Building function
- Height
- Usable area

Then, there is the entity "Thermal Zone", which would also be based on building ID. In this thesis, the assumption was made that every building has one thermal zone since there was not detailed data available about the thermal zone distribution within the Rijssen-Holten building stock. However, this capability should still be added since a building has one or more thermal zones. This table would store the following attributes:

- Thermal zone ID (Primary Key)
- Building ID (Foreign Key)
- Thermal zone area

Then, there is the entity "Surface", which would also be based on building ID, since a building has one or more surfaces and it would store the following attributes:

- Surface ID (Primary Key)
- Building ID (Foreign Key)
- Surface type
- Surface area
- Surface inclination
- Surface orientation
- Surface perimeter

A "Thermal Property" look-up table that allows you to search for thermal attributes based on a data entry building's typology and construction year is also needed to store the following attributes:

- Building type
- Construction period
- U-Value per surface type
- Type of ventilation system
- Type of heating system

A "Weather Properties" look-up table is also required to store all the relevant NTA 8000 weather attributes such as:

- Indoor temperature
- Outdoor temperature
- Solar radiation
- Shading factor

In addition, an entity is needed for heat demand, to be able to store the final computation results. The entity "Heat demand" would have the following attributes:

- Building ID (Foreign Key)
- Month
- Heat transmission
- Ventilation
- Internal gain
- Solar gain
- Space heating demand

When these entities are in place in the database, a possible query can be formulated that encompasses all the relevant building attributes needed to compute the heat demand in the model (see BuildingQuery in Figure 5.1).

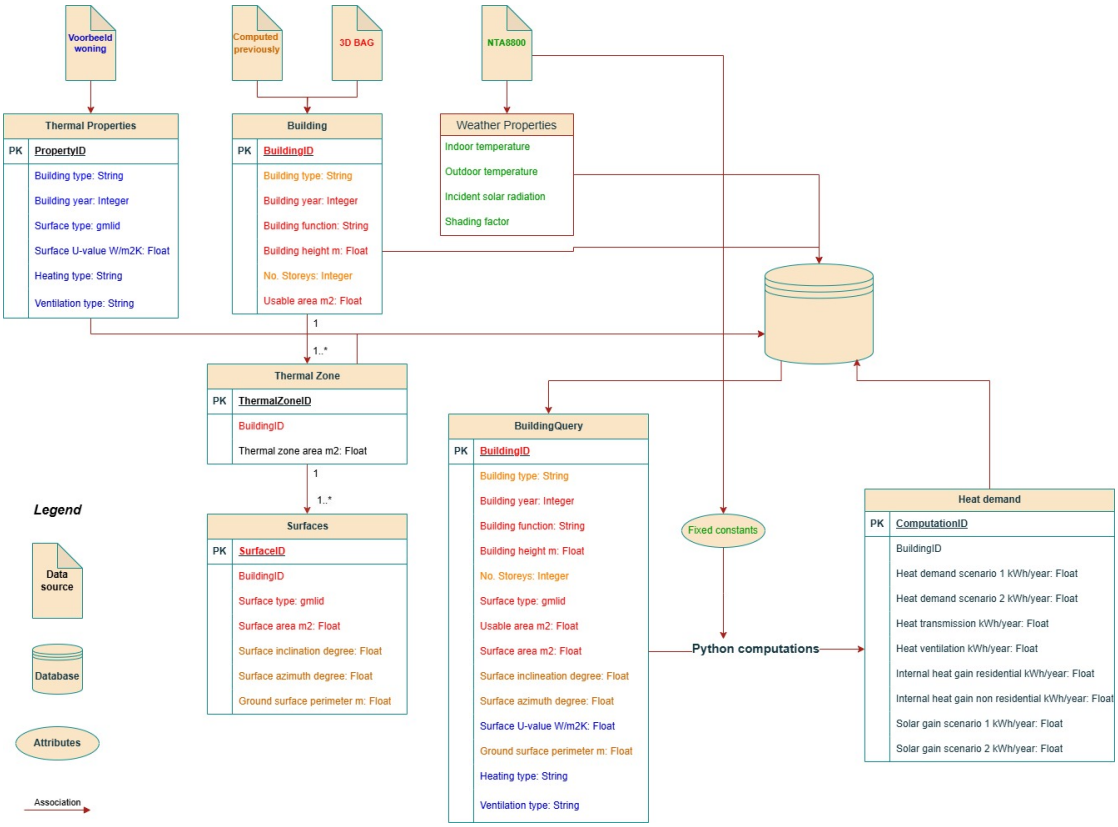

Figure 5.1: Entity relationship diagram of the heat demand model implementation

5.1.3. Logical design: Data mapping

For the logical design phase, the entity and attributes need to be specified as tables with the attribute name and data type and hence Table 5.1 outlines the entity table name, with the attributes and data type and at the same time shows where these attributes can already be stored in the CityGML 2.0 and Energy ADE V1 data model. Figure 5.2 demonstrates where the final space heating demand result from the model can be stored in the CityGML 2.0 and Energy ADE V1 data model. The final space heating demand can be stored in each building in a CityObject through the table "EnergyDemand" with endUse classification "SpaceHeating" with the values stored as a time series in energyAmount. As can be concluded from this data mapping, CityGML with Energy ADE has the required data attributes outlined in the data model that are necessary for computing and storing the NTA 8800 space heating demand, making it an effective data model for storing the space heating demand results.

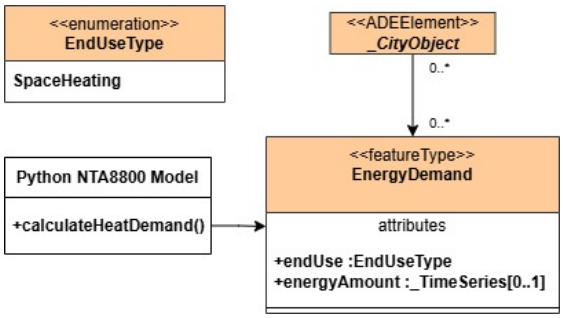

Figure 5.2: Overview of the data mapping of the NTA 8800 space heating demand output in CityGML 2.0 and Energy ADE V1

Entity/Attribute	CityGML Module	EnergyADE Module
Buildings		
BuildingID (PK)	Building (core)	
YearOfConstruction (INT)	Building (core)	
BuildingTypeClassification (VARCHAR)	Building (core)	
BuildingFunctionClassification (VARCHAR)	Building (core)	
Height (DECIMAL)	Building (core)	
UsableArea (DECIMAL)		Building (ADE) or UsageZone
Thermal Zone		
ThermalZoneID (PK)		ThermalZone
BuildingID (FK)	Building (core)	
ThermalZoneArea (DECIMAL)		ThermalZone
Surfaces		
SurfaceID (PK)	BoundarySurface	
BuildingID (FK)	Building (core)	
SurfaceType (VARCHAR)	BoundarySurface	
SurfaceArea (DECIMAL)		ThermalBoundary
SurfaceInclination (DECIMAL)		ThermalBoundary
SurfaceOrientation (DECIMAL)		ThermalBoundary
SurfacePerimeter (DECIMAL)		ThermalBoundary
HeatingDemand		
ComputationID (PK)		EnergyDemand
BuildingID (FK)	Building (core)	
Month (INT)		TimeSeries
HeatTransmissionValue (DECIMAL)		-
VentilationValue (DECIMAL)		-
InternalGainValue (DECIMAL)		-
SolarGainValue (DECIMAL)		-
TotalSpaceHeatingDemand (DECIMAL)		EnergyDemand
Lookup WeatherProperties		
IndoorTemperature (DECIMAL)		WeatherData
OutdoorTemperature (DECIMAL)		WeatherData
SolarRadiation (DECIMAL)		WeatherData
ShadingFactor (DECIMAL)		WeatherData
Lookup ThermalProperties		
BuildingType (VARCHAR)	Building (core)	
ConstructionPeriod (VARCHAR)	Building (core)	
UValuePerSurfaceType (DECIMAL)		Construction or SolidMaterial
VentilationSystemType (VARCHAR)		EnergyConversionSystems
HeatingSystemType (VARCHAR)		EnergyConversionSystems

Table 5.1: Data mapping to CityGML and Energy ADE

5.1.4. Database implementation

It is important to note that at the time of thesis documentation, a rough database schema was created to perform the operations. However, there is an existing database, CityGML 3D City Database, also known as 3DCityDB, supported by CityGML, which contains the Rijssen-Holten dataset. The Python model was created to facilitate the rough database schema operations such as data retrieval and storage through the usage of DataFrames and Pandas SQL.

A critical component of the model implementation was the usage of databases for data storage and retrieval. The proposal for the rough database creation is to use PostgreSQL since it is an open-source option that supports many data types and functions, which would follow the FAIR implementation principles. PostgreSQL 16 was installed on the computer with Pg Admin v4. After installing the DBMS software and configuring it to the system specification, a database instance within PostgreSQL can be created. The next step would be to implement the conceptual schema into the physical table and for this, the following tables below would need to be queried in PostgreSQL. After the tables are queried through the PostgreSQL environment, the dataset needs to be formatted similarly and can be imported into the database.

```
CREATE SCHEMA NTA8800;

CREATE TABLE Buildings (
    BuildingID INT PRIMARY KEY,
    YearOfConstruction INT,
    BuildingTypeClassification VARCHAR(100),
    BuildingFunctionClassification VARCHAR(100),
    Height DECIMAL(10,2),
    UsableArea DECIMAL(10,2)
);

CREATE TABLE ThermalZone (
    ThermalZoneID INT PRIMARY KEY,
    BuildingID INT,
    ThermalZoneArea DECIMAL(10, 2),
    FOREIGN KEY (BuildingID) REFERENCES Buildings(BuildingID)
);

CREATE TABLE Surfaces (
    SurfaceID INT PRIMARY KEY,
    BuildingID INT,
    SurfaceType VARCHAR(255),
    SurfaceArea DECIMAL(10, 2),
    SurfaceInclination DECIMAL(10, 2),
    SurfaceOrientation DECIMAL(10, 2),
    SurfacePerimeter DECIMAL(10, 2),
    FOREIGN KEY (BuildingID) REFERENCES Buildings(BuildingID)
);

CREATE TABLE HeatingDemand (
    ComputationID INT PRIMARY KEY,
    BuildingID INT,
    Month VARCHAR(255),
    HeatTransmissionValue DECIMAL(10, 2),
    VentilationValue DECIMAL(10, 2),
    InternalGainValue DECIMAL(10, 2),
```

```
    SolarGainValue DECIMAL(10, 2),
    TotalSpaceHeatingDemand DECIMAL(10, 2),
    FOREIGN KEY (BuildingID) REFERENCES Buildings(BuildingID)
);

CREATE TABLE Lookup_WeatherProperties (
    IndoorTemperature DECIMAL(10, 2),
    OutdoorTemperature DECIMAL(10, 2),
    SolarRadiation DECIMAL(10, 2),
    ShadingFactor DECIMAL(10, 2),
);

CREATE TABLE Lookup_ThermalProperties (
    PropertyID INT PRIMARY KEY AUTO_INCREMENT,
    BuildingType VARCHAR(255),
    ConstructionPeriod VARCHAR(255),
    UValuePerSurfaceType DECIMAL(10, 2),
    VentilationSystemType VARCHAR(255),
    HeatingSystemType VARCHAR(255)
);
```

5.2. Model implementation

In this section, an overview of the technical specifications of the tools used during the thesis is listed to encourage transparency for this research's reproducibility and a pseudo-code explanation is provided for the four main heat demand components implementations to broadcast the primary programming logic. For a full version of the model script, see link.

5.2.1. Tools

5.2.1.1.Hardware

The following are the specifications of the computer that was utilized to implement the model:

- Processor: Intel(R) Core(TM) i7-1065G7 CPU @ 1.30GHz 1.50 GHz
- RAM: 32.0 GB (31.6 GB usable)
- Operating System: Windows 11 Home

The model was also tested on a 2016 MacBookPro, of which the specifications are:

- Processor: 2.3 GHz Quad-Core Intel Core i5
- RAM: 8 GB
- Operating System: macOS 14 Sonoma

5.2.1.2.Python packages

The programming language used for the model implementation is Python, version 3.11, using the interpreter Pycharm Professional during the thesis. An overview of the library packages used during the thesis are listed:

- Pandas version: 2.1.4
- NumPy version: 1.26.4
- Pandasql version: 0.7.3
- Openpyxl version: 3.0.10

5.2.2. Heat transfer transmission

Below an overview is given of how heat transfer transmission is implemented using pseudo-code. A key aspect to mention that is not mentioned in the previous chapter is how the negative heat transmission is tackled. I added a correction condition that depends on the heating period month in the Netherlands (see Figure 5.3 for the heating degree days in the Netherlands). The correction occurs at the end for the heat transmission computation. This was implemented since in the initial test, negative heat transmissions results appeared, which means the building is heating up. This can happened during the heating period months, which in the model case, appeared mostly for July or August. This implies that in those months, cooling is needed but since this component is not included in the model, I set a condition to turn the negative heat transmissions to 0 during the heat period months. I set this condition so that I am not summing negative values when computing the total demand.

Algorithm 1 Computation of Heat Transmission

Data: Provide $\Theta_{e\_avg\_mi}$ (external temperature), $\Theta_{int\_set\_H\_zi\_mi}$ (indoor temperature), Ag (ground surface area), Ufl (ground surface u-value), P (ground surface perimeter), AT_i (surface areas), UC_i (Surface u-value), $nbouwlaag\_j$ (no. of storeys) and tmi (time measurement) from the database

Input: $\Theta_{e\_avg\_mi}, \Theta_{int\_set\_H\_zi\_mi}, Ag, Ufl, P, AT_i, UC_i, nbouwlaag\_j, tmi$

Output: $QHtr_{zi\_mi}$

Constant values:

$HH_{U\_zi\_mi} \leftarrow 0\,\mathrm{W/K}$

$HH_{A\_zi\_mi} \leftarrow 0\,\mathrm{W/K}$

$none\_heating\_months \leftarrow$ ["May","June","July","August","September"] ; // None heating periods

Semantic 3D model data:

$Ag \leftarrow$ from 3DBAG in the CityGML file m^2 ; // Ground surface area

$P \leftarrow$ computed beforehand from 3DBAG in the CityGML file in m ; // Perimeter

$AT_i \leftarrow \mathrm{m}^2$; // Surface area

$nbouwlaag\_j \leftarrow$ from 3DBAG in the CityGML file ; // No. of storeys

Conditional look up from the database:

$Ufl \leftarrow$ depends on building type and construction year $\mathrm{W/m^2}K$; // Ground heat transfer coefficient

$UC_i \leftarrow \mathrm{W/m^2}K$; // Heat transfer coefficient

$HH_{p\_spec\_j} \leftarrow$ depends on building heating system $\mathrm{W/m^2}K$; // Heat transfer coefficient

Computations:

$\Theta_{\text{int\_cal\_H\_zi\_mi}} \leftarrow (\Theta_{\text{int\_set\_H\_zi\_mi}} - \Theta_{e\_avg\_mi}) + \Theta_{e\_avg\_mi}\,^{\circ}\mathrm{C}$ (Calculation temperature)

$Hg_{an\_zi\_mi} \leftarrow Ag \cdot Ufl + 0.5 \cdot P$; // Ground contact heat transfer coefficient

$HH_{D\_zi\_mi} \leftarrow AT_i \cdot UC_i$; // Direct heat transfer coefficient

$HH_{p\_zi} \leftarrow nbouwlaag\_j \cdot HH_{p\_spec\_j}$; // Vertical pipe heat transfer coefficient

$HH_{tr\_exclgfm\_zi\_mi} \leftarrow HH_{D\_zi\_mi} + HH_{U\_zi\_mi} + HH_{A\_zi\_mi} + HH_{p\_zi}$; // Total heat transfer coefficient

$QHtr_{zi\_mi} \leftarrow (HH_{tr\_exclgfm\_zi\_mi} \cdot (\Theta_{int\_calc\_H\_zi\_mi} - \Theta_{e\_avg\_mi}) + Hg_{an\_zi\_mi} \cdot (\Theta_{int\_calc\_H\_zi\_mi} - \Theta_{e\_avg\_an})) \cdot 0.001 \cdot tmi$; // Heat Transmission

Set none-heating months to 0 if negative:

for *month* ***in*** *non_heating_months* **do**-

$QHtr\_zi\_mi[month] \leftarrow QHtr\_zi\_mi[month].\text{apply}(\lambda x : \max(x, 0))$

=0

5.2.3. Heat transfer ventilation

Here an overview is given of how heat transfer ventilation is implemented using pseudo-code:

Algorithm 2 Computation of Heat Ventilation

Data: Provide $\Theta_{e\_avg\_mi}$ (external temperature), $\Theta_{int\_set\_H\_zi\_mi}$ (indoor temperature), $\Theta_{int\_set\_H\_stc\_zi\_mi}$ (set point temperature), $\Theta_{sup\_k\_H\_mi}$ (supply temperature), and tmi (time measurement) from the database

Input: $\Theta_{e\_avg\_mi}$, $\Theta_{int\_set\_H\_zi\_mi}$, $\Theta_{int\_set\_H\_stc\_zi\_mi}$, $\Theta_{sup\_k\_H\_mi}$, tmi

Output: $QHve_{zi\_mi}$

Constant values:

$pa \leftarrow 1.205\,\mathrm{kg/m^3}$; // Air density

$ca \leftarrow 1005\,\mathrm{J/kgK}$; // Specific heat capacity of air

$qv_{k\_H\_zi\_mi} \leftarrow 50\,\mathrm{m^3/h}$; // Ventilation flow rate

$fv_{dyn\_k\_zi\_mi} \leftarrow 1$; // Dynamic volume flow factor

$bv_{k\_H\_zi\_mi} \leftarrow 1$; // Correction factor

Conditional look up from the database:

$\Theta_{int\_set\_H\_stc\_zi\_mi} \leftarrow$ depends on building function $^\circ C$; // Set supply temperature correction factor

Computations:

$\Theta_{\mathrm{int\_cal\_H\_zi\_mi}} \leftarrow (\Theta_{\mathrm{int\_set\_H\_zi\_mi}} - \Theta_{e\_avg\_mi}) + \Theta_{e\_avg\_mi}\,^\circ\mathrm{C}$ (Calculation temperature)

$HHve_{zi\_mi} \leftarrow (pa \cdot ca) \cdot ((qv_{k\_H\_zi\_mi} \cdot bv_{k\_H\_zi\_mi} \cdot fv_{dyn\_k\_zi\_mi})/3600)$; // Total heat transfer coefficient

$QHve_{zi\_mi} \leftarrow HHve_{zi\_mi} \cdot (\Theta_{int\_calc\_H\_zi\_mi} - \Theta_{e\_avg\_mi}) \cdot 0.001 \cdot tmi$; // Heat ventilation

5.2.4. Heat gain internal

Here an overview is given of how heat gain internal is implemented using pseudo-code:

Algorithm 3 Computation of Internal Heat Gains

Data: Provide Ag_{zi} (usable area), $Nwoon_{zi}$ (building units), $Function$ (building function), and tmi (time measurement) from the database

Input: $Ag_{zi}, Nwoon_{zi}, Function, tmi$

Output: $QHint_{zi\_mi}$

Constant values:

$tan \leftarrow 8760$; // Hours in year

$Wt \leftarrow 46.94$; // Energy consumption for lighting

$fL \leftarrow 1$; // Reduction factor

$QW_{ls\_rbl\_si\_zi\_mi} \leftarrow 7718.4$; // Energy lost from DHW

$\Phi_{int\_Vzi} \leftarrow 0$; // Heat flux

$\Phi_{int\_proc_{zimi}} \leftarrow 0$; // Heat flux

Semantic 3D model data:

$Function \leftarrow$ from 3DBAG in the CityGML file ; // Building function

$Ag_{zi} \leftarrow$ from 3DBAG in the CityGML file m^2 ; // Usable area

$Nwoon_{zi} \leftarrow$ from 3DBAG in the CityGML file ; // Building units

Conditional look up from the database:

$qOc_{usi} \leftarrow$ depends on building function in W/m^2 ; // Specific internal heat

$f_{r_{usi}} \leftarrow$ depends on building function in W/m^2 ; // Correction factor

$qA_{usi} \leftarrow$ depends on building function in W/m^2 ; // Specific internal heat

For Residential Buildings:

$Area \leftarrow Ag_{zi}/Nwoon_{zi}$

if $Area \leq 30$ **then**

  $NP_{woon_{zi}} \leftarrow 1$

else

  if $Area \leq 100$ **then**

    $NP_{woon_{zi}} \leftarrow 2.28 - (1.28/70) \times (100 - Area)$

  else

    $NP_{woon_{zi}} \leftarrow 1.28 + 0.01 \times Area$

  end

end

$QHint_{zi\_mi\_R} \leftarrow 180 \times Nwoon_{zi} \times NP_{woon_{zi}} \times 0.001 \times tmi$; // Internal heat gain

For Non-residential Buildings:

$\Phi_{int\_Oczi} \leftarrow qOc_{usi} \times f_{r_{usi}} \times Ag_{zi}$; // Heat flux

$\Phi_{int\_Azi} \leftarrow qA_{usi} \times Ag_{zi}$; // Heat flux

$\Phi_{int\_Lzi} \leftarrow fL \times (Wt \times Ag_{zi}) \times 1000/tan$; // Heat flux

$\Phi_{int\_Wzi} \leftarrow QW_{ls\_rbl\_si\_zi\_mi} \times 1000/tmi$; // Heat flux

$QHint_{dir_{zi\_mi\_non\_R}} \leftarrow (\Phi_{int\_Oczi} + \Phi_{int\_Azi} + \Phi_{int\_Lzi} + \Phi_{int\_Wzi} + \Phi_{int\_Vzi} + \Phi_{int\_proc_{zimi}}) \times 0.001 \times tmi$; // Internal heat gain

5.2.5. Heat gain solar

Below an overview is given of how heat gain solar is implemented using pseudo-code. A key aspect to mention that is not mentioned in the previous chapter is how the negative heat solar gain is tackled. I added a correction condition in the model for the heat solar gain computation that checks if there are negative values and turns them into 0. This was implemented since in the

initial test, a couple of buildings had negative heat solar gain results appearing during the winter months, mostly January, when there are hardly any solar gains in the Netherlands. So to avoid summing the negative solar gain to the total heat demand, I set a condition to turn the negative heat solar gain to 0.

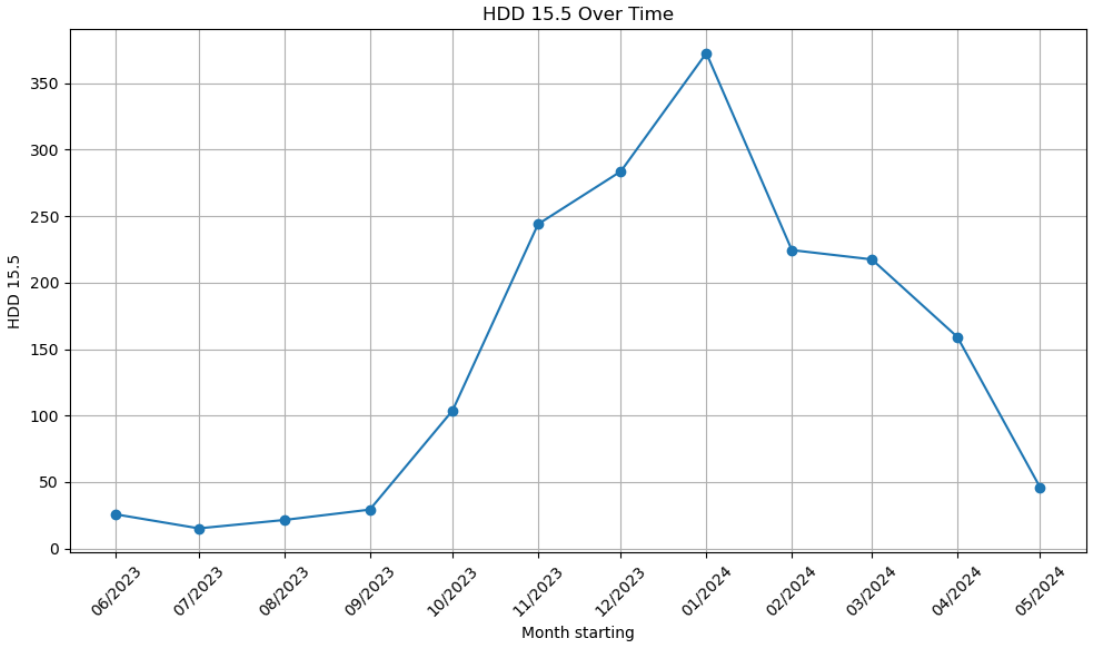

Figure 5.3: Heating degree days (HDD) for the Netherlands (BizEE Software, 2008–2024)

Algorithm 4 Computation of Solar Heat Gains

Data: Provide Aw (surface area), $angle$ (inclination and azimuth), and tmi (time measurement) from the database

Input: $Aw, angle, tmi$

Output: $QHsol_{zi\_mi}$

Constant values:

$ratio \leftarrow 0.3$; // Window to facade ratio

$hlr_{ek} \leftarrow 4.14\ \mathrm{W/m^2K}$; // Heat transfer coefficient for long-wave radiation

$deltasky_mi \leftarrow 11\ \mathrm{K}$; // Temperature difference factor

$asol \leftarrow 0.6$; // Absorption coefficient

$F_rw_i \leftarrow 0.25$; // Frame fraction of window

$Rse \leftarrow 0.04\ \mathrm{m^2K/W}$; // Heat transfer resistance

Semantic 3D model data:

$angle \leftarrow$ computed beforehand from 3DBAG in the CityGML file ; // Inclination and azimuth

$Aw \leftarrow$ from 3DBAG in the CityGML file $\mathrm{m^2}$; // Surface area

Conditional look up from the database:

$Uw \leftarrow$ depends on building type and construction year $\mathrm{W/m^2}K$; // Heat transfer coefficient

$Isol \leftarrow$ depends on inclination and azimuth $\mathrm{W/m^2}$; // Solar radiation

$F_shobst \leftarrow$ depends on inclination and azimuth ; // Shading factor

Function `calculate_f_sky`(*angle*)**:**

  if *angle* ≤ 5 **then**

    return 1 // Horizontal structure

  else if *angle* ≤ 75 **then**

    return 0.75 // Inclined structure

  else

    return 0.5 // Vertical structure

  end

// Form Factor

Function `calculate_g_gl_wi`(*type_of_glass*)**:**

  g_gl_n_wi $\leftarrow$ Query glass type g-value

  return `calculate_g_gl_sh_wi`(*g_gl_n_wi*)

// Scenario 1

Function `calculate_g_gl_sh_wi`(*g_gl_n_wi*)**:**

  F_w $\leftarrow$ 0.90 // Correction factor for glass shading

  return F_w $\times$ g_gl_n_wi

// Scenario 2

type_of_glass $\leftarrow$ "Double glass" // Glass type (sensitivity parameter)

Computations:

g_gl_wi $\leftarrow$ `calculate_g_gl_wi`(type_of_glass) // Glass scenario for g-value

F_sky $\leftarrow$ `calculate_f_sky`(*angle*) // Form Factor

$Q_{\mathrm{sky}} \leftarrow 0.001 \cdot F_{\mathrm{sky}} \cdot R_{\mathrm{se}} \cdot U_{\mathrm{w}} \cdot A_{\mathrm{w}} \cdot hlr_{\mathrm{ek}} \cdot \Delta\theta_{\mathrm{skymi}} \cdot t_{\mathrm{mi}}$ (Heat radiation to the sky)

if *condition_for_window* **then**

  $QH_{\mathrm{sol\_window}} \leftarrow g_{\mathrm{gl\_wi}} \cdot A_{\mathrm{w}} \cdot (1 - F_{\mathrm{frwi}}) \cdot F_{\mathrm{sh;obst}} \cdot I_{\mathrm{sol}} \cdot 0.001 \cdot t_{\mathrm{mi}} - Q_{\mathrm{sky}}$; // Heat gain through window

else

  $QH_{\mathrm{sol\_facade}} \leftarrow \alpha_{\mathrm{sol}} \cdot R_{\mathrm{se}} \cdot U_{\mathrm{w}} \cdot A_{\mathrm{w}} \cdot I_{\mathrm{sol}} \cdot 0.001 \cdot t_{\mathrm{mi}} - Q_{\mathrm{sky}}$; // Heat gain through facade

end

$QHsol_{zi\_mi} \leftarrow QH_{\mathrm{sol\_window}} + QH_{\mathrm{sol\_facade}}$; // Total Solar Heat Gain

Set to 0 if negative:

  for *month* ***in*** *months* **do-**

$QHsol\_zi\_mi[month] \leftarrow QHsol\_zi\_mi[month].\mathrm{apply}(\lambda x : \max(x, 0))$

5.3. Model testing

The model was initially developed and tested for two test buildings and later on, expanded to make it suitable for entire semantic 3D city model computations.

5.3.1. Test buildings

Two test buildings were selected in Rijssen-Holten to test the model implementation. The two test buildings contained the required data attributes as outlined in Figure 5.2. The two buildings have the BAG ID 1742100000006518 and 1742100000004574. Building 1742100000006518 is currently in use and was built in 1965. Figure 5.4 displays where the building is located according to the Kadaster and provides the 3D geometry of the building in yellow and the surrounding buildings in grey. Building 1742100000004574 is currently in use and was built in 1923. Figure 5.5 displays where the building is located according to the Kadaster and provides the 3D geometry of the building in yellow and the surrounding buildings in grey. A detailed overview of the two building's thermal properties, taken from the Voorbeeldwoning 2022, scenario *Current*, can be found in Appendix C.

Attribute	**Value**
Year of construction	1965
Roof type	Slanted
Roof area	50.3
Height	27.8

Table 5.2: Overview of some BAG building attributes of building ID 1742100000006518

Attribute	**Value**
Year of construction	1923
Roof type	Slanted
Roof area	104.1
Height	23.82

Table 5.3: Overview of some BAG building attributes of building ID 1742100000004574

kadaster

Pand ID 17421000000006518

Samenvatting

Oorspronkelijk bouwjaar
1965

Status
Pand in gebruik

Gemeente
Rijssen-Holten

(a) Kadaster building ID 1742100000006518, see for more details the following link

(b) 3DBAG building ID 1742100000006518

Figure 5.4: Building ID 1742100000006518 attributes

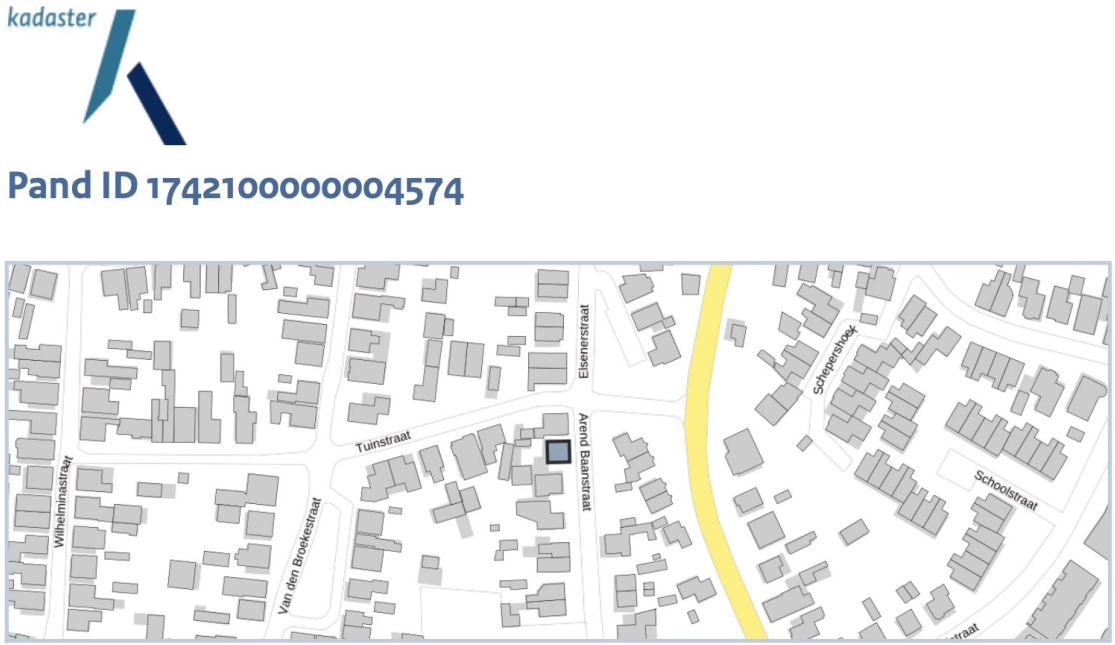

(a) Kadaster building ID 1742100000004574, see for more details the following link

(b) 3DBAG building ID 1742100000004574

Figure 5.5: Building ID 1742100000004574 attributes

5.3.1.1. Test buildings results

The model computed the following space heating demand results for the two test buildings, see Figure 5.7-5.9. Figure 5.7 displays the monthly heat transfer for each building by displaying the heat transfer through ventilation as green, heat transfer through transmission as purple and the total heat transfer as dashed blue. From the plots, it is noticeable that the ventilation remains relatively low and constant throughout the year with slight increases during the winter months. The results from the model imply that the impact of ventilation is minor in comparison to transmission. This is contradictory to the literature that suggests that 33% of the heat loss is attributed to ventilation (Everett, 2023), showcasing that there is a component missing in the current implementation that increases the impact of heat transfer through ventilation. A possible reason as to what is missing can be attributed to the norm ventilation formula interpretation.

According to Everett (2023), ventilation loss can also be computed as:

$$Q_v = 0.33 \times n \times V \times \Delta T \tag{5.1}$$

Where:

- Q_v is the heat transfer for ventilation
- 0.33 is the energy required to raise one cubic metre of air through one kelvin is 0.33 watt-hours, i.e. its heat capacity per cubic metre is 0.33 $\text{Whm}^{-3}\text{K}^{-1}$
- n is the number of air changes per hour (ACH)
- V is the volume of the house in m^3
- ΔT is the difference in indoor and outdoor temperature

This formulation displays that the impact of ventilation depends on the building volume. This is an attribute that does not appear in the norm formulation of the ventilation loss computation as seen in subsubsection 4.1.1.2. However, the addition of building volume to the ventilation implementation could improve the model and showcase also more variability in the output since the current implementation is based on a fixed value q_v for every building, making the ventilation outcome the same for each building.

Transmission on the other hand shows significant seasonal variation with higher values in the winter months, peaking for both around 5000 kWh in January. Transmission seems to steadily decrease from January to May and is low during the summer months, displaying the impact of external temperatures on heat loss. From the model computations, it was noticed that the highest heat transfer coefficient comes from H_D and the second largest from H_g (see Table 5.4), implying that the largest share of transmission lost comes from wall and roof surfaces and secondly from floor surfaces. These two coefficients significantly influence the size of the heat transmission output in the model. This is not completely in line with theory since it is known that the largest impact of transmission comes from windows and doors (Everett, 2023). However, the current model implementation does not consider these two components based on the reader's interpretation of the norm, the norm did not mention the formulas to compute the impact of these components. In fact, as mentioned in paragraph 4.1.1.1.2, the norm even specifically outlines that H_D only considers opaque surfaces, not window or door surfaces. Yet, excluding these components, while it is known to have an impact on heat transmission, can lead to an underlying model limitation. Because the transmission transfer is significant, the total heat transfer mirrors this trend. Overall, theoretically speaking, the heat transfer trends are displaying the seasonal patterns as expected, e.g. higher values during the winter months and lower values during the summer months.

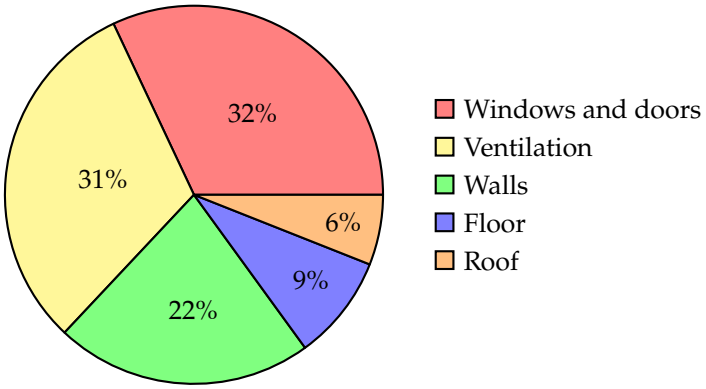

Figure 5.6: Energy loss distribution (Everett, 2023)

Heat transfer coefficient	Value
Ground H_g	118.8
Direct H_D	560.1
Vertical pipes H_{Hp}	3.6
Via adjacent unheated spaces H_U	0
Via adjacent heated spaces H_A	0

Table 5.4: Extract of the heat transfer coefficients for building 1742100000004574

Figure 5.8 displays the monthly heat gain for each building by displaying the heat gain through solar as orange, heat gain through internal as yellow and the total heat transfer as dashed red. From the plots, it is noticeable that the internal gain remains relatively constant throughout the year, with values around 400 kWh. This consistency indicates that internal heat sources contributed the same amount of heat regardless of the season, which was expected. Solar gain increases significantly from January to June, peaking at 2600 kWh for the first building, and 3500 kWh for the second one. It gradually decreases from July to December. Solar heat gains demonstrate expected trends of being the highest during the summer months when days are longer and the sunlight is more intense. The total heat gain is significantly impacted by the solar gain because this gain is more dominant in size in comparison to the internal gain.

Figure 5.9 shows the monthly space heating demand results per building with the total heat transfer in blue, the total heat gain in red and the space heating demand in dashed black. Overall, the space heating demand trends generated by the model are in line with other studies that show how space heating demand behaves per month (de Geus et al., 2015), showcasing that the model at least can simulate the expected heat flows of space heating demand. In addition to the plots, Table 5.5 provides a tabular overview of the total yearly space heating demand and the mean space heating demand per month for each building. From these results, the yearly space heating demand lies between 178.6-218.85 kWh/m² for the two buildings, which in the next chapter assesses whether these values are viable.

Statistic	**1742100000006518**	**1742100000004574**
Usable area in m^2	90	144
Total space heating demand kWh/yr	19706	25176
Total space heating demand kWh/m^2/yr	218.95	178.6
Mean space heating demand kWh/month	1642	2098
Mean space heating demand kWh/m^2/month	18.24	14.6

Table 5.5: Descriptive statistics of the space heating demand estimates for the buildings

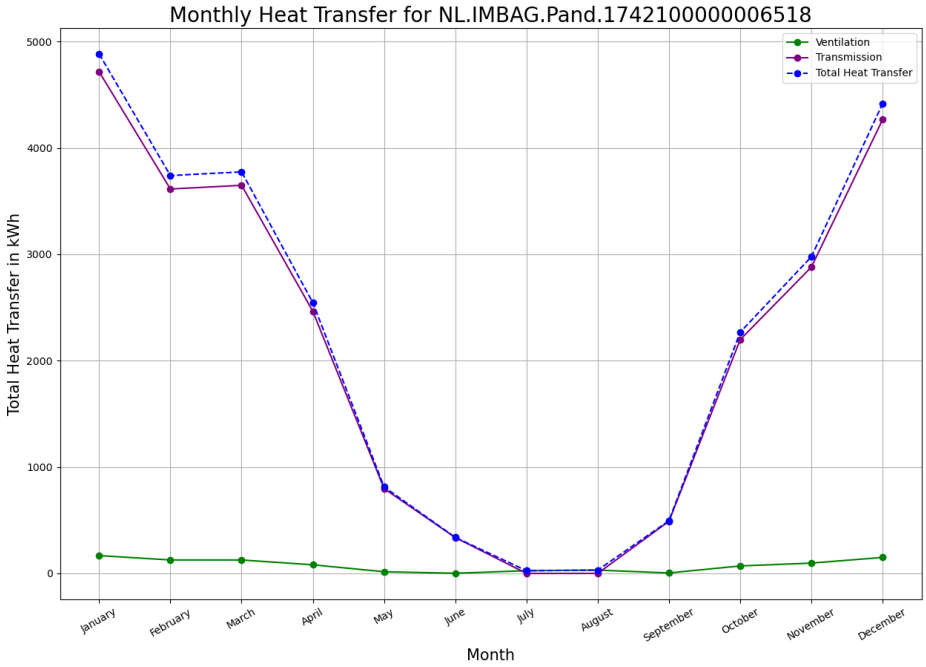

(a) Heat transfer for building 1742100000006518

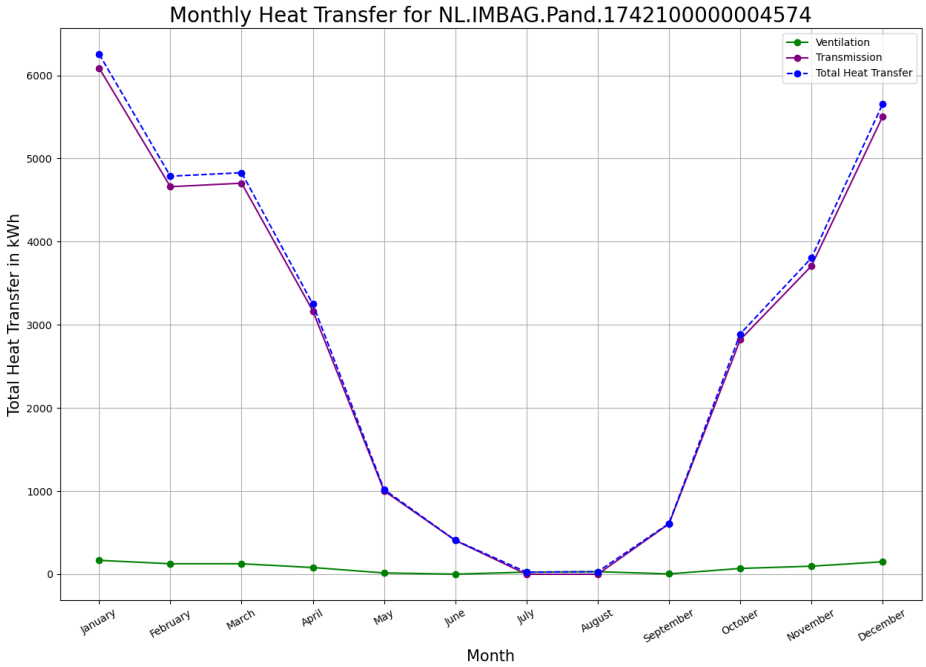

(b) Heat transfer for building 1742100000004574

Figure 5.7: Model results for heat transfer

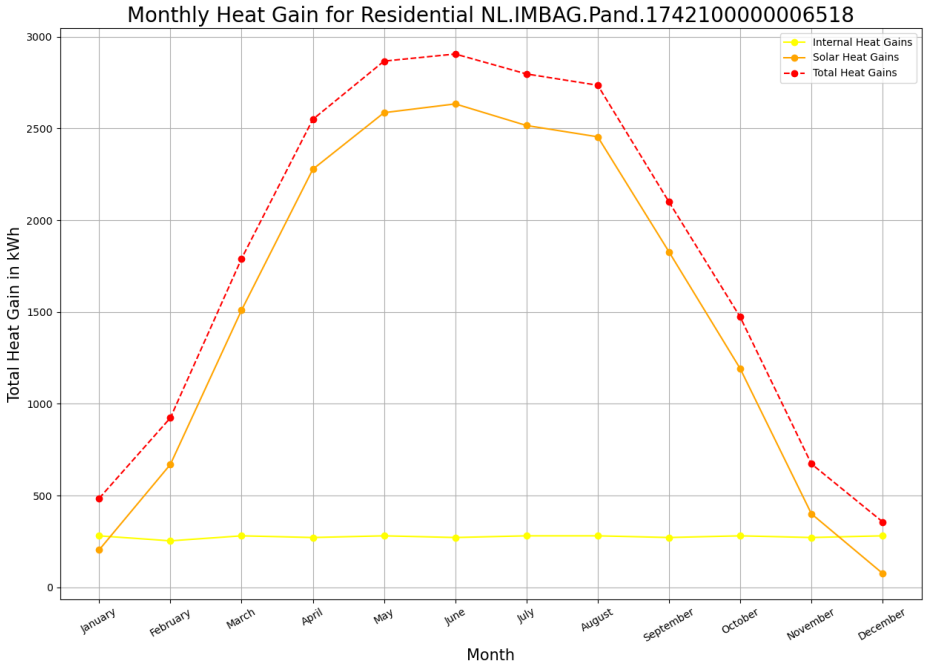

(a) Heat gain for building 1742100000006518

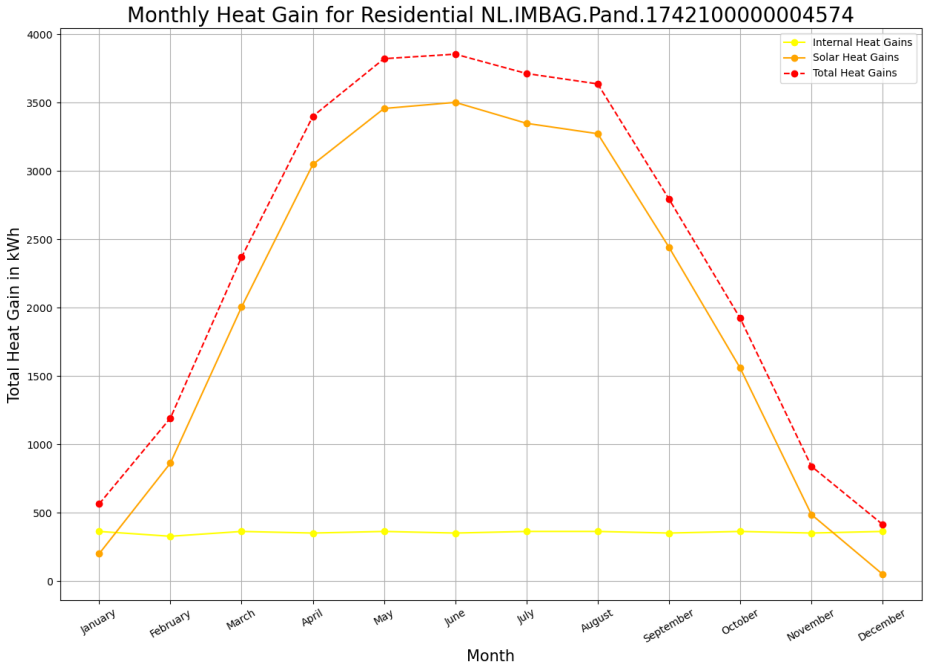

(b) Heat gain for building 1742100000004574

Figure 5.8: Model results for heat gain

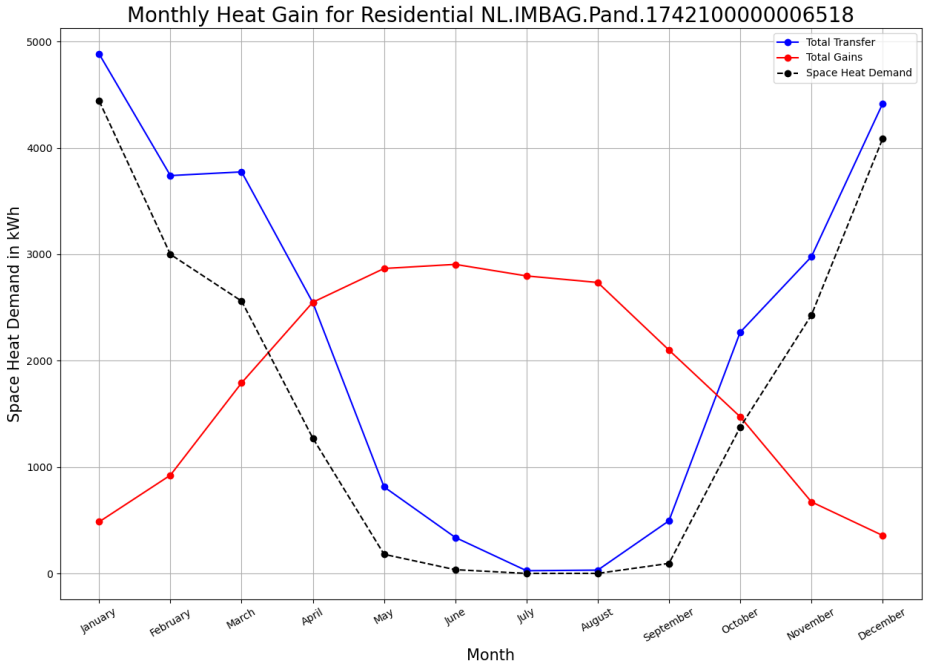

(a) Heat demand for building 1742100000006518

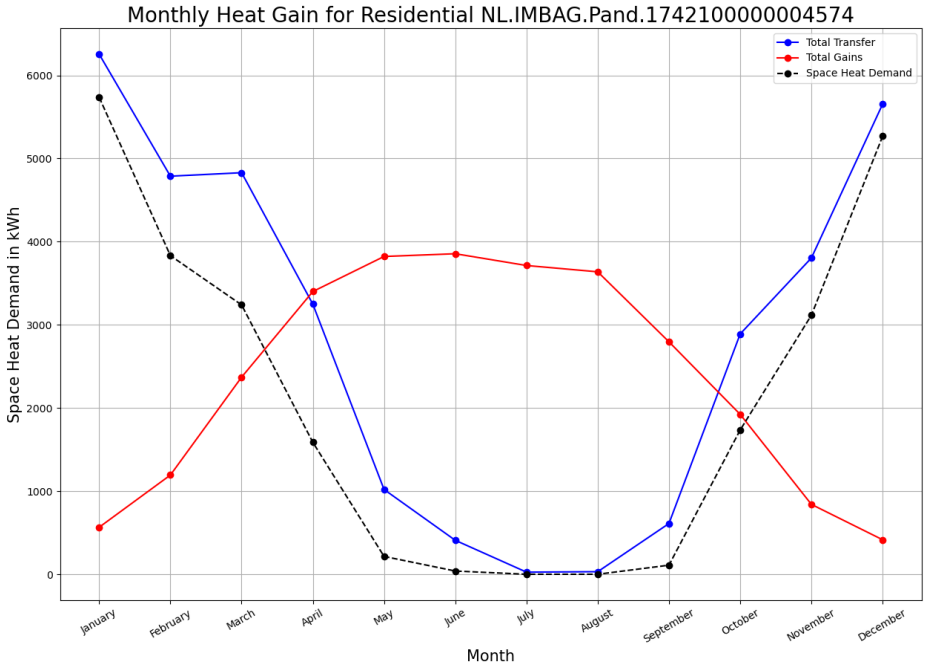

(b) Heat demand for building 1742100000004574

Figure 5.9: Model results for heat demand

5.3.2. Test semantic 3D city model: Rijssen-Holten

5.3.2.1.Rijssen-Holten results

Figure 5.10 shows the space heating demand per building in a normalised unit of kWh/m²/year and Table 5.6 provides a statistical overview of the space heating demand. The average heat demand of the 323 buildings that were simulated was 117.4 kWh/m², with a distribution range of 16.8-741.3 kWh/m². The spatial distribution of the space heating demand varies across different areas, however, from Figure 5.10, it seems clear that the majority of the distribution lies between 50-250 kWh/m² and there is one outlier with a space heating demand of 741.3 kWh/m². When consulting Figure 6.9, it becomes clear that the older buildings lie in the 200-300 kWh/m² range and the newer buildings have a lower heat demand.

Descriptive statistics	Model results
Count	324
Mean	117.4
Min	16.8
Max	741.3

Table 5.6: Descriptive statistics of the total heating demand estimates for Rijssen-Holten

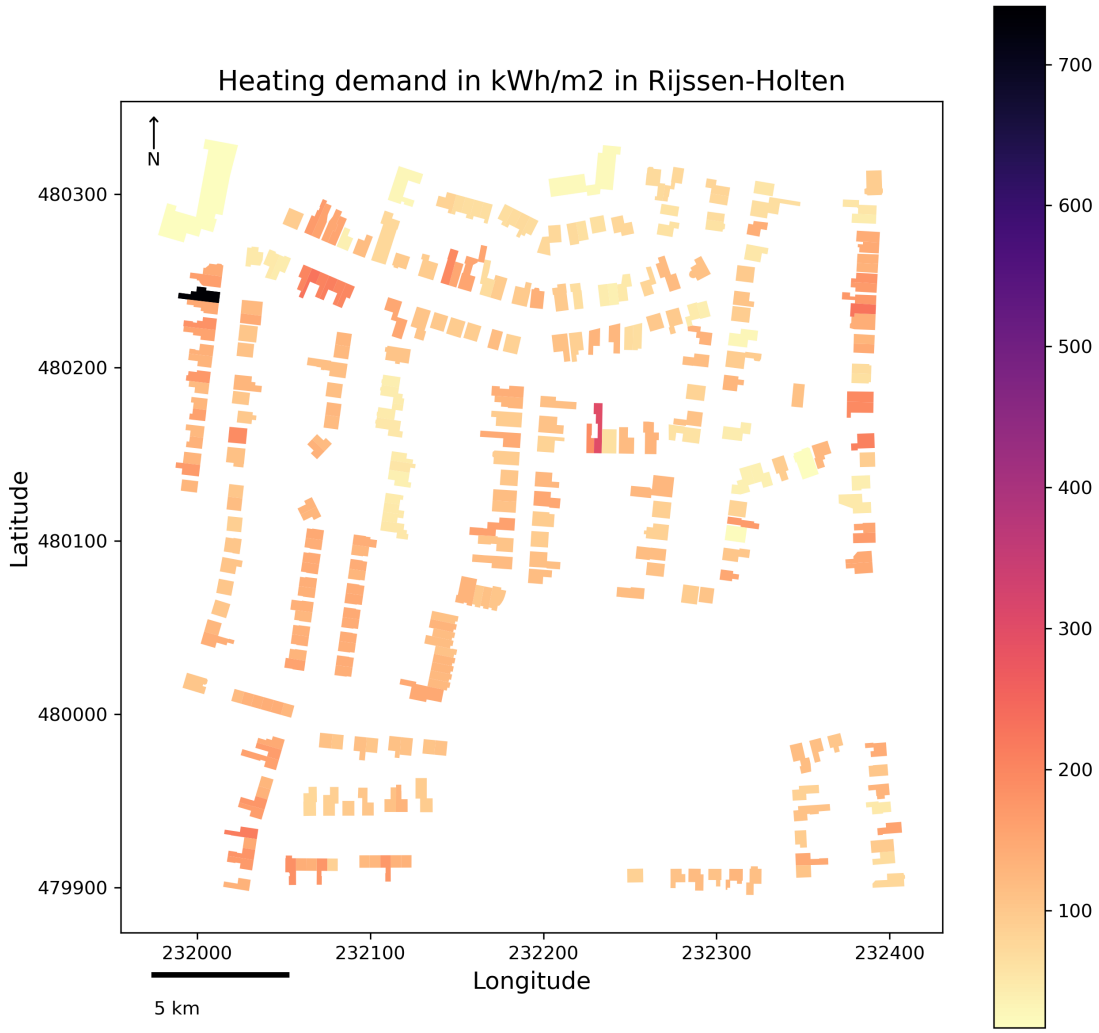

Figure 5.10: Model results per building in kWh/m²/year

5.3.3. Solar gain sensitivity analysis

Solar gain scenarios were tested based on glass type to see the impact of different g-values on the total solar gain since as mentioned in the previous chapter, window information is not openly available for every building in Rijssen-Holten. Figure 5.11 displays the results of solar gain (in kWh per month) for different window types on building ID 1742100000004574. The four scenarios are:

- Scenario 1: Single glazing
- Scenario 2: Double glazing
- Scenario 3: Triple glazing
- Scenario 4: Triple glazing with two spectrally (low) selective and low emissivity coatings

In general, all scenarios exhibit the trend that solar gain increases from January peaks around June to July, and decreases towards December. Yet, the magnitude of the solar gain varies significantly. Scenario 1 has the largest solar gain throughout the year, peaking at around 3500 kWh per month in June and July. This high solar gain can contribute significantly to passive solar

heating, reducing heating requirements in winter but potentially increasing cooling loads in summer. Scenario 2 has a somewhat lower solar gain compared to single glazing, with a peak of around 3000 kWh per month. This reduction indicates better insulation properties, leading to a balanced approach between solar gain and thermal insulation. Scenario 3 reduces solar gain to about 2000 kWh per month at its peak, exhibiting significant energy performance. Scenario 4 has the lowest solar gain, peaking at around 1500 kWh per month. The low emissivity coatings significantly reduce the amount of solar heat entering the building, providing the best thermal insulation.

From Table 5.7, it is observed that there is a significant reduction in solar gain when comparing the solar gain from single glazing to all other glazing types, the most significantly from triple glazing with coating for January and December. From Table 5.7, it is noticeable that there isn't a significant difference between single and double glazing in the summer months as the per cent difference is around 7% but there is for triple glazing (e.g. 65%-110%). From these results, it is clear that triple glazing has a high impact on the solar gain reduction that can ultimately lead to better thermal performance, minimizing the heat transfer, however, single glazing can be more beneficial in the winter months since it can reduce the heating demand but unfortunately leads to overheating in the summer.

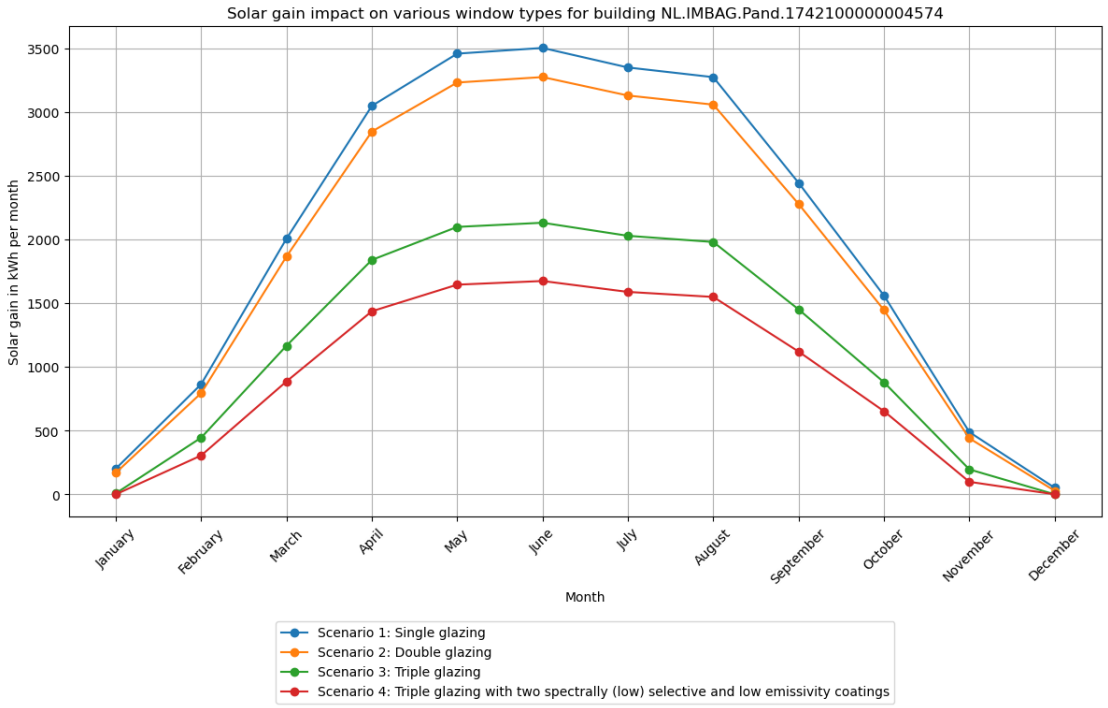

Figure 5.11: Overview of the impact of the glass type (g-value) on the model solar gain computation

Month	% Difference (S1 vs S2)	% Difference (S1 vs S3)	% Difference (S1 vs S4)
January	19.09	2518.09	inf
February	8.81	94.41	183.68
March	7.50	72.06	126.45
April	7.08	65.71	112.20
May	7.01	64.80	110.20
June	6.98	64.36	109.25
July	7.03	65.11	110.88
August	7.05	65.33	111.35
September	7.26	68.43	118.21
October	7.84	77.41	139.11
November	11.10	149.72	398.52
December	84.23	inf	inf

Table 5.7: Percentage differences in solar gain between Scenario 1 and other scenarios. S1 = scenario 1: single glazing, S2: scenario 2: double glazing, S3 = scenario 3: triple glazing, and S4 = scenario 4: triple glazing with two spectrally (low) selective and low emissivity coatings

6

To what extent can the computed heat demand values be validated?

This sub-question aims to assess the model results' validity. To verify whether the theoretical heating demand calculated from the model implementation corresponds with reality, the values are compared to another BES tool, named *CitySim Pro* and the actual energy consumption levels. Also, as a supplementary comparison, the Voorbeeldwoning 2022 dataset (Ministerie van Binnenlandse Zaken en Koninkrijksrelaties, 2023) also provides energy performance indicators benchmarks on average heating demand and total primary energy estimates per building typology and construction year, which were used to compare with the NTA 8800 computed model values.

6.1. Heat demand modelling with CitySim Pro

A BES tool was deployed to compare with the NTA 8800 energy balance model's heat demand estimations. Many bottom-up BES tools, as noted in subsection 2.2.4, require time-consuming computations for a single building (Langevin et al., 2020). On the other hand, *CitySim Pro* is a bottom-up urban energy modelling tool that can computationally quickly quantify the energy demand of a building for an entire neighbourhood or city (Ferrando et al., 2020). Semantic 3D city models can be entered into *CitySim Pro* using the CityGML, XML, DXF, or other data formats as input. The primary advantage of utilizing *CitySim Pro* is that it facilitates fast and efficient model validation testing by enabling high-quality analysis of energy flows for large-scale study regions in a relatively short amount of time.

For this thesis, the BES tool utilized was *CitySim Pro*. A conceptual overview of the procedure for energy simulations is given by Figure 6.1. The first step is to load climatic data into *CitySim Pro* and add building geometry and physics attributes. Based on the input data, the software estimates the heating demand.

The *CitySim Pro* software interface is shown in Figure 6.2. In *CitySim Pro*, modelling is often done

by uploading input data and clicking the *simulate* button. For the case study area, the simulation took around two hours, and the output could be exported as tab-separated values (TSV) files. These files then needed to have geometry added to them to be visualised as a map.

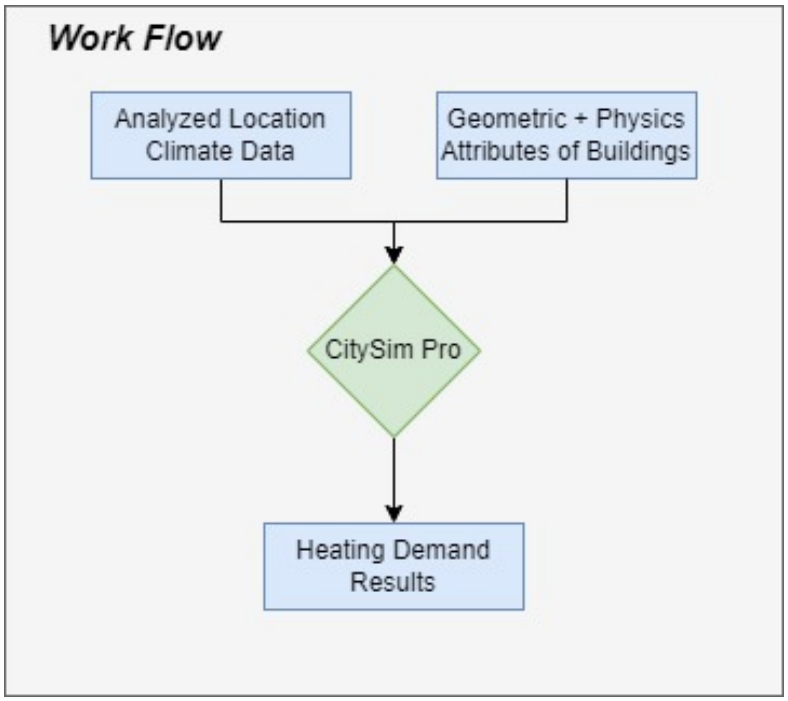

Figure 6.1: Schematic overview of the *CitySim Pro* workflow for heat demand computation, adapted from Jin (2022)

Figure 6.2: An overview of the *CitySim Pro* interface

6.1.1. Data collection and processing

Before simulating the heat demand in *CitySim Pro*, there were a few procedures that needed to be completed. Reliability of analysis depends on the quality of the data, which is not always guaranteed in GIS-related analysis (Srivastava, 2008). Selecting pertinent, well-established data sources and utilizing trustworthy automated software solutions are necessary to ensure high quality. Therefore, an overview of the data collection decisions is presented in the next section to guarantee the high-quality input data needed for the energy simulations performed for the geographical scope; Rijssen-Holten, the Netherlands. To prepare for the energy calculations, several datasets needed to be gathered and analyzed. The following input data had to be obtained:

1. Horizon file (Mutani et al., 2018)
2. Climate file (Jin, 2022; Mutani et al., 2018)
3. CityGML buildings (Jin, 2022; Mutani et al., 2018)
4. Building physics data (Jin, 2022)

An overview of how this thesis handles the data collection decisions for each necessary input can be found below. Using publicly available GIS data was a crucial data collection decision made during the data gathering process to adhere to the FAIR principles. In addition, another main criterion is that the GIS data collected is available for the Netherlands. Since the acquired data may not be available for other nations, this limits the method's reproducibility for other countries outside of the Netherlands.

6.1.1.1.Horizon file

The horizon file in this case refers to the storage of the viewshed information, e.g. the visibility of surfaces from a particular point, accounting for the curvature of the Earth as well as any impediments on the ground, such as mountains (Pulumbarit, 2023). This information is needed for the shortwave and longwave radiation calculation aspects in the *CitySim Pro* environment. It is possible to purchase the horizon file for the study region of choice via Meteonorm (Mutani et al., 2018). However, as the goal of this thesis was to use open data, no purchase was made for this dataset. Since the horizon file is a necessary input for *CitySim Pro*, it had to be computed. Utilizing C. Leon-Sanchez's research (date: under review), the horizon file was produced. This requests a digital surface model (DSM) covering the case study region in addition to the position of the nearest weather station in Rijssen-Holten, and the weather station itself.

The *Actueel Hoogtebestand Nederland* (AHN) DSM was utilized in GeoTIFF format (AHN, 2020) for DSM, with a resolution of five meters. AHN is a reputable company that creates high-resolution digital elevation models that encompass the whole Netherlands and makes their data publicly available (AHN, n.d.). From Lawrie and Crawley (2022), the weather station location data in .kml format can be collected. This dataset is freely accessible and also available for more regions than only the Netherlands. The site of the weather station and the Rijssen-Holten area are both covered by the AHN DSM file that was obtained, as shown by Figure 6.3. Given the lack of elevation in the Netherlands, the horizon file (in .HOR format) that resulted from applying C. Leon-Sanchez's algorithm produced a sky view (see Figure 6.4 for the horizon file result).

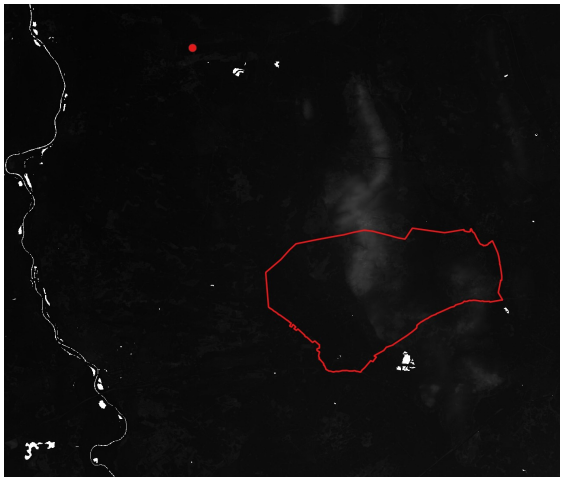

Figure 6.3: The AHN DSM dataset displayed in the QGIS interface with Rijssen-Holten shown in read with the nearest weather station location indicated as red as well. Elevation range between -6-300m

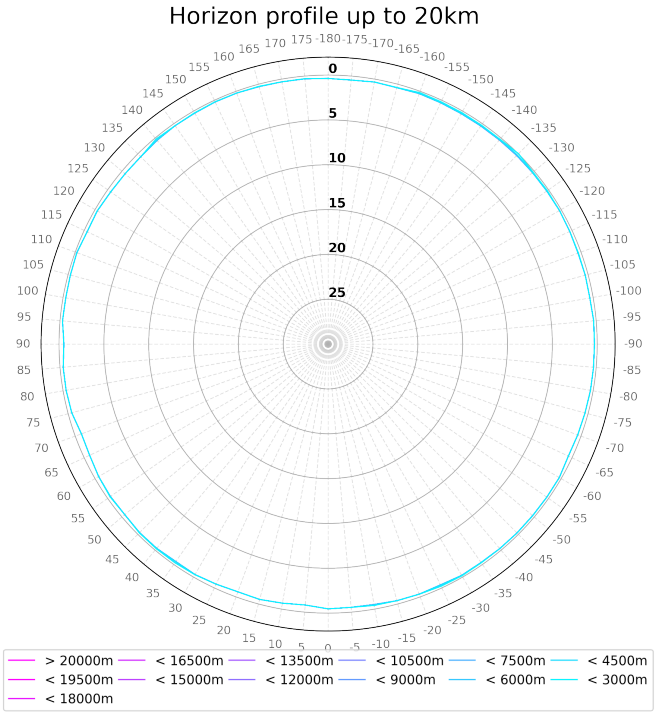

Figure 6.4: The output of the horizon file by C. Leon-Sanchez

6.1.1.2.Climate file

A climate file in the .CLI format must be entered into *CitySim Pro* to carry out certain tasks, like the solar radiation analysis that determines how much heat gain the buildings receive. As a result, this climate file had to be calculated. Jin (2022) devised a method to do so, which is accessible to the public on GitHub via the link. An overview of Jin (2022)'s algorithm and a schematic UML diagram of the script operations are shown in Figure 6.5.

In principle, the algorithm reads and parses an EnergyPlus Weather (EPW) file to obtain the pertinent climate data, and then converts and writes the data into a .CLI file format. The climatic

data, which is accessible for a wide geographic area outside of the Netherlands, was obtained in the .epw file type for Heino, Netherlands, Europe, in the year 2023 from Lawrie and Crawley (2022). That being said, Lawrie and Crawley (2022) also offer other climatic dataset formats, which could potentially be used alternatively, such as:

- CLM (ESP-r weather format)
- WEA (Daysim weather format)
- PVSyst (PV Solar weather design format)
- DDY (ASHRAE Design Conditions or "file" design conditions in EnergyPlus format)
- RAIN (hourly precipitation in m/hr, where available)
- STAT (expanded EnergyPlus weather statistics)

The resultant .CLI file includes climate-related data for the case study region, including solar radiation, air and surface temperatures, wind direction and speed, humidity and precipitation, and cloud cover. For point of reference, Figure 6.6 plotted the monthly average air temperature that was saved in the .CLI file and utilized in the analysis.

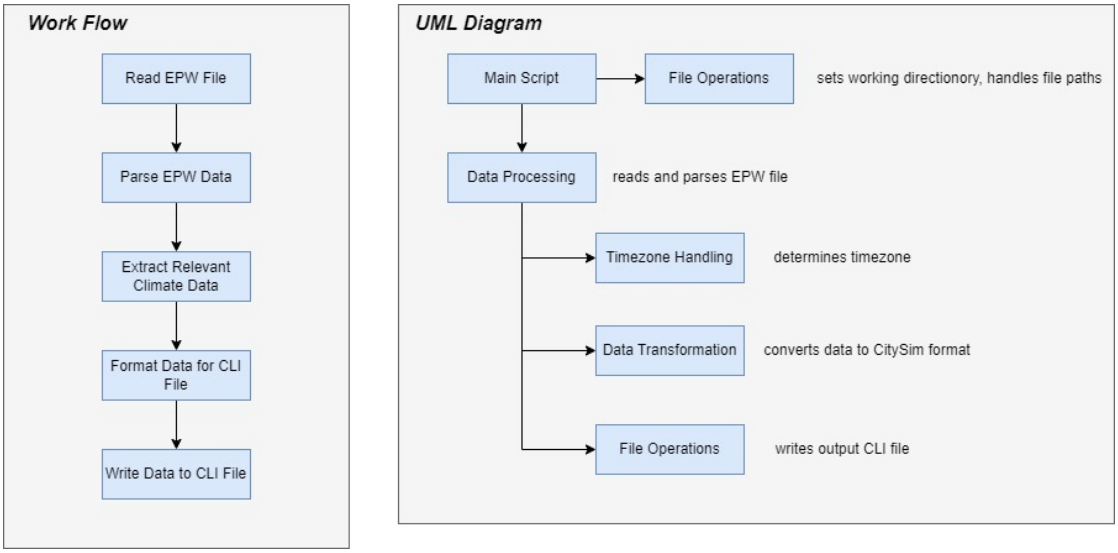

Figure 6.5: Overview of the workflow and UML diagram to compute the CLI file

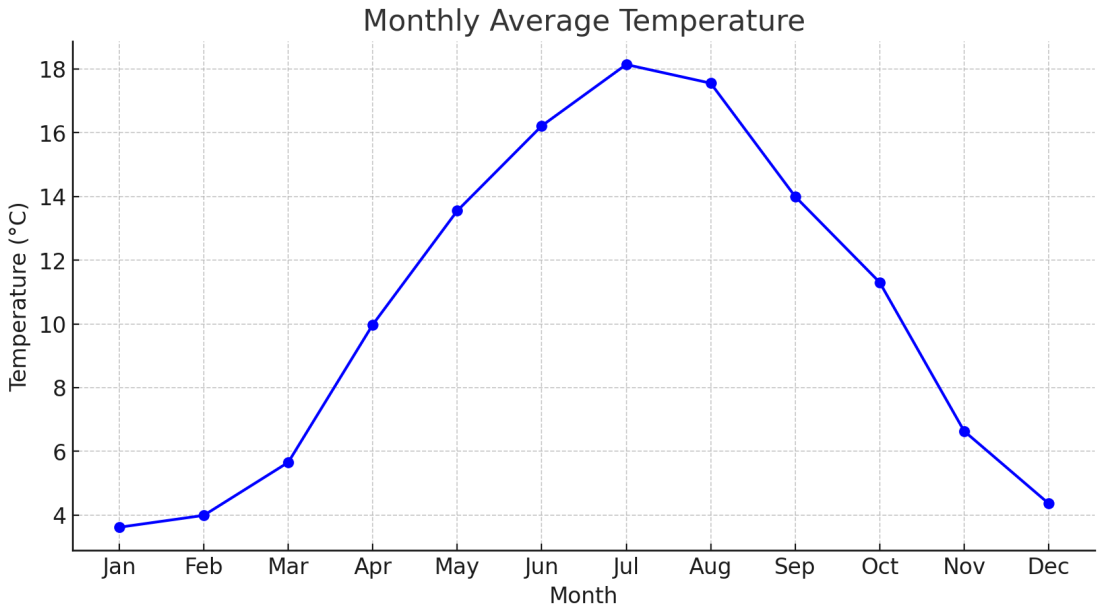

Figure 6.6: Overview of the .CLI monthly average air temperature

6.1.1.3.Semantic 3D city model

CitySim Pro can read a variety of data formats that reflect the built environment, such as CityGML, XML, etc and a semantic 3D city model can store the building stock's geometry and physical characteristics needed for the energy simulation. Therefore, the same semantic 3D city model used in subsection 4.4.1 is used for the *CitySim Pro* modelling.

The option to manually change each building's physical properties, such as U-values and g-values, is provided by *CitySim Pro*. A database of building physical properties is included in *CitySim Pro*, and users may utilize it by manually changing the component they want to simulate for each unit of analysis. Because editing the building physics attributes for 2500 buildings can be time-consuming, Jin (2022) developed an algorithm (see link) that allows editing the building physics attributes for all the buildings at once.

The algorithm by Jin (2022) for producing CitySim XML files was put into use. A UML diagram explaining the script structure and a simplified schematic overview of the algorithm's functions are provided via Figure 6.7. To put it briefly, it takes a CityGML file uploaded to a database, extracts out building information like material, construction, and geometry, does the necessary calculations for the XML file, and then writes the result.

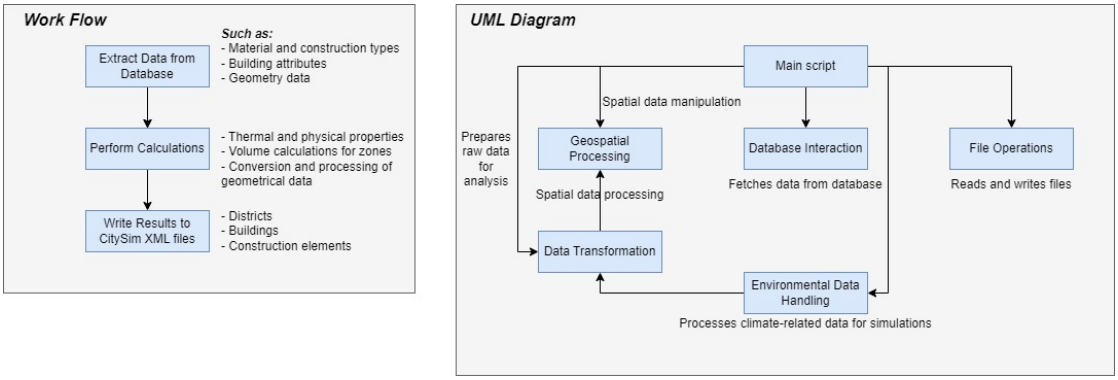

Figure 6.7: Overview of the workflow and UML diagram to compute the CitySim XML file

The CityGML building file was uploaded to a database. Since executing modifications for XML files may sometimes be complicated, the approach of extracting the pertinent data using a database was chosen for its simplicity of data collecting and rewriting the result to prevent any errors.

The ability to automate all of the buildings' building physics features simultaneously, based on the building type categorization and construction year, is the primary advantage of utilizing Jin's (2022) work. The semantic 3D city model contains the building type classification and construction year and thus with those two attributes, building physics data was able to be inserted into the semantic 3D city model.

The European TABULA project (Loga et al., 2012) compiled building physics data by building typology and construction year. From this project, the data available for the Netherlands was used. Since the goal was to model the existing conditions as closely as possible and the building features in *Existing State* followed the energy regulation in "Bouwbesluit" that was in effect at the time, TABULA scenario *Existing State* attributes were gathered and used for the energy simulation to answer the third sub-question (Loga et al., 2012). All of the typologies' building physics data characteristics were gathered and added to a database so that extraction operations could be carried out to generate a CitySim XML file. According to Loga et al. (2012), the ventilation system is mechanical with an alternative current, and the heating system is modelled as a single condensing gas-fired boiler for the *Existing State*.

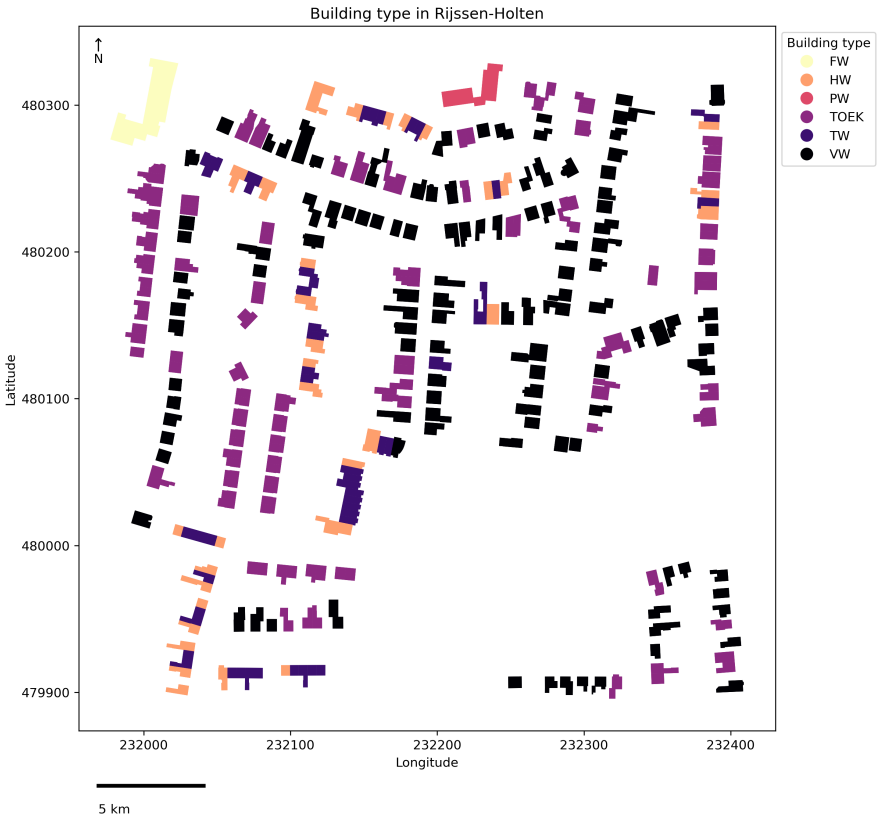

Figure 6.8: Building types in Rijssen-Holten

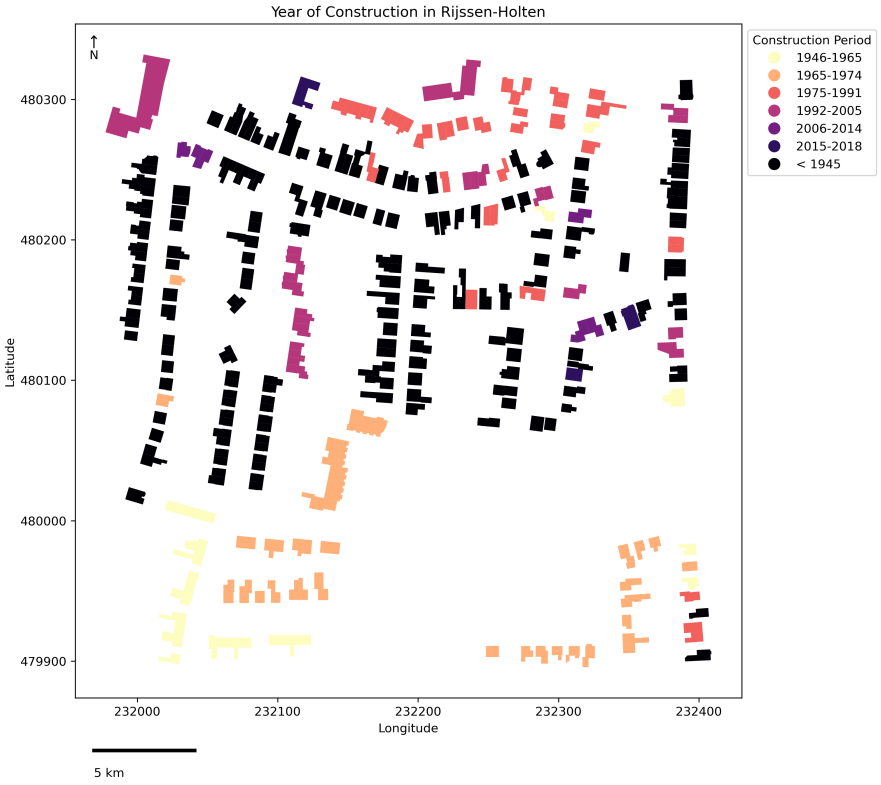

Figure 6.9: Building years in Rijssen-Holten

6.1.2. CitySim Pro heating demand result

The results of the *CitySim Pro* heat demand estimates for each building in Rijssen-Holten are shown in Figure 6.10.

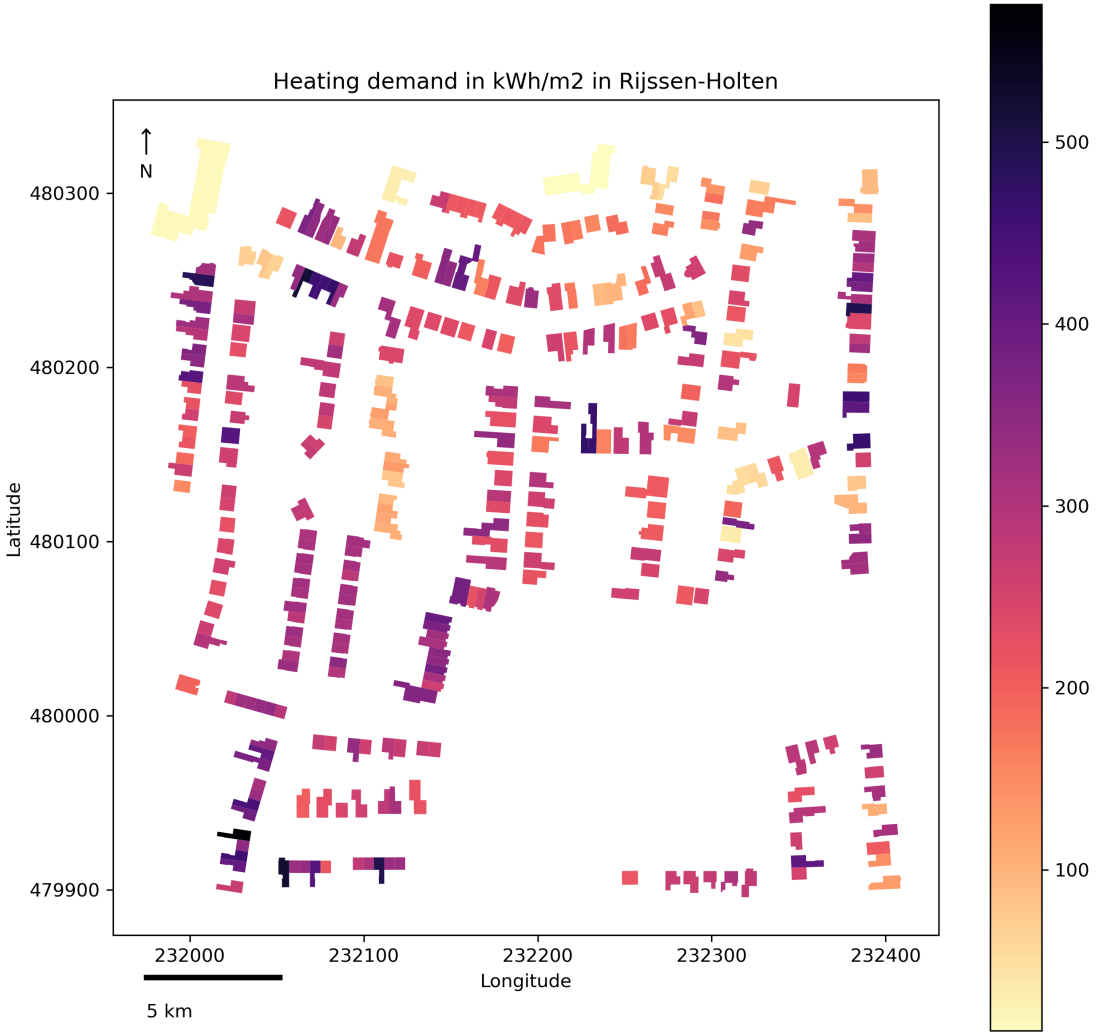

Figure 6.10: Heating demand in kWh/m² for Rijssen-Holten for the scenario *Existing State*. For reference, VW stands for detached house, TOEK stands for semi-detached house, TW stands for terraced house, HW stands for corner house, FW stands for flat or apartment, and PW stands for porch house

A summary of some descriptive data on the semantic 3D city model's estimated total heat demand is given by Table 6.1. The average heat demand of the 323 buildings that were simulated was 260.7 kWh/m², with a distribution range of 11.5-575.7 kWh/m².

Descriptive statistics	Existing State
Count	324
Mean	260.7
Min	11.5
Max	575.7

Table 6.1: Descriptive statistics of the total heating demand estimates for Rijssen-Holten for the scenario *Existing State*

An overview of the annual average heating demand, derived from the simulation, in kWh/m² per building type per construction year, is given by Figure 6.11.

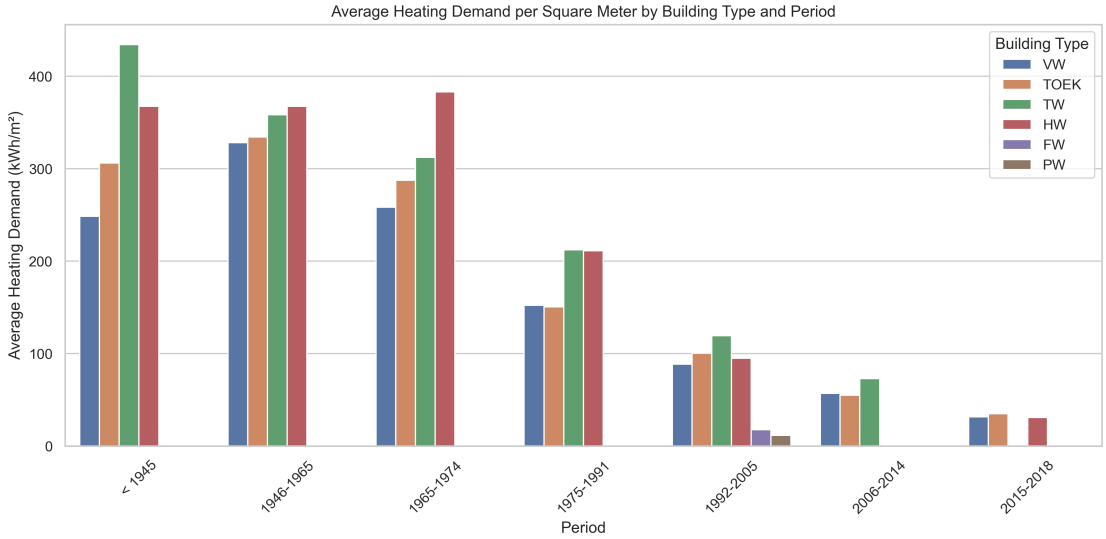

Figure 6.11: Average heating demand in kWh/m² per building typology per construction year for Rijssen-Holten for the scenario *Existing State*

6.2. Actual energy consumption and energy performance indicator comparison

6.2.1. Actual energy consumption data collection

The estimates computed from the developed NTA 8800 energy balance heat demand model has to be compared with statistical consumption data to verify whether the theoretical heating demand calculated corresponds with reality. Comparing the theoretical estimates with actual consumption statistics allows for the model to be evaluated as a sanity check. The statistical consumption dataset used for this study comes from the Centraal Bureau voor de Statistiek (CBS) of which two types were found, one dataset being: "Energie postcode 6 2021", year 2021, downloaded on December 7, 2023 in CSV format from the website link (Centraal Bureau voor de Statistiek (CBS), 2023) and another dataset being: "Energieverbruik particuliere woningen; woningtype en regio's", year 2021, downloaded on March 12th, 2024 in CSV format from the website link (Centraal Bureau voor de Statistiek (CBS), 2024).

Both datasets come from network operators, which CBS links through registries *Basisregistratie Adressen en Gebouwen* (BAG), Dataland and Locatus. CBS grouped the information into postal code 6 to preserve anonymity for the initial dataset and into building types for the second dataset.

Figure 6.12 presents the statistical consumption values for gas, which can be used to compare the Python-based model results as a sanity check for program development. As can be seen in Figure 6.12a, the gas consumption data is displayed in the energy unit m^3 using the spatial PC6 zones. In Rijssen-Holten, it seems that the majority of the gas consumption varies between 500-3940 m^3. Figure 6.12a shows the gas consumption in m^3 per building type, which lies between 1000 and 2500 m^3.

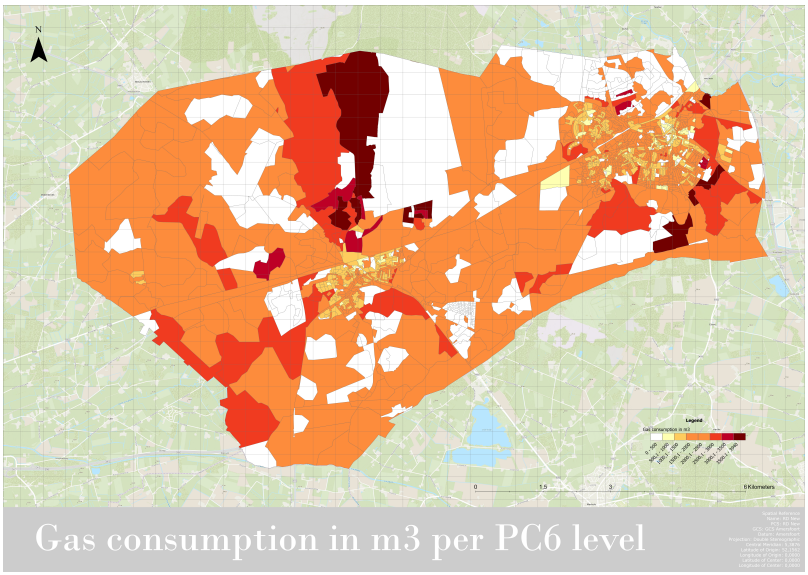

(a) Overview of the gas consumption estimates in m^3 for Rijssen-Holten PC6 level (Centraal Bureau voor de Statistiek (CBS), 2023)

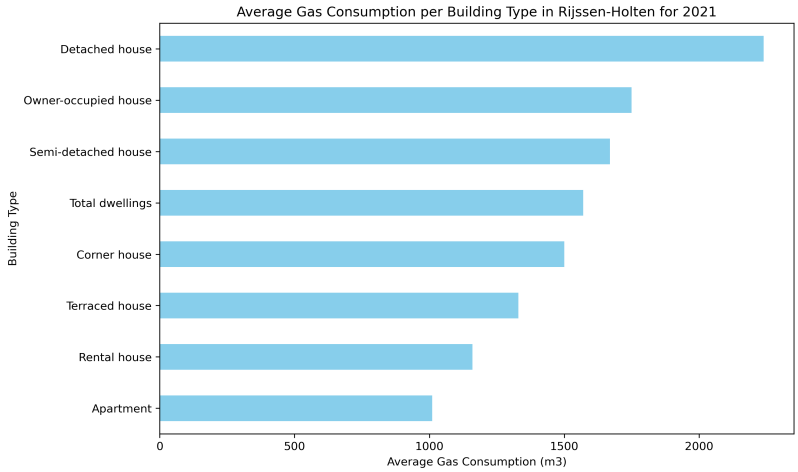

(b) Overview of the gas consumption estimates in m^3 for Rijssen-Holten per building type for year 2021 (Centraal Bureau voor de Statistiek (CBS), 2023)

Figure 6.12: Overview of the energy consumption estimates from CBS (2021) to use as a comparison reference

6.2.2. Energy conversion

There is a limitation that needs to be addressed when directly comparing the actual consumption with theoretical estimates, which is that they do not correspond to the same energy unit semantically. The theoretical numbers derived from the simulation reflect the heating demand, whereas the historical consumption data from the CBS dataset represents the yearly gas consumption reported by the network operator. Furthermore, the theoretical value is calculated for every building, but the CBS dataset shows the average gas consumption level per building type or per PC6 zone.

Both units must be properly converted to a semantically similar energy unit. To do this, it is necessary to define what energy conversion implies and what the energy system boundaries are. Energy generation, conversion and consumption can never be considered in isolation, all operations occur within the energy system (see Figure 6.13).

The extraction of energy carriers (such as coal, uranium, oil, natural gas, or biomass) via mining, extraction, or cultivation is the first stage. Natural forms of energy, such as coal, natural gas, or crude oil, are the resultant primary energy. Another name for it is primary energy carriers. To convert the primary energy carriers produced into a form that can be used, they must be processed through facilities like refineries or power plants (Blok & Nieuwlaar, 2020).

The energy left behind after conversion is known as secondary energy. However, to get that energy to consumers, it often needs to be transported, distributed, or stored, which consumes additional energy (Blok & Nieuwlaar, 2020).

Thus, the final energy is the energy that also includes the distribution energy required to deliver the energy. Even when energy is obtained by the consumer, it might still not be in the right form and requires further conversion through for example converting the fuel to heat in a boiler (Blok & Nieuwlaar, 2020). This energy is defined as usable energy that has undergone conversion to end-use. The energy can serve a specific purpose for the user when it is in its ultimate state e.g. heating or lighting a room (Blok & Nieuwlaar, 2020).

As a result, the final energy is the energy that also contains the distribution energy needed to deliver the energy. Even after the energy is acquired by the end user, energy may still need to be converted further, e.g. fuel used to generate heat needs to be converted by boiler (Blok & Nieuwlaar, 2020). This is also known as usable energy, when it can be used for a specified purpose by the end-user, such as illuminating or heating a space (Blok & Nieuwlaar, 2020).

Theoretical and actual consumption values are converted into primary energy carriers in the unit MJ to align the units for result comparison.

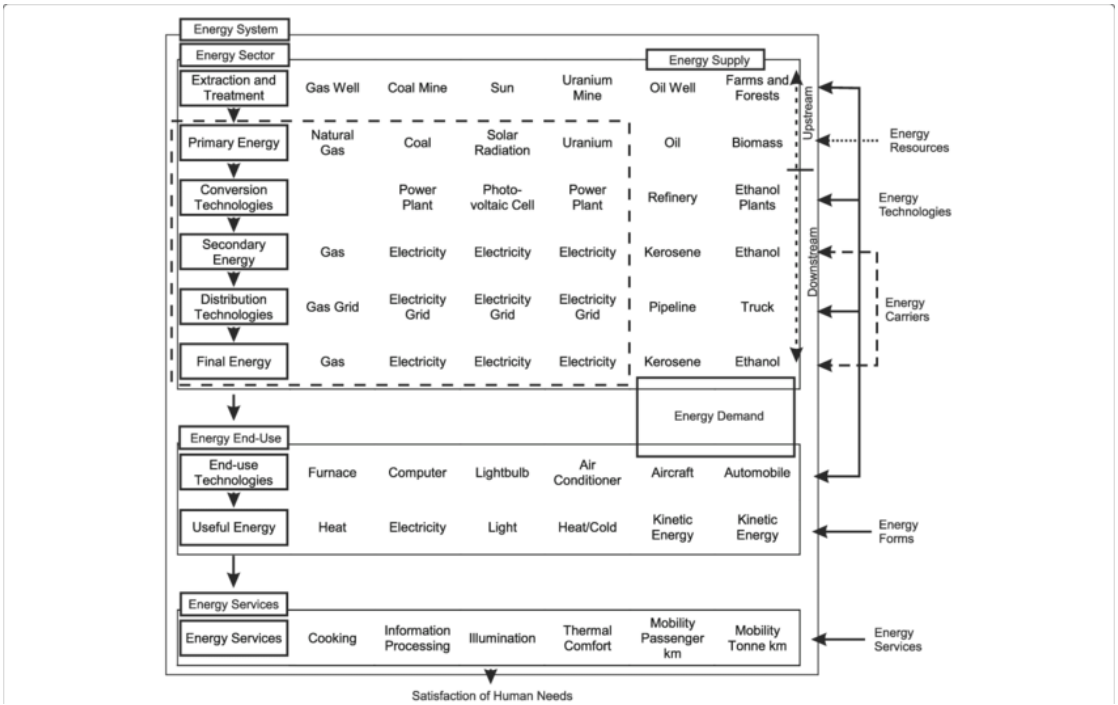

Figure 6.13: A schematic diagram of the energy system to demonstrate the conversion steps of energy supply to energy demand and to end-use and services (Kriechbaum et al., 2018)

6.2.2.1.Computing the primary energy from gas consumption

Equation 6.1 converts the gas consumption into primary energy (MJ) to make the comparison easier. It involves multiplying the yearly consumption found in the CBS dataset by the energy content of natural gas. Assuming the Netherlands utilizes Groningen gas, which has a high energy content, 35 MJ/m^3 was utilized, as the energy content of natural gas typically ranges from 31 to 36 MJ/m^3 (Blok & Nieuwlaar, 2020). In addition, only a share of 76.84% of the total gas consumption is used for the comparison since gas consumption is not only used for space heating but also for hot water or cooking usage and 76.84% represents the share of gas used for space heating (see Figure 6.14).

$$E_{0th} = C \times \varepsilon \times \eta_{sp} \tag{6.1}$$

Where:

- E_{0th}: The total primary energy in MJ
- C: Annual consumption for natural gas in m^3 from the CBS dataset (Centraal Bureau voor de Statistiek (CBS), 2023)
- ε: Energy content for natural gas; 35 MJ/m^3
- η_{sp}: Share of space heating demand on gas consumption; 76.84%

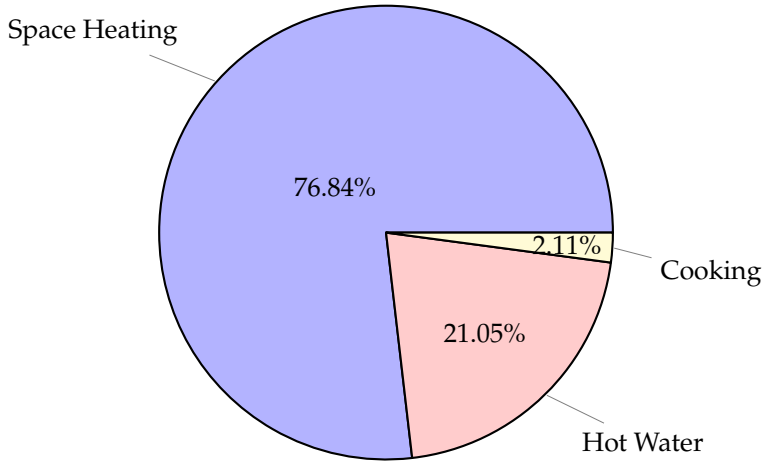

Figure 6.14: Gas consumption distribution per energy service within boilers (Knol, 2018)

6.2.2.2.Computing the primary energy from heating demand

Equation 6.2 converts the heating demand, which was computed in *CitySim Pro* in kWh, into the primary energy (MJ). For simplification, a standard HR107 boiler efficiency is used for the comparison for every building. This is chosen since the main heating system type specified in the Voorbeeldwoning 2022 is HR107 boiler (Ministerie van Binnenlandse Zaken en Koninkrijksrelaties, 2023). Only detached houses built between 2015-2018 use the electric heat pump and gallery houses and flat houses from 1965-1974 use VR boilers (see Table C.5). From Figures 6.8-6.8 it is visible that there are no gallery houses in the *CitySim Pro* output and no flat houses from 1965-1974. There is one detached house built between 2015-2018, but it is only one of the 324 buildings, so for the conversion, the HR107 boiler efficiency is used, which ranges between 85-90% efficiency (Knol, 2018), and I chose the upper limit of 90% since literature named this boiler a highly efficient boiler.

$$E_{0th} = \frac{E \times c_f}{\eta_b} \tag{6.2}$$

Where:

- E_{0th}: The total primary energy in MJ
- E: Space heating demand represented in kWh from the model results
- c_f: Conversion factor of kWh to MJ; 3.6
- η_b: Boiler efficiency; 90%

6.2.3. Energy performance indicator data collection

Figure 6.15 shows the benchmark values of the expected energy performance per building type and construction period based on the Voorbeeldwoning 2022. The heating demand does not only consist of space heating but also on other components (e.g. hot water use and cooking), and since in subsubsection 6.2.2.1, I am assuming space heating demand contributes to 76.84% of the gas consumption, I am also going to assume that 76.84% of the heating demand consists of space heating demand. In this assumption, I am also assuming that all gas consumption in buildings is used for the heating demand energy services, which can be a limitation depending what the building's heating system truly is.

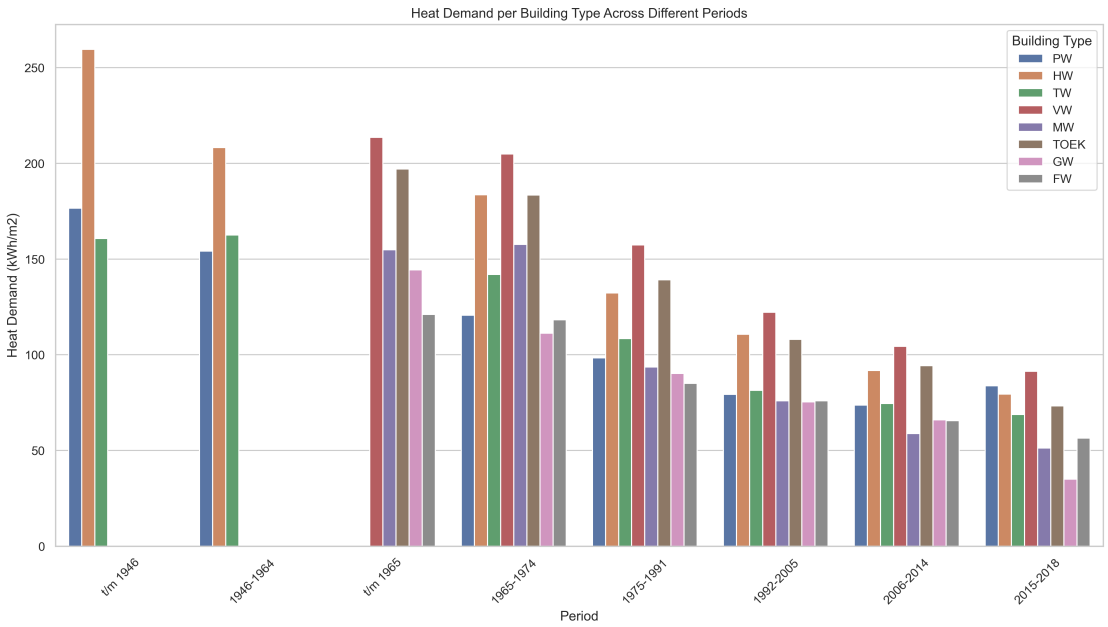

Figure 6.15: Overview of the expected heat demand (kWh/m^2) per building typology and construction period. For reference of the building typologies in the legend, PW stands for porch house, HW stands for corner house, TW stands for terraced house, VW stands for detached house, MW stands for maisonette, TOEK stands for semi-detached house, GW stands for gallery, and FW stands for flat or apartment

6.3. Result comparison

The results were compared using statistical metrics. The main method explored here is statistically comparing the NTA 8800 computed values with the other heat demand estimate values using metrics like mean absolute error (MAE) and root mean squared error (RMSE). The MAE is calculated using Equation 6.1 and is the average of all absolute errors (Everitt & Skrondal, 2010; Kotz et al., 2006):

$$\text{MAE} = \frac{1}{n}\sum_{i=1}^{n}|x_i - x| \tag{6.3}$$

Where:

- n is no. of errors
- $|x_i - x|$ is absolute errors

A comparison of anticipated and observed values (e.g. x_i vs x) is included in the measure of errors between paired observations to express the same phenomena (Everitt & Skrondal, 2010; Kotz et al., 2006). For this thesis, a comparison between paired observations is reflected in the actual primary energy consumption of heating, another BES tool heating needs, and benchmark estimates with the NTA 8800 computed primary energy consumption of heating. MAE calculates the absolute disparities between the primary energies types without accounting for the direction of such errors (Everitt & Skrondal, 2010; Kotz et al., 2006).

The residuals (prediction errors) standard deviation is known as RMSE (Barnston, 1992; Kenney & Keeping, 1962). Residuals can be used to quantify the dispersion of data points, e.g. the data point's distance from the line of best fit (Barnston, 1992; Kenney & Keeping, 1962). Hence, RMSE

was used to give higher weight to errors resulting from high deviations to assess whether there was a substantial discrepancy between certain NTA 8800 computed values and the other values. Equation 6.2 is used to calculate the RMSE (Barnston, 1992):

$$\text{RMSE} = \sqrt{\frac{1}{N}\sum(x_{fi} - x_{oi})^2} \tag{6.4}$$

Where:

- $(x_{fi} - x_{oi})^2$ are squared differences
- N is sample size

Table 6.2 summarizes the MAE and RMSE results of the model comparison with the BES tool results, historical statistical consumption patterns, and benchmark patterns. When comparing the model results versus the *CitySim Pro* results, the MAE is 148.9, and the RMSE is 162.8. The MAE demonstrates that there is a difference of 149 kWh/m^2 between the two results, with larger errors being more prominent (indicated by RMSE being higher than MAE). Both metric results are relatively close, suggesting that while there are errors, they may not be significant outliers causing significant deviations. The variation was expected to be high considering the limitation that I am comparing the output of two different energy method tools, the NTA 8800 norm method and a dynamic modelling method which both also have different thermal properties, e.g. the NTA 8800 uses the Voorbeeldwoning 2022 and the *CitySim Pro* results uses the TABULA project. I acknowledge that this is not a fair comparison, yet, despite this, the distribution between the errors is not as large as anticipated, especially since I am also comparing space heating demand from the NTA 8800 model with heating needs from the *CitySim Pro* which could also include the share of hot water or cooking in the computation.

When comparing the model results with the benchmark, the model surprisingly is close in range with an MAE of 49.8 and a RMSE of 63.5. These lower values indicate that the model's predictions are closer to the benchmark results. Similarly, as before, the MAE and RMSE difference is small but shows that some larger errors slightly affect the RMSE value. Lastly, when comparing the model results with the historical consumption data, it becomes apparent that the variation between theoretical values and reality is significant as the MAE is 19886 kWh and RMSE is 31862 kWh. This implies that the models cannot accurately estimate the space heating demand of the building stock. This result does not come as a surprise as many studies point out that the BES tool cannot accurately predict the actual energy consumption (van den Brom, 2020), and in addition, these MAE and RMSE seem also higher than the previous two because it was not possible to normalise the value beforehand since the actual energy consumption dataset did not come with area size, making it not a fair comparison either.

Metric	**CitySim Pro vs model values**	**CBS ground truth vs model values**	**Voorbeeldwoning benchmark vs model values**
MAE	148.9	19886	39.8
RMSE	162.8	31862	63.5

Table 6.2: Metric evaluation results for comparing both simulation results, the ground truth and the NTA 8800 computed simulation values and the benchmark estimate and the NTA 8800 computed simulation values

Figure 6.16 highlights the average heat demand results per building type and construction period for the model results, the BES tool results, and the energy performance benchmark results. For reference, PW stands for porch house, HW stands for corner house, TW stands for terraced house, VW stands for detached house, MW stands for maisonette, TOEK stands for semi-detached house, GW stands for gallery, and FW stands for flat or apartment.

For the FW buildings from 1992-2005, it seems like the model results and the *CitySim Pro* results are comparable, which could indicate that for this building year and type, the Voorbeeldwoning and TABULA project have similar thermal properties values. The model seems to estimate the demand as the lowest and significantly differs from the benchmark performances, implying that the model predicts that the newer FW buildings are more energy-efficient than in reality. For the HW, TOEK, and VW buildings, the model estimates space heating demand as the lowest but is closer in range with the benchmark. For HW, TOEK, TW and VW buildings, it becomes apparent that the *CitySim Pro* result has a higher heating demand which can be attributed to higher thermal properties. For the PW buildings, the benchmark heating demand is significantly higher than either tool result with the *CitySim Pro* being significantly lower. For TW buildings, it seems like the model estimates space heating demand higher than the benchmark but is still far lower than the *CitySim Pro* result. A trend is noticed in all plots that the BES tools typically estimate the demand higher in older buildings than the benchmark suggests and often underestimate demand with newer buildings than what the benchmark suggests, indicating that both tool results require calibration to estimate the demand better.

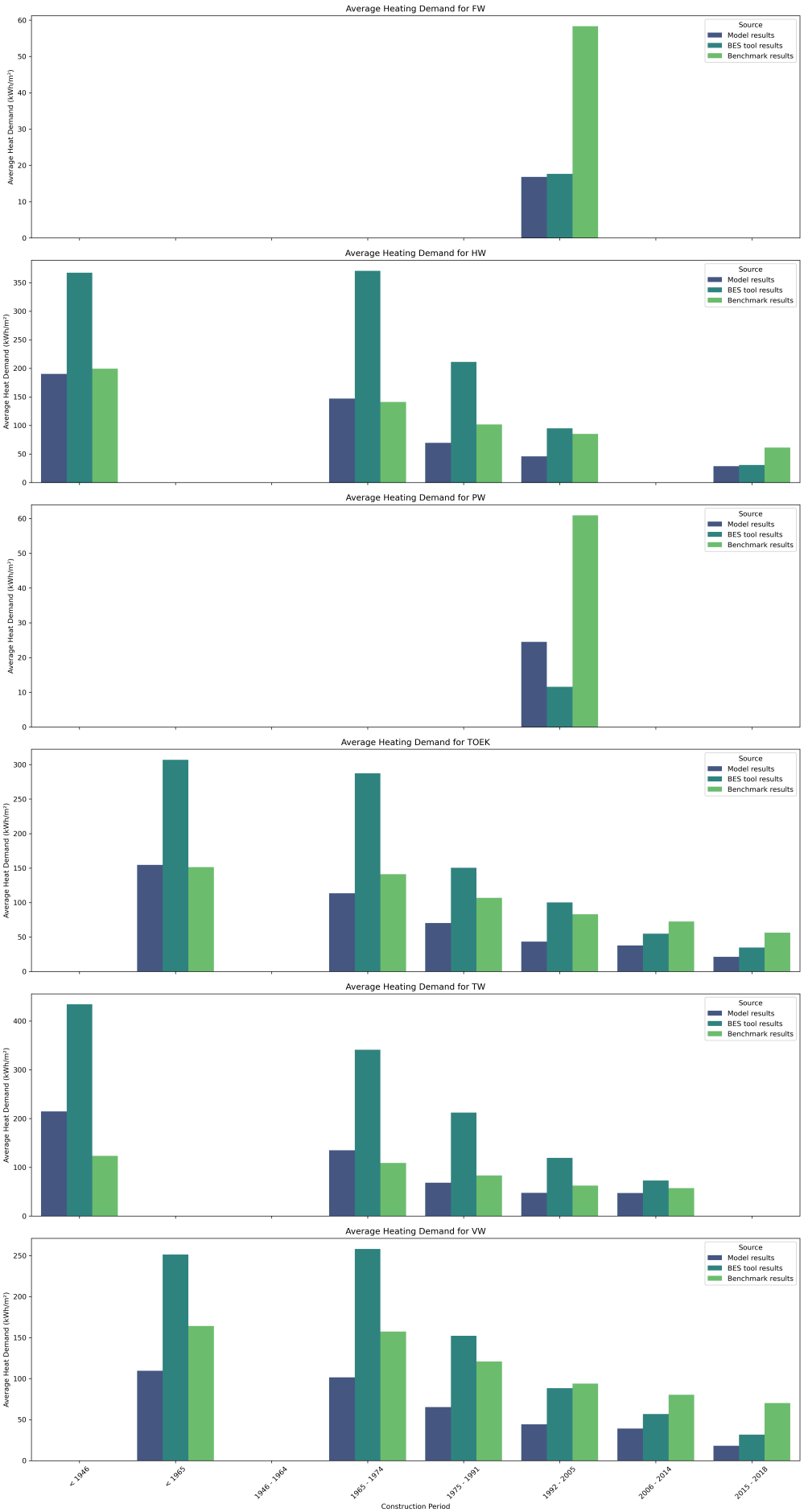

Figure 6.16: Average heat demand per building type and construction period for model results, BES tool results, and energy performance benchmark results

6.3.1. Result comparison for the two test buildings

Table 6.3 shows the difference in heating demand for the two buildings. The *CitySim Pro* values are higher than the model implementation, e.g. by 27.24% for building ID 1742100000006518 and 42.67% for building ID 1742100000004574. However, this could be attributed to the fact that *CitySim Pro* result "heating needs" consists of more energy services contribution than just space heating demand, the use of different thermal properties between the two BES methods, and because the model implementation seems to be missing certain component implementation such as heat transmission through window and doors or the impact of building volume on ventilation losses.

Statistic	**1742100000006518**	**1742100000004574**
Usable area in m^2	90	144
Total space heating demand kWh/yr in the model	19706	25176
Total heating demand kWh/yr in *CitySim Pro*	25074	36697.5
Total space heating demand kWh/m^2/yr in the model	218.95	178.6
Total heating demand kWh/m^2/yr in*CitySim Pro*	278.6	254.8

Table 6.3: Descriptive statistics of the total heating demand estimates for the buildings

6.3.2. Energy label comparison between model and CitySim Pro results

As an additional result comparison between the model implementation and *CitySim Pro* results, the energy label was computed for each building to see what label each building receives from each tool. Using the energy label range outlined in Table 6.4 for the primary fossil fuel energy usage from (CFP Green Buildings, 2024), multiplied by 76.84% to only consider the space heating demand contribution to this usage, the energy label for each building was computed and are displayed in Figure 6.17-6.18. The main takeaway in this comparison is that the model implementation estimated a far lower energy label value in comparison to the *CitySim Pro* model. As is seen in Table 6.5, the *CitySim Pro* model has 124 buildings classified as label G while this is only 3 for the model. The model estimates Rijssen-Holten's building stock energy performance higher since most buildings fall in the energy label A range (186) or B (78), indicating that the model implementation is producing lower expected space heating demand results, which could be attributed to the missing components mentioned in subsubsection 5.3.1.1.

Energy label category	Primary energy demand in kWh/m²/year
A	0 < PED < 160
B	160 < PED < 190
C	190 < PED < 250
D	250 < PED < 290
E	290 < PED < 335
F	335 < PED < 380
G	> 380

Table 6.4: Energy label ranges (CFP Green Buildings, 2024)

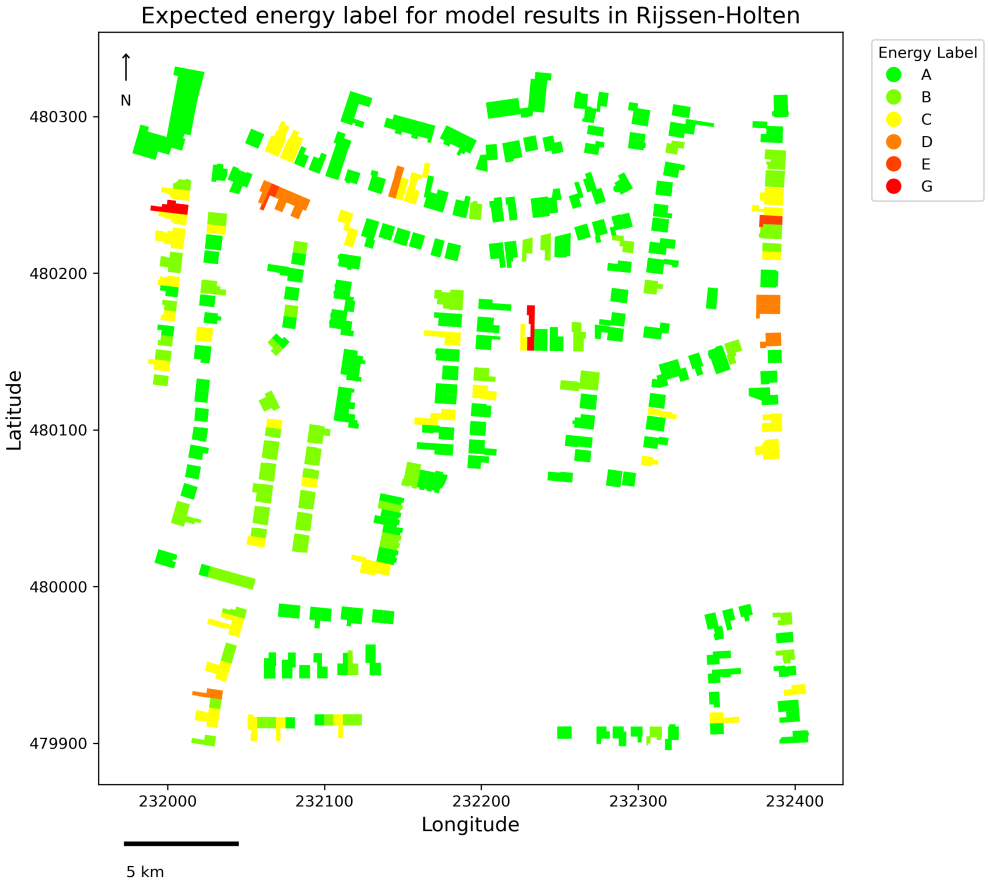

Figure 6.17: Model energy label result

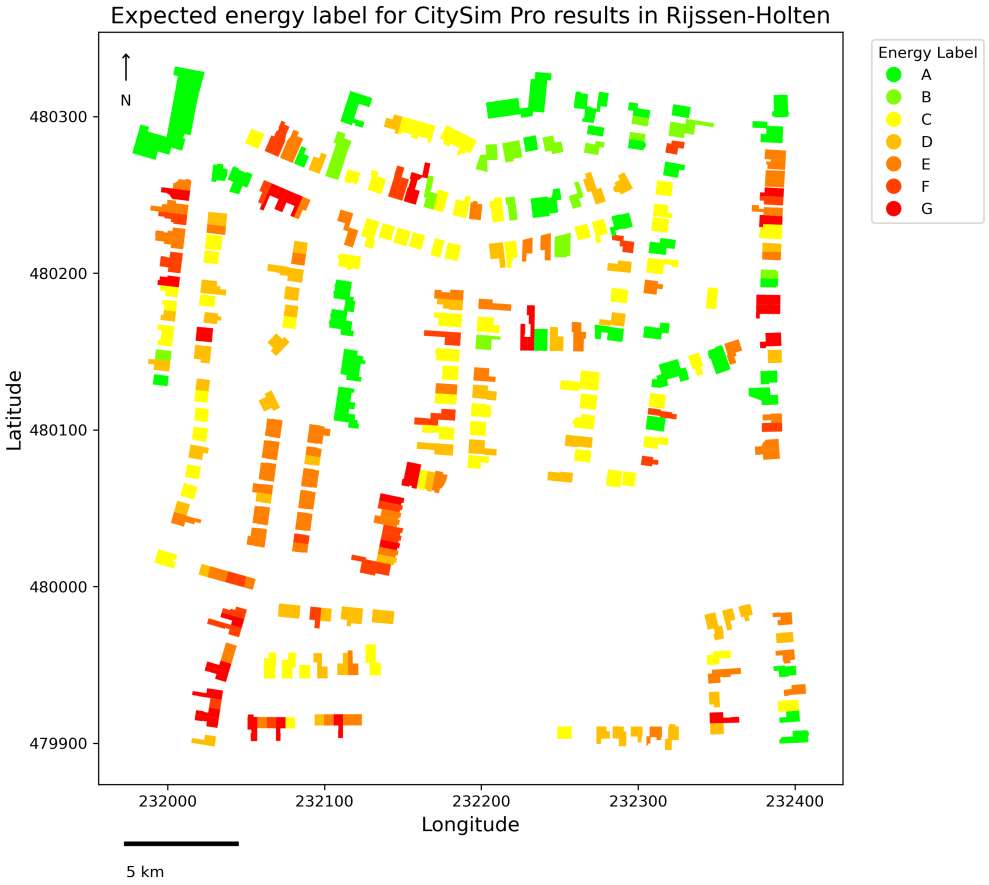

Figure 6.18: *CitySim Pro* energy label result

Energy label category	Model result count	CitySim Pro result count
A	186	49
B	78	17
C	45	72
D	10	59
E	2	71
F	0	28
G	3	28

Table 6.5: The distribution of energy label categories in each tool result

7

Discussion

7.1. Research implications

The Dutch built environment is lagging in terms of reducing its energy consumption, which results in an excess of greenhouse gases being released into the atmosphere and magnifies the impacts of climate change. The EU is pressuring Dutch authorities to decarbonise, so policymakers must devise plans to reduce energy use in the built environment. This means that to accelerate the transition, structural adjustments within the built environment must be implemented. Tools that can help the decision-making process are necessary, and hence, the main research question of the thesis became:

To what extent can a heat demand model be developed that adapts and implements the NTA 8800 to be coupled with CityGML-based semantic 3D city models?

The thesis aimed to develop a model that follows the NTA 8800 norm and accepts a semantic 3D city model as input and to an extent, this goal was achieved. The model calculates the space heating demand based on the student's interpretation of the NTA 8800 formulas. This was achieved by initially outlining the important formulas and parameters of the NTA 8800. The output was sketched in the form of mind maps. This allowed for the creation of a data requirement checklist, which form the basis of the data mapping for the model. The appropriate data was collected that can be stored in a semantic 3D city model, compatible with CityGML and Energy ADE, and additional assumptions were made for variables that were not easily collected.

This research step helped shape the model implementation. Since the data was initially stored in a CityGML XML file, it became apparent that to retrieve relevant data from the building file or store it in the building file, databases had to play a certain role in the model implementation to simplify the operations. This led to the creation of a Python model with database interactions. To aid the model implementation, data mapping was outlined together with the potential database storage with the CityGML and Energy ADE data model, to assess whether the data models were appropriate for the model function. The conclusion gathered from the data mapping is that CityGML and Energy ADE are suitable for NTA 8800 space heating demand computations and a

functioning model was developed in Python and tested for Rijssen-Holten.

The model was initially tested for two buildings which revealed several critical insights and potential implications for the field of energy modelling. The first is that the model heat transfer through ventilation is low and constant, which as mentioned before, contradicts existing literature on the impact of ventilation loss (Everett, 2023). This disparity draws attention to a possible weakness or missing element in the model, specifically, the building volume that was not included in the ventilation loss computation, which other formulations have pointed out is necessary for the computation or the impact of infiltration (Everett, 2023), which is not considered in the model. Solving this problem could greatly increase the accuracy of the model.

Conversely, heat transfer by transmission exhibits significant seasonal variation, consistent with patterns of larger losses in the winter. In contrast to accepted theoretical assumptions, the model currently does not consider the effect of windows and doors on transmission losses. This suggests a possible model limitation implementation due to the student's interpretation of the norm. The results of the solar gain show the expected patterns, with higher gains in the summer and lower gains in the winter, with solar heat being the dominant flow in the total heat gain. Because there was no viable window information dataset about the building stock in Rijssen-Holten and the norm outlining several assumptions required to compute the window conditions, solar gain scenarios based on different window's g-values were simulated to assess the impact of the glass type on the solar gain. The scenarios revealed the energy-saving potential in space heating demand if better window quality was implemented. The magnitude of potential energy savings by just changing the window type can be significant and relevant for policymakers.

The model reproduces space heating demand trends for the two buildings that are in line with the expected pattern, highlighting the model's capability of replicating the building's heat demand. The total space heating demand for the two buildings was, however, lower than expected, implying that the model underestimates the space heating demand. This only further suggests that the model is indeed missing certain components. Nevertheless, the model was tested for all the buildings in Rijssen-Holten, which led to the average space heating demand being 117.4 $kWh/m^2/yr$.

As an attempt to validate the model, the model results were compared with another BES tool, such as *CitySim Pro* results, and the average statistical consumption data per building type and benchmark results per building type and year. When comparing the Rijssen-Holten case study model results with these three comparisons, it proved that the model results were most similar to benchmark estimates and the least with the ground-truth values. The analysis of MAE and RMSE results reveals that while the model aligns reasonably well with benchmark results, it deviates significantly from historical consumption data. This indicates the need for model refinement and validation using diverse data sources. By addressing these discrepancies, the model can be improved to provide more accurate predictions, which are essential for effective energy policy and planning.

The findings of this thesis show that this model could be used for modelling building energy consumption but should be cautioned since the model values deviate significantly from actual

consumption patterns, which has been emphasized to be a common BES tool limitation (van den Brom, 2020) and therefore, any policy decision made based on BES tools should be cautioned. Nevertheless, the BES tool can serve as a guideline or provide a range of what the potential heat demand can be within the built environment and the insights derived from the model can still shed some light on what the consequences are of implementing certain renovation strategies, such as with changing the glass type within buildings.

A key benefit of this model implementation is promptly generating space heat demand results for an entire city. The results can be computed within 5 minutes using the Python script for the Rijssen-Holten study area, while this took 2 hours with *CitySim Pro*. Another benefit of my model implementation is that it is less sensitive to not watertight geometries in comparison to *CitySim Pro*. During simulating Rijssen-Holten in *CitySim Pro*, several buildings were not computed because the geometry was not watertight, which is not an issue in the Python script. As for the societal benefit of the model implementation, this model was developed to follow the NTA 8800 space heating computation method and therefore is specially tailored towards the Dutch built environment context and regulation, which policymakers can benefit from testing renovation strategies and compute the energy performance of buildings.

7.2. Research limitations

Full disclosure, the results presented are indicative of the research analysis conditions in which the thesis study is conducted. Each sub-question chapter has identified the constraints of the thesis in terms of data collection and technique assumptions. This section summarizes the key limitations of the thesis approach regarding the model implementations. From the heat flow results, it becomes apparent that the model implementation is missing some components that result in a lower space heating demand than expected. This could be attributed to how transmission and ventilation were implemented based on the student's understanding of the norm, which has a significant impact on the model accuracy.

The norm often asked for detailed information for the transmission computation that was not available and hence generalisations were made to allow for the computation to occur. Examples of missing variables include the transmission factors between the separation surfaces between the heated space and adjacent unheated spaces, the separation surfaces between the heated space and adjacent heated spaces or the linear thermal bridges that form a separation between separating surfaces and the ground (or water). As a result, the flat rate method, e.g. the simplified method, was implemented for the transmission computation since the high-level detailed data was often not available.

Another model assumption for transmission was made with the computation of the heat transmission for vertical pipes. Because no information on vertical pipe insulation level was found at the building level or in the building typology database, assumptions were made based on the HVAC systems specification outlined in the building typology. If a building had the heating system VR or H107 boiler, I assumed the building would have an uninsulated pipe value from the NTA 8800 table, while if the building had an electric heat pump, I assumed the higher efficiency

pipe value.

Certain factors were also outlined to be generalised in a simplistic manner for computing the total heat transmission. For example, the heat transfer coefficient via adjacent unheated and heated spaces was assumed to be 0 according to the norm, which is a strong generalisation of these two components' behaviour. Other factors such as the heat transfer coefficient through windows and doors were not even considered as it was excluded in the H_D formulation.

Another limitation of this thesis is the fact that the NTA 8800 norm outlines the different specifications of the area zones types (see subsection 2.2.2 for a reminder of the different zones definitions), however throughout the thesis model implementation, only two area attribute types were available and was used for computations, e.g. the usable area or surface area. This is an assumption limitation used because the thermal or calculation zone that the norm outlined to be necessary for the computation was not possible to determine since there was no indoor floor plan available to determine the zones. Hence, the main assumption used in the model implementation is that each building has one thermal zone or calculation zone, which is not the case in reality.

The ventilation computation also has limitations regarding the data availability. For the ventilation, the effective volume flow rate was assumed to be one single fixed value, used for all building types and years, while in reality, this can vary significantly. This leads to a constant ventilation value outcome for most buildings, only varying minimally depending on the building function. Also, the assumption of using a factor of 1 for the correction factors in the heat transfer coefficient for ventilation was used due to the lack of data availability on the ventilation system of the building stock conditions. This also limits the ventilation loss output.

As for internal gain, fixed value assumptions had to be made for the heat flux of lighting and the DHW system since I could not find varying building typology information regarding these components. This leads to a significant generalisation in the internal gains for each building type in the heat demand outputs for the non-residential buildings since I am using the same fixed value for each building, which I acknowledge, is a major limitation.

During the debugging of the model, another interesting consideration was discovered due to the norm formulation of the variable $N_{P;woon;zi}$. This variable is supposed to represent the average number of residents per calculation zone and yet it turns out that when you implement the area range limit per person, it seems like the norm wants you to use a smaller factor when the area size is larger than 100m^2 (see Table 7.1). This felt contradicting to implement as I assumed you want to use a higher factor when you have a larger area size. This ultimately results in a lower internal gain for larger residential buildings, which suggests that the impact of internal gain is restricted to building area conditions.

Condition	$N_{\mathbf{P;woon;zi}}$ Value
When $\frac{A_{g;zi}}{N_{woon;zi}} \leq 30m^2$	1
When $30m^2 < \frac{A_{g;zi}}{N_{woon;zi}} \leq 100m^2$	3.08
When $\frac{A_{g;zi}}{N_{woon;zi}} > 100m^2$	2.72

Table 7.1: The average number of residents per calculation zone according to the NTA 8800 formulation of Equations 4.23-4.25

The semantic 3D city model does not contain information regarding window surface area or whether there is a frame or not or what the material type even is and hence several generalisations had to be made for the solar gain computation. The first one is that each building surface, besides the ground floor, was multiplied by 30% (Yang et al., 2020) to get the window area. This assumption was made based on the literature review regarding window to facade ratio range in the Netherlands, which was also taken as the average from Yang et al. (2020) study. This ratio assumption was also used on roof surfaces since no viable literature was found on window-to-roof ratio, which can lead to overestimations of window areas on roof surfaces by the model. The situation with the window frame became a fixed value using method B from the NTA 8800 due to a lack of data. To avoid making many more assumptions with the windows, the glass type with non-scattering glazing was set as a sensitivity analysis parameter to allow for multiple scenario testing for solar heat gain since the real situation regarding windows conditions is not stored within semantic 3D city models e.g. if there are glazed windows or blinds or rotating or both etc.

Some general model assumptions that were also made include the monthly computations, assuming an infinite power system and the exclusion of the cooling demand in heat demand computation. The capacity to precisely represent time-dependent interactions with engineering building systems is limited by the monthly time interval of the model. This limitation leads to the usage of simplified modelling, which frequently makes use of correlation coefficients. However, variables like user behaviour, system kind and control, and climate all affect how accurate these coefficients are. The model also uses the assumption that the system's power is unlimited to compute the energy needs for heating and cooling, which could not correctly represent actual situations. Also, the model does not include estimates for cooling demand in the space heating demand computations, even though heating and cooling demands are intertwined. In fact, a conditional was implemented to change negative heat transfer to 0 during the heating period months and for the negative solar gain during the inverse of those months. This could have been avoided perhaps if cooling demand was implemented.

Lastly, misinterpretation of the norm is highly likely since there were often mismatches discovered during the reading process, e.g. mislabeling or misuse of units occurred and certain formula requirements had to be generalised due to lack of data availability. This was the case for each model component.

As for result comparison limitations, the lack of semantically similar datasets required me to make significant assumptions such as using an H7107 boiler, or a share of space heating contribution of 76.84%, etc., to align the space heating demand units for comparison. Every assumption used

there is a limitation.

7.3. Future research

This thesis explored the idea of implementing a heat demand model prototype that can always be improved through more research. The main future area of research for this thesis is concerning improving the model input data and assumptions with more accurate data. One possible future research suggestion is to conduct an analysis that compares the NTA 8800 solar radiation fixed table values with a solar radiation model. The outcome of this analysis can shed light on whether the NTA 8800 fixed table could potentially be replaced by an alternative, geomatic-related solution, that works as the model's solar radiation input data. The same goes for the ventilation effective volume flow rate assumption. Now, one single value is used for all building types and years, while in reality, this can vary significantly. A possible future research topic is the development of ventilation system building typology libraries to enhance this model computation or alternatively implement the ventilation loss formulation that considers the building volume (Everett, 2023) and see if the results significantly vary. The same could be tested for heat transmission impact of windows and doors by implementing a formula that takes care of this heat flow in the model.

8

Conclusion

The built environment is a complex system, and making improvements to the built environment is a difficult process. Implementing changes requires careful consideration to assess the long-term consequences of a decision. To do so, policymakers need clear methods of evaluation to make well-informed decisions on how the built sector will develop. This thesis aims to provide such a tool to help policymakers decide on the building stock on a large urban scale more expeditious and informed. The thesis describes techniques for modelling building-level energy use for an entire neighbourhood while adhering to NTA 8800 guidelines.

The thesis's main research question was: "To what extent can a heat demand model be developed that adapts and implements the NTA 8800 to be coupled with CityGML-based semantic 3D city models?", and to answer this question a Python model with database interaction was developed that explored spatial energy modelling using semantic 3D city models, tested for Rijssen, the Netherlands, which led to the average space heating demand being 117.4 kWh/m^2/yr. The thesis research uses a mixed-method research approach, using qualitative and quantitative research methods to answer the research question.

The model's capacity to estimate space heating demand shows its potential usefulness in decision-making processes regarding building energy efficiency upgrades, even though it nearly matches the benchmark results, producing the lowest MAE and RMSE results. Notwithstanding its achievements, the model's shortcomings—such as its underestimating of the space heating demand and its low, continuous heat transfer through ventilation—indicate areas that still need improvement. These problems draw attention to elements that are absent from the model, such as the effect of building volume on ventilation and the omission of windows and doors from computations of heat transmission. Resolving these gaps can greatly improve the accuracy and dependability of the model.

The availability of data and model assumptions were the main sources of the research's shortcomings. As a result, even though the developed model appears to have the potential to help reduce energy consumption in the Dutch built environment, more research is needed to address

its limitations and improve the model's dependability in real-world applications.

8.1. Self reflection

The methodology used in this thesis closely resembles the lessons learned through the Master of Geomatics program, which places a strong emphasis on a methodical approach to spatial data analysis and modelling. As part of my thesis, several datasets were gathered and integrated, a framework for data mapping was established, and a Python-based model that communicates with semantic 3D city models was developed, all while trying to adhere to the FAIR principles as much as possible. Due to the toolkit I developed during my Geomatics program, I was able to implement a building energy simulation tool that performs faster than *CitySim Pro* and can handle more buildings in comparison to using *EnergyPlus*.

This thesis is an example of how geomatics principles can be applied practically, showing how modelling approaches and geospatial data can be used to solve practical issues to real-world questions such as how to decarbonise the built environment. To simulate space heating demand, the model uses OGC-approved city data models like CityGML and Energy ADE. This application demonstrates how spatial data and modelling may support sustainable development objectives, showcasing the potential of geomatics in urban planning and energy efficiency. Hopefully, this thesis showcased how relevant geomatics is in developing solutions for energy management in the built environment.

Not only does this model have geomatics-related applications, but this model also has a social wider value. As shown with the sensitivity analysis, glass-type scenarios were able to be conducted with the help of the model to see how much the potential energy savings can be for the built environment concerning heat demand, giving policymakers important information about efficient remodelling techniques. This type of information can help asses how to lower energy consumption within buildings but also lower people's energy bills, overall reducing energy poverty.

References

Agugiaro, G. (2016). Energy planning tools and citygml-based 3d virtual city models: Experiences from trento (italy). *Applied Geomatics*, *8*(1), 41–56. https://doi.org/10.1007/s12518-015-0163-2

Agugiaro, G., Benner, J., Cipriano, P., & Nouvel, R. (2018). The energy application domain extension for citygml: Enhancing interoperability for urban energy simulations. *Open Geospatial Data, Software and Standards*, *3*(1), 2. https://doi.org/10.1186/s40965-018-0042-y

AHN. (2020). Ahn dsm 5m geotiff dataset. https://www.ahn.nl/ahn-viewer

AHN. (n.d.). Kwaliteitsbeschrijving. https://www.ahn.nl/kwaliteitsbeschrijving

Allegrini, J., Orehounig, K., Mavromatidis, G., Ruesch, F., Dorer, V., & Evins, R. (2015). A review of modelling approaches and tools for the simulation of district-scale energy systems. *Renewable and Sustainable Energy Reviews*, *52*(100), 1391–1404. https://doi.org/10.1016/j.rser.2015.07.12

Association of the European Heating Industry. (2024). Electric heat pumps. https://ehi.eu/heating-technologies/electric-heat-pumps/

Attia, S., Beltran, L., De Herde, A., & Hensen, J. (2009). Architect friendly: A comparison of ten different building performance simulation tools. *11th IBPSA Building Simulation Conference, 27-30 July*, 204–211.

Barnston, A. (1992). Correspondence among the correlation [root mean square error] and heidke verification measures; refinement of the heidke score.

Benner, J. (2018, March). *Citygml energy ade v. 1.0 specification*. Version 1.0. KIT. https://www.citygmlwiki.org/images/3/38/Energy_ADE_specification_2018_03_25.pdf

Bhattacherjee, A. (2012). *Social science research: Principles, methods, and practices*. Open Access Textbooks.

Biljecki, F., Ledoux, H., & Stoter, J. (2016). An improved lod specification for 3d building models. *Computers, Environment and Urban Systems*, *59*, 25–37. https://doi.org/10.1016/j.compenvurbsys.2016.04.005

BizEE Software. (2008–2024). Degree days.net: Weather data for energy saving. https://www.degreedays.net

Blok, K., & Nieuwlaar, E. (2020). *Introduction to energy analysis* (3rd ed.). Routledge. https://doi.org/10.4324/9781003003571

Bodelier, M., & Herfkens, J. (2021). *Every new building in the netherlands must be almost energy neutral starting jan. 1, 2021*. https://www.gtlaw.com/en/insights/2021/1/every-new-building-in-the-netherlands-must-be-almost-energy-neutral-starting-jan-1-2021

Borowski, M., Mazur, P., Kleszcz, S., & Zwolińska, K. (2020). Energy monitoring in a heating and cooling system in a building based on the example of the turówka hotel. *Energies*, *13*(8). https://doi.org/10.3390/en13081968

Bottino-Leone, D., Balest, J., Cittati, V. M., Pezzutto, S., Fraboni, R., & Beltrami, F. (2024). Review of existing tools for the assessment of european building stock energy demand for space heating and cooling. *Sustainability*, *16*(6). https://doi.org/10.3390/su16062462

Bramiana, C., Entrop, A., & Halman, J. (2016). Relationships between building characteristics and airtightness of dutch dwellings. *Energy procedia*, *96*, 580–591.

Centraal Bureau voor de Statistiek (CBS). (2023, November). *Energielevering aan woningen en bedrijven naar postcode*. Centraal Bureau voor de Statistiek. https://www.cbs.nl/nl-nl/maatwerk/2023/46/energielevering-aan-woningen-en-bedrijven-naar-postcode

Centraal Bureau voor de Statistiek (CBS). (2024, March). *Energieverbruik particuliere woningen; woningtype en regio's*. Centraal Bureau voor de Statistiek. https://opendata.cbs.nl/#/CBS/nl/dataset/81528NED/table

CFP Green Buildings. (2024, March). *Green residential buildings methodology assessment document*.

CitySimPro. (2023). Citysim pro. http://www.kaemco.ch/download.php

Conti, P., Bartoli, C., Franco, A., & Testi, D. (2020). Experimental analysis of an air heat pump for heating service using a "hardware-in-the-loop" system. *Energies*, *13*, 4498. https://doi.org/10.3390/en13174498

Crawley, D. B., Hand, J. W., Kummert, M., & Griffith, B. T. (2008). Contrasting the capabilities of building energy performance simulation programs. *Building and Environment*, *43*(4), 661–673. https://doi.org/10.1016/j.buildenv.2006.10.027

Creswell, J. W., & Clark, V. L. P. (2017). *Designing and conducting mixed methods research*. Sage publications.

Dang, M. (2023). Estimating window-to-wall ratio for urban energy modelling of amsterdam centrum by deep learning. *AMS Institute Blog*. https://amsterdamintelligence.com/posts/estimating-window-to-wall

de Geus, A., de Beijer, H., & Krosse, L. (2015). The solabcool®, cooling of dwellings and small offices by using waste or solar heat [International Conference on Solar Heating and Cooling for Buildings and Industry, SHC 2014]. *Energy Procedia*, *70*, 23–31. https://doi.org/10.1016/j.egypro.2015.02.093

De Rosa, M., Bianco, V., Scarpa, F., & Tagliafico, L. A. (2014). Heating and cooling building energy demand evaluation; a simplified model and a modified degree days approach. *Applied Energy*, *128*, 217–229. https://doi.org/10.1016/j.apenergy.2014.04.067

Everett, B. (2023). *2.3 cutting ventilation losses* [OpenLearn]. Retrieved June 12, 2024, from https://www.open.edu/openlearn/nature-environment/energy-buildings/content-section-2.3#:~:text=The%20energy%20required%20to%20raise,%C3%97%20V%20%C3%97%20%CE%94T%20watts

Everitt, B. S., & Skrondal, A. (2010). *The cambridge dictionary of statistics*. Cambridge University Press.

Ferrando, M., Causone, F., Hong, T., & Chen, Y. (2020). Urban building energy modeling (ubem) tools: A state-of-the-art review of bottom-up physics-based approaches. *Sustainable Cities and Society*, *62*, 102408. https://doi.org/10.1016/j.scs.2020.102408

Fonseca, J. A., Nguyen, T.-A., Schlueter, A., & Marechal, F. (2016). City energy analyst (cea): Integrated framework for analysis and optimization of building energy systems in neighborhoods and city districts. *Energy and Buildings*, *113*, 202–226. https://doi.org/10.1016/j.enbuild.2015.11.055

Future Cities Laboratory Global. (2024). City energy analyst (cea). https://fclg-ep.ethz.ch/tool/city-energy-analyst

Garg, V., Mathur, J., & Bhatia, A. (2020). *Building energy simulation: A workbook using designbuilder*. CRC Press.

Gröger, G., Kolbe, T. H., Nagel, C., & Häfele, K.-H. (2012). Ogc city geography markup language (citygml) encoding standard [Publication Date: 2012-04-04, Approval Date: 2012-03-09], (OGC 12-019). http://www.opengis.net/spec/citygml/2.0

Hamburg, A., Mikola, A., Parts, T.-M., & Kalamees, T. (2021). Heat loss due to domestic hot water pipes. *Energies*, *14*(20). https://doi.org/10.3390/en14206446

Hong, T., Chen, Y., Lee, S. H., & Piette, M. A. (2016). Citybes: A web-based platform to support city-scale building energy efficiency. *Urban Computing*, *14*, 2016.

Hong, W. Y., & Rahmat, B. N. N. N. (2022). Energy consumption, co2 emissions and electricity costs of lighting for commercial buildings in southeast asia. *Scientific Reports*, *12*(1), 13805. https://doi.org/10.1038/s41598-022-18003-3

Jin, Y. (2022, June). *Dynamic energy simulations based on the 3d bag 2.0* [Master's Thesis]. Delft University of Technology. http://resolver.tudelft.nl/uuid:3ae123bd-cae4-45b2-be48-27ffe5cab980

Kenney, J. F., & Keeping, E. S. (1962). Root mean square. In *Mathematics of statistics, pt. 1* (3rd, pp. 59–60). Van Nostrand.

Kmeťková, J. B., Petráš, D., Corgnati, S. P., & Becchio, C. (2018). Energy and financial evaluation of envelope retrofit measures for an apartment block in slovakia. https://api.semanticscholar.org/CorpusID:169560010

Knol, A. (2018, August). Local power-to-heat (p2h) district heating cooperatives : An exploration of the technical, economic, social and legal aspects of the establishment of a local p2h district heating cooperative in an existing residential area, particularly in the netherlands. http://essay.utwente.nl/77442/

Kolbe, T. H., & Donaubauer, A. (2021). Semantic 3d city modeling and BIM. In W. Shi, M. F. Goodchild, M. Batty, M.-P. Kwan, & A. Zhang (Eds.), *Urban informatics* (pp. 609–636). Springer. https://doi.org/10.1007/978-981-15-8983-6_34

Kotz, S., et al. (Eds.). (2006). *Encyclopedia of statistical sciences*. Wiley.

Kriechbaum, L., Scheiber, G., & Kienberger, T. (2018). Grid-based multi-energy systems—modelling, assessment, open source modelling frameworks and challenges. *Energy, Sustainability and Society*, *8*. https://doi.org/10.1186/s13705-018-0176-x

Langevin, J., Reyna, J., Ebrahimigharehbaghi, S., Sandberg, N., Fennell, P., Nägeli, C., Laverge, J., Delghust, M., Mata, É., Van Hove, M., Webster, J., Federico, F., Jakob, M., & Camarasa, C. (2020). Developing a common approach for classifying building stock energy models. *Renewable and Sustainable Energy Reviews*, *133*, 110276. https://doi.org/10.1016/j.rser.2020.110276

Ledoux, H. (2021). Semantic 3d city models [Licensed under a Creative Commons Attribution 4.0 International License]. https://3d.bk.tudelft.nl/courses/backup/geo1004/2020/data/handout6.1.pdf

Leon-Sanchez, C., Giannelli, D., Agugiaro, G., & Stoter, J. (2021). Testing the new 3d bag dataset for energy demand estimation of residential buildings [6th International Conference on Smart Data and Smart Cities, SDSC 2021 ; Conference date: 15-09-2021 Through 17-09-2021]. *International Archives of the Photogrammetry, Remote Sensing and Spatial Information Sciences*, *46*(4/W1-2021), 69–76. https://doi.org/10.5194/isprs-archives-XLVI-4-W1-2021-69-2021

León-Sánchez, C., Agugiaro, G., & Stoter, J. (2022a). Creation of a citygml-based 3d city model testbed for energy-related appications [7th International Conference on Smart Data and

Smart Cities, SDSC 2022 ; Conference date: 19-10-2022 Through 21-10-2022]. *International Archives of the Photogrammetry, Remote Sensing and Spatial Information Sciences - ISPRS Archives*, *48*(4/W5-2022), 97–103. https://doi.org/10.5194/isprs-archives-XLVIII-4-W5-2022-97-2022

León-Sánchez, C., Agugiaro, G., & Stoter, J. (2022b). Creation of a citygml-based 3d city model testbed for energy-related applications. *The International Archives of the Photogrammetry, Remote Sensing and Spatial Information Sciences*, *XLVIII-4/W5-2022*, 97–103. https://doi.org/10.5194/isprs-archives-XLVIII-4-W5-2022-97-2022

Loga, T., Diefenbach, N., Stein, B., et al. (2012). Iee project tabula - typology approach for building stock energy assessment. https://episcope.eu/iee-project/tabula/

Majcen, D., Itard, L., & Visscher, H. (2013). Actual and theoretical gas consumption in dutch dwellings: What causes the differences? *Energy Policy*, *61*, 460–471.

Ministerie van Binnenlandse Zaken en Koninkrijksrelaties. (2011). Bouwbesluit 2012. *Building Decree*, *31*, 2022.

Ministerie van Binnenlandse Zaken en Koninkrijksrelaties. (2023, February). Voorbeeldwoningen bestaande bouw. https://www.rvo.nl/onderwerpen/wetten-en-regels-gebouwen/voorbeeldwoningen-bestaande-bouw

Monien, D., Strzalka, A., Koukofikis, A., et al. (2017). Comparison of building modelling assumptions and methods for urban scale heat demand forecasting. *Future Cities and Environment*, *3*(2). https://doi.org/10.1186/s40984-017-0025-7

Morton, A. (n.d.). *Utm grid zones of the world*. http://www.dmap.co.uk/utmworld.htm

Mutani, G., Coccolo, S., Kaempf, J., & Bilardo, M. (2018, September). *Citysim guide: Urban energy modelling*. CreateSpace Independent Publishing Platform.

NEN. (2024, January). *Nta 8800: Energy performance of buildings - determination method* [NTA 8800:2024 nl, Current Standard. Replaces NTA 8800:2023 nl]. NEN.

Open Geospatial Consortium. (2023). Citygml standards. https://www.ogc.org/standards/

Pulumbarit, M. (2023). Horizon file format. *HelioScope, an Aurora Inc. Company*. https://helpcenter.helioscope.com/hc/en-us/articles/8317031304979-Horizon-File-Format

Robinson, D., Haldi, F., Leroux, P., Perez, D., Rasheed, A., & Wilke, U. (2009). Citysim: Comprehensive micro-simulation of resource flows for sustainable urban planning. *Proceedings of the Eleventh International IBPSA Conference*, 1083–1090. https://doi.org/10.26868/25222708.2009.1083-1090

Saiedian, H. (1997). An evaluation of extended entity-relationship model. *Information and Software Technology*, *39*(7), 449–462. https://doi.org/10.1016/S0950-5849(97)00002-5

Salim, F. D., Dong, B., Ouf, M., Wang, Q., Pigliautile, I., Kang, X., Hong, T., Wu, W., Liu, Y., Rumi, S. K., Rahaman, M. S., An, J., Deng, H., Shao, W., Dziedzic, J., Sangogboye, F. C., Kjærgaard, M. B., Kong, M., Fabiani, C., … Yan, D. (2020). Modelling urban-scale occupant behaviour, mobility, and energy in buildings: A survey. *Building and Environment*, *183*, 106964. https://doi.org/10.1016/j.buildenv.2020.106964

SimStadt. (2023). Simstadt. https://simstadt.hft-stuttgart.de

Sola, A., Corchero, C., Salom, J., & Sanmarti, M. (2020). Multi-domain urban-scale energy modelling tools: A review. *Sustainable Cities and Society*, *54*, 101872. https://doi.org/10.1016/j.scs.2019.101872

Srivastava, R. N. (2008). Spatial data quality: An introduction. *Geography Realm*. https://www.geographyrealm.com/spatial-data-quality-an-introduction/

Swan, L. G., & Ugursal, V. I. (2009). Modeling of end-use energy consumption in the residential sector: A review of modeling techniques. *Renewable and Sustainable Energy Reviews*, *13*(8), 1819–1835. https://ideas.repec.org/a/eee/rensus/v13y2009i8p1819-1835.html

Technische Universiteit Delft. (n.d.). *Energieberekening*. https://www.tudelft.nl/beyondthecurrent/benadering/energieberekening

The CEA Team. (2024). The city energy analyst (version 3.35.6). https://doi.org/10.5281/zenodo.598221

van den Brom, P. (2020). Energy in dwellings: A comparison between theory and practice. *A+BE | Architecture and the Built Environment*. https://doi.org/10.7480/abe.2020.3

Watt, A. (2014). *Database design - 2nd edition*. Open University. https://opentextbc.ca/dbdesign01/chapter/chapter-13-database-development-process/

Yang, X., Hu, M., Heeren, N., Zhang, C., Verhagen, T., Tukker, A., & Steubing, B. (2020). A combined gis-archetype approach to model residential space heating energy: A case study for the netherlands including validation. *Applied Energy*, *280*, 115953. https://doi.org/10.1016/j.apenergy.2020.115953

Yao, Z., Nagel, C., Kunde, F., Hudra, G., Willkomm, P., Donaubauer, A., Adolphi, T., & Kolbe, T. H. (2018). 3dcitydb - a 3d geodatabase solution for the management, analysis, and visualization of semantic 3d city models based on CityGML. *Open Geospatial Data, Software and Standards*, *3*(1), 5. https://doi.org/10.1186/s40965-018-0046-7

Yoshino, H., Murakami, S., Akabayashi, S., Kurabuchi, T., Kato, S., Tanabe, S., & Adachi, M. (2004). Survey on minimum ventilation rate of residential buildings in fifteen countries. *Proceedings of the 25th AIVC Conference-Ventilation and retrofitting, Prague*, 227–238.

A

Enlarged mind maps

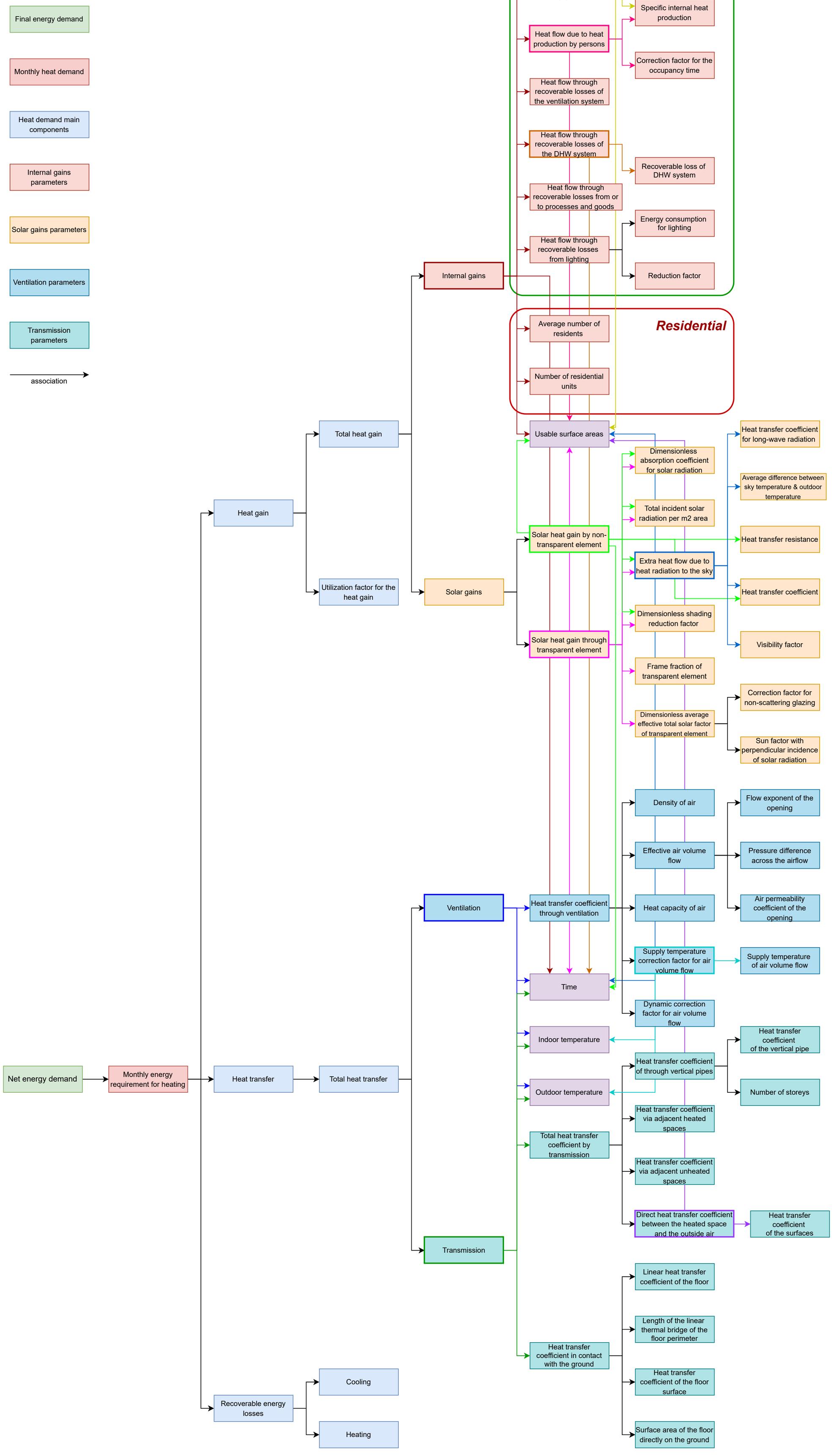
Legend
Final energy demand
Monthly heat demand
Heat demand main components
Internal gains parameters
Solar gains parameters
Ventilation parameters
Transmission parameters
association
Non-Residential
Heat flow due to heat production by equipment
Specific internal heat production
Heat flow due to heat production by persons
Correction factor for the occupancy time
Heat flow through recoverable losses of the ventilation system
Heat flow through recoverable losses of the DHW system
Recoverable loss of DHW system
Heat flow through recoverable losses from or to processes and goods
Energy consumption for lighting
Heat flow through recoverable losses from lighting
Reduction factor
Internal gains
Residential
Average number of residents
Number of residential units
Usable surface areas
Heat transfer coefficient for long-wave radiation
Dimensionless absorption coefficient for solar radiation
Average difference between sky temperature & outdoor temperature
Total incident solar radiation per m2 area
Heat gain
Total heat gain
Solar heat gain by non-transparent element
Heat transfer resistance
Extra heat flow due to heat radiation to the sky
Heat transfer coefficient
Utilization factor for the heat gain
Solar gains
Dimensionless shading reduction factor
Solar heat gain through transparent element
Visibility factor
Frame fraction of transparent element
Correction factor for non-scattering glazing
Dimensionless average effective total solar factor of transparent element
Sun factor with perpendicular incidence of solar radiation
Density of air
Flow exponent of the opening
Effective air volume flow
Pressure difference across the airflow
Heat capacity of air
Air permeability coefficient of the opening
Supply temperature correction factor for air volume flow
Supply temperature of air volume flow
Ventilation
Heat transfer coefficient through ventilation
Time
Dynamic correction factor for air volume flow
Indoor temperature
Heat transfer coefficient of through vertical pipes
Heat transfer coefficient of the vertical pipe
Outdoor temperature
Number of storeys
Heat transfer coefficient via adjacent heated spaces
Total heat transfer coefficient by transmission
Heat transfer coefficient via adjacent unheated spaces
Direct heat transfer coefficient between the heated space and the outside air
Heat transfer coefficient of the surfaces
Transmission
Linear heat transfer coefficient of the floor
Length of the linear thermal bridge of the floor perimeter
Heat transfer coefficient in contact with the ground
Heat transfer coefficient of the floor surface
Surface area of the floor directly on the ground
Net energy demand
Monthly energy requirement for heating
Heat transfer
Total heat transfer
Recoverable energy losses
Cooling
Heating

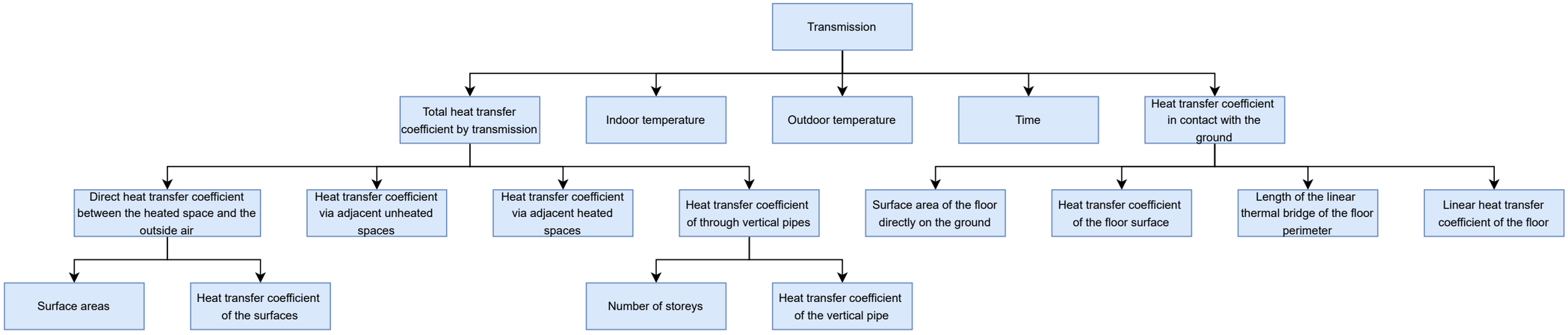
Transmission
Total heat transfer coefficient by transmission
Indoor temperature
Outdoor temperature
Time
Heat transfer coefficient in contact with the ground
Direct heat transfer coefficient between the heated space and the outside air
Heat transfer coefficient via adjacent unheated spaces
Heat transfer coefficient via adjacent heated spaces
Heat transfer coefficient of through vertical pipes
Surface area of the floor directly on the ground
Heat transfer coefficient of the floor surface
Length of the linear thermal bridge of the floor perimeter
Linear heat transfer coefficient of the floor
Surface areas
Heat transfer coefficient of the surfaces
Number of storeys
Heat transfer coefficient of the vertical pipe

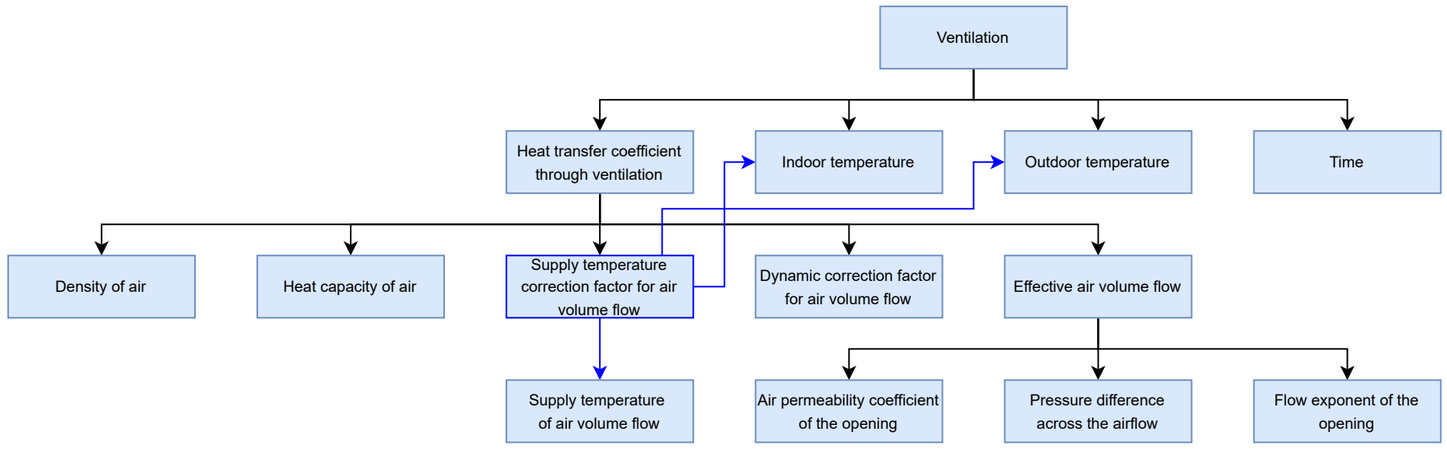
Ventilation
Heat transfer coefficient through ventilation
Indoor temperature
Outdoor temperature
Time
Density of air
Heat capacity of air
Supply temperature correction factor for air volume flow
Dynamic correction factor for air volume flow
Effective air volume flow
Supply temperature of air volume flow
Air permeability coefficient of the opening
Pressure difference across the airflow
Flow exponent of the opening

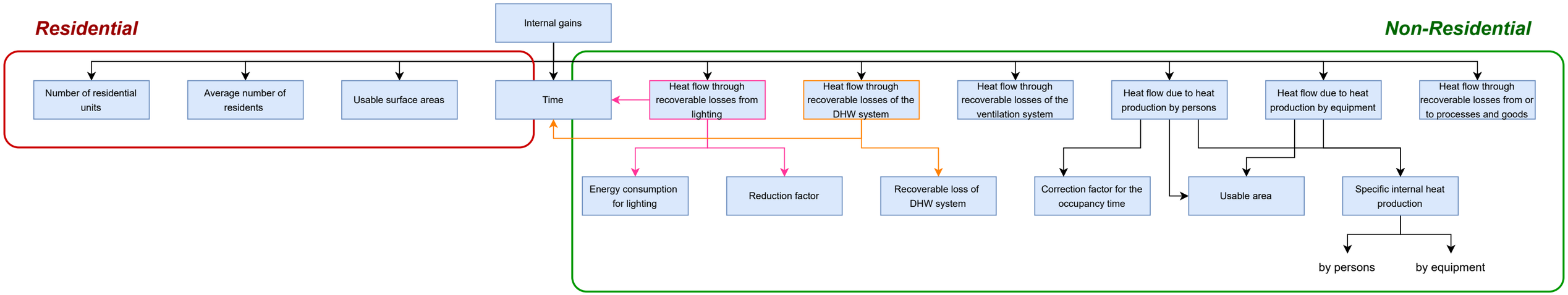
Residential
Internal gains
Non-Residential
Number of residential units
Average number of residents
Usable surface areas
Time
Heat flow through recoverable losses from lighting
Heat flow through recoverable losses of the DHW system
Heat flow through recoverable losses of the ventilation system
Heat flow due to heat production by persons
Heat flow due to heat production by equipment
Heat flow through recoverable losses from or to processes and goods
Energy consumption for lighting
Reduction factor
Recoverable loss of DHW system
Correction factor for the occupancy time
Usable area
Specific internal heat production
by persons
by equipment

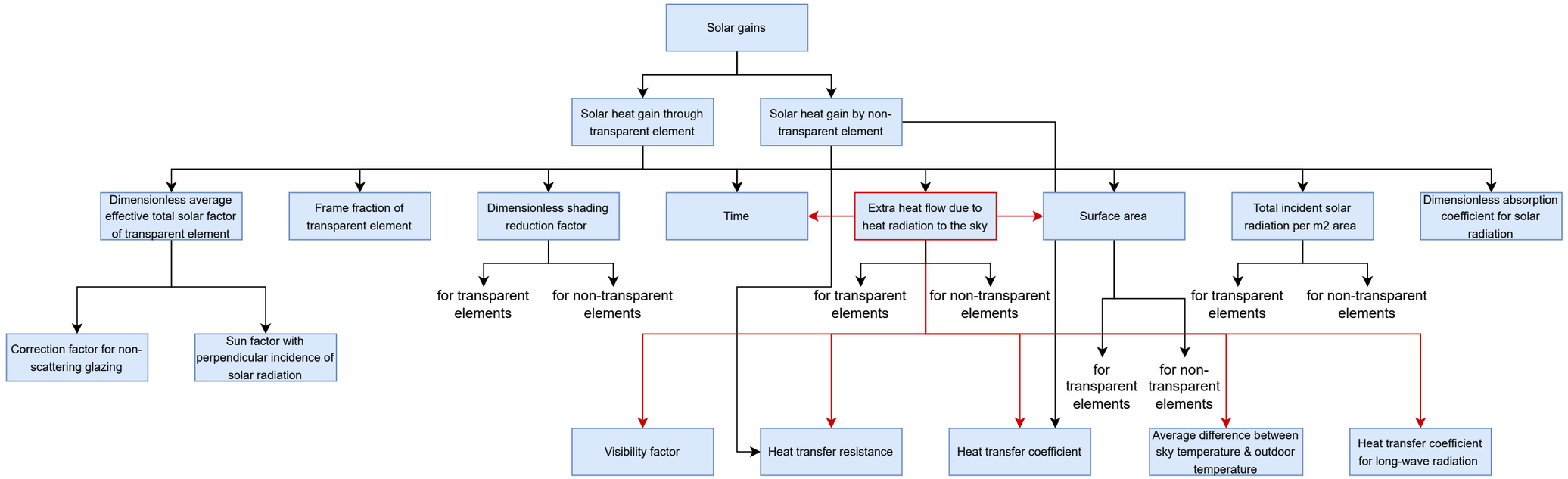
Solar gains
Solar heat gain through transparent element
Solar heat gain by non-transparent element
Dimensionless average effective total solar factor of transparent element
Frame fraction of transparent element
Dimensionless shading reduction factor
Time
Extra heat flow due to heat radiation to the sky
Surface area
Total incident solar radiation per m2 area
Dimensionless absorption coefficient for solar radiation
Correction factor for non-scattering glazing
Sun factor with perpendicular incidence of solar radiation
for transparent elements
for non-transparent elements
for transparent elements
for non-transparent elements
for transparent elements
for non-transparent elements
for transparent elements
for non-transparent elements
Visibility factor
Heat transfer resistance
Heat transfer coefficient
Average difference between sky temperature & outdoor temperature
Heat transfer coefficient for long-wave radiation

B

NTA 8800 Tables

B.1. Shading reduction factor

Orientation	South												
Month	90°	75°	60°	45°	30°	15°	0°	105°	120°	135°	150°	165°	180°
January	0,23	0,24	0,26	0,29	0,34	0,42	1,00	0,23	0,23	0,26	0,35	0,82	1,00
February	0,91	0,92	0,92	0,93	0,94	0,95	1,00	0,91	0,91	0,91	0,92	0,99	1,00
March	1,00	1,00	1,00	1,00	1,00	1,00	1,00	1,00	0,99	0,99	1,00	1,00	1,00
April	1,00	1,00	1,00	1,00	0,99	0,99	1,00	1,00	1,00	1,00	1,00	1,00	1,00
May	1,00	1,00	0,99	0,99	0,98	0,97	1,00	1,00	1,00	1,00	1,00	1,00	1,00
June	1,00	0,99	0,97	0,96	0,94	0,92	1,00	1,00	1,00	1,00	1,00	1,00	1,00
July	1,00	1,00	0,99	0,98	0,97	0,96	1,00	1,00	1,00	1,00	1,00	1,00	1,00
August	1,00	1,00	1,00	0,99	0,99	0,99	1,00	1,00	1,00	1,00	1,00	1,00	1,00
September	1,00	1,00	1,00	1,00	1,00	1,00	1,00	1,00	1,00	1,00	1,00	1,00	1,00
October	0,97	0,97	0,97	0,97	0,98	0,98	1,00	0,96	0,96	0,96	0,97	0,99	1,00
November	0,61	0,62	0,64	0,66	0,69	0,73	1,00	0,61	0,61	0,62	0,67	0,95	1,00
December	0,19	0,21	0,23	0,27	0,32	0,42	1,00	0,19	0,20	0,22	0,31	0,75	1,00

Table B.1: Shading reduction factor ($F_{sh,obst,m}$) for heat demand calculation for south facing surfaces (NEN, 2024)

Orientation	Southwest												
Month	90°	75°	60°	45°	30°	15°	0°	105°	120°	135°	150°	165°	180°
January	0,49	0,51	0,53	0,57	0,61	0,68	1,00	0,47	0,46	0,46	0,50	0,80	1,00
February	0,83	0,85	0,86	0,87	0,89	0,90	1,00	0,82	0,80	0,80	0,83	0,95	1,00
March	0,93	0,94	0,94	0,94	0,94	0,93	1,00	0,92	0,91	0,91	0,93	0,98	1,00
April	0,92	0,93	0,93	0,93	0,91	0,90	1,00	0,91	0,90	0,90	0,93	0,99	1,00
May	0,99	0,98	0,97	0,95	0,93	0,90	1,00	0,99	0,98	0,98	0,99	1,00	1,00
June	1,00	0,99	0,97	0,94	0,91	0,87	1,00	1,00	1,00	1,00	1,00	1,00	1,00
July	1,00	0,99	0,96	0,93	0,90	0,86	1,00	1,00	1,00	1,00	1,00	1,00	1,00
August	0,99	0,98	0,98	0,96	0,95	0,92	1,00	0,98	0,98	0,98	0,99	1,00	1,00
September	0,91	0,91	0,91	0,91	0,90	0,90	1,00	0,90	0,89	0,89	0,91	0,99	1,00
October	0,88	0,89	0,89	0,90	0,91	0,91	1,00	0,87	0,85	0,85	0,87	0,96	1,00
November	0,71	0,72	0,74	0,77	0,80	0,84	1,00	0,69	0,68	0,68	0,72	0,93	1,00
December	0,58	0,60	0,62	0,65	0,69	0,74	1,00	0,57	0,56	0,57	0,59	0,85	1,00

Table B.2: Shading reduction factor ($F_{sh,obst,m}$) for heat demand calculation for southwest facing surfaces (NEN, 2024)

Orientation	Southeast												
Month	90°	75°	60°	45°	30°	15°	0°	105°	120°	135°	150°	165°	180°
January	0.48	0.50	0.53	0.56	0.60	0.66	1.00	0.47	0.46	0.47	0.54	0.87	1.00
February	0.81	0.83	0.85	0.86	0.88	0.90	1.00	0.80	0.79	0.78	0.80	0.94	1.00
March	0.87	0.88	0.89	0.89	0.90	0.90	1.00	0.86	0.85	0.85	0.88	0.97	1.00
April	0.95	0.95	0.94	0.93	0.91	0.88	1.00	0.95	0.94	0.94	0.96	1.00	1.00
May	1.00	1.00	0.98	0.96	0.93	0.89	1.00	1.00	1.00	1.00	1.00	1.00	1.00
June	1.00	1.00	0.98	0.96	0.92	0.88	1.00	0.99	0.99	1.00	1.00	1.00	1.00
July	0.99	0.99	0.98	0.96	0.93	0.90	1.00	0.99	0.99	0.99	1.00	1.00	1.00
August	0.98	0.98	0.96	0.94	0.92	0.88	1.00	0.97	0.97	0.97	0.99	1.00	1.00
September	0.92	0.92	0.92	0.92	0.91	0.90	1.00	0.91	0.90	0.89	0.92	0.99	1.00
October	0.86	0.87	0.88	0.89	0.90	0.91	1.00	0.85	0.84	0.83	0.84	0.96	1.00
November	0.70	0.72	0.74	0.76	0.79	0.83	1.00	0.69	0.67	0.67	0.69	0.91	1.00
December	0.40	0.42	0.44	0.48	0.53	0.60	1.00	0.39	0.39	0.40	0.47	0.81	1.00

Table B.3: Shading reduction factor ($F_{sh,obst,m}$) for heat demand calculation for southeast facing surfaces (NEN, 2024)

Orientation	West												
Month	90°	75°	60°	45°	30°	15°	0°	105°	120°	135°	150°	165°	180°
January	0.85	0.86	0.86	0.86	0.84	0.81	1.00	0.83	0.82	0.82	0.84	0.91	1.00
February	0.85	0.86	0.86	0.85	0.83	0.79	1.00	0.83	0.83	0.84	0.88	0.97	1.00
March	0.89	0.89	0.88	0.86	0.82	0.77	1.00	0.87	0.87	0.88	0.91	0.97	1.00
April	0.82	0.82	0.81	0.79	0.75	0.70	1.00	0.80	0.79	0.80	0.85	0.96	1.00
May	0.88	0.87	0.84	0.80	0.75	0.69	1.00	0.87	0.86	0.87	0.91	0.98	1.00
June	0.93	0.92	0.90	0.86	0.81	0.75	1.00	0.92	0.92	0.92	0.95	0.99	1.00
July	0.92	0.91	0.89	0.85	0.79	0.73	1.00	0.91	0.91	0.91	0.94	0.99	1.00
August	0.89	0.88	0.86	0.83	0.79	0.74	1.00	0.88	0.87	0.88	0.91	0.98	1.00
September	0.85	0.85	0.83	0.81	0.77	0.72	1.00	0.84	0.84	0.85	0.89	0.97	1.00
October	0.83	0.85	0.86	0.86	0.84	0.79	1.00	0.82	0.82	0.83	0.88	0.97	1.00
November	0.90	0.92	0.93	0.92	0.90	0.86	1.00	0.89	0.89	0.89	0.92	0.98	1.00
December	0.87	0.86	0.85	0.85	0.82	0.79	1.00	0.86	0.85	0.85	0.88	0.95	1.00

Table B.4: Shading reduction factor ($F_{sh,obst,m}$) for heat demand calculation for west facing surfaces (NEN, 2024)

Orientation	East												
Month	90°	75°	60°	45°	30°	15°	0°	105°	120°	135°	150°	165°	180°
January	0.92	0.93	0.93	0.92	0.90	0.86	1.00	0.91	0.90	0.90	0.92	0.96	1.00
February	0.79	0.81	0.82	0.83	0.83	0.81	1.00	0.77	0.76	0.77	0.83	0.96	1.00
March	0.82	0.84	0.84	0.83	0.81	0.78	1.00	0.81	0.80	0.81	0.87	0.96	1.00
April	0.91	0.92	0.91	0.88	0.83	0.77	1.00	0.90	0.90	0.90	0.93	0.98	1.00
May	0.95	0.96	0.93	0.89	0.83	0.76	1.00	0.94	0.94	0.95	0.96	0.99	1.00
June	0.90	0.91	0.89	0.85	0.80	0.73	1.00	0.89	0.89	0.90	0.93	0.99	1.00
July	0.93	0.94	0.92	0.89	0.84	0.79	1.00	0.92	0.92	0.92	0.95	0.99	1.00
August	0.94	0.95	0.93	0.88	0.82	0.75	1.00	0.94	0.94	0.94	0.96	0.99	1.00
September	0.87	0.88	0.88	0.86	0.84	0.79	1.00	0.86	0.85	0.86	0.90	0.98	1.00
October	0.84	0.83	0.83	0.81	0.78	0.74	1.00	0.83	0.82	0.83	0.87	0.96	1.00
November	0.92	0.90	0.88	0.86	0.83	0.79	1.00	0.91	0.90	0.90	0.91	0.96	1.00
December	0.86	0.87	0.89	0.90	0.90	0.88	1.00	0.84	0.83	0.83	0.86	0.94	1.00

Table B.5: Shading reduction factor ($F_{sh,obst,m}$) for heat demand calculation for east facing surfaces (NEN, 2024)

Orientation	Northwest												
Month	90°	75°	60°	45°	30°	15°	0°	105°	120°	135°	150°	165°	180°
January	0.97	0.97	0.98	0.97	0.94	0.77	1.00	0.98	0.98	0.99	0.99	1.00	1.00
February	0.97	0.97	0.96	0.93	0.87	0.74	1.00	0.97	0.97	0.97	0.98	0.99	1.00
March	0.96	0.96	0.94	0.89	0.79	0.67	1.00	0.96	0.96	0.96	0.97	0.99	1.00
April	0.87	0.87	0.85	0.79	0.69	0.58	1.00	0.87	0.87	0.88	0.92	0.98	1.00
May	0.85	0.83	0.78	0.70	0.61	0.53	1.00	0.84	0.85	0.87	0.92	0.98	1.00
June	0.91	0.88	0.83	0.75	0.66	0.59	1.00	0.90	0.90	0.92	0.94	0.98	1.00
July	0.90	0.88	0.84	0.77	0.67	0.59	1.00	0.90	0.90	0.91	0.94	0.99	1.00
August	0.88	0.86	0.83	0.76	0.66	0.58	1.00	0.87	0.88	0.89	0.93	0.99	1.00
September	0.96	0.96	0.93	0.87	0.76	0.63	1.00	0.96	0.96	0.96	0.97	0.99	1.00
October	0.97	0.98	0.96	0.92	0.82	0.66	1.00	0.97	0.98	0.98	0.99	1.00	1.00
November	0.99	0.99	0.98	0.97	0.93	0.75	1.00	0.99	0.99	0.99	0.99	1.00	1.00
December	1.00	1.00	1.00	1.00	0.99	0.86	1.00	1.00	1.00	1.00	1.00	1.00	1.00

Table B.6: Shading reduction factor ($F_{sh,obst,m}$) for heat demand calculation for northwest facing surfaces (NEN, 2024)

Orientation	Northeast												
Month	90°	75°	60°	45°	30°	15°	0°	105°	120°	135°	150°	165°	180°
January	1.00	0.99	0.99	0.99	0.95	0.79	1.00	1.00	1.00	1.00	1.00	1.00	1.00
February	0.96	0.96	0.95	0.92	0.85	0.73	1.00	0.96	0.96	0.97	0.98	1.00	1.00
March	0.97	0.96	0.93	0.88	0.78	0.66	1.00	0.97	0.97	0.97	0.98	0.99	1.00
April	0.97	0.94	0.89	0.80	0.68	0.56	1.00	0.97	0.97	0.97	0.98	0.99	1.00
May	0.93	0.90	0.84	0.74	0.63	0.53	1.00	0.94	0.94	0.95	0.97	1.00	1.00
June	0.88	0.88	0.85	0.78	0.68	0.60	1.00	0.87	0.88	0.90	0.94	0.99	1.00
July	0.91	0.91	0.87	0.81	0.72	0.64	1.00	0.91	0.91	0.92	0.95	0.99	1.00
August	0.98	0.95	0.89	0.80	0.67	0.55	1.00	0.98	0.98	0.98	0.99	1.00	1.00
September	0.97	0.96	0.93	0.85	0.75	0.62	1.00	0.97	0.97	0.97	0.98	0.99	1.00
October	0.96	0.96	0.95	0.90	0.80	0.66	1.00	0.96	0.96	0.96	0.98	0.99	1.00
November	0.98	0.97	0.96	0.95	0.90	0.73	1.00	0.98	0.98	0.99	1.00	1.00	1.00
December	1.00	1.00	1.00	0.99	0.98	0.84	1.00	1.00	1.00	1.00	1.00	1.00	1.00

Table B.7: Shading reduction factor ($F_{sh,obst,m}$) for heat demand calculation for northeast facing surfaces (NEN, 2024)

Orientation	North												
Month	90°	75°	60°	45°	30°	15°	0°	105°	120°	135°	150°	165°	180°
January	1.00	1.00	1.00	1.00	1.00	0.95	1.00	1.00	1.00	1.00	1.00	1.00	1.00
February	1.00	1.00	1.00	1.00	1.00	0.78	1.00	1.00	1.00	1.00	1.00	1.00	1.00
March	1.00	1.00	1.00	1.00	0.82	0.61	1.00	1.00	1.00	1.00	1.00	1.00	1.00
April	0.99	0.98	0.96	0.84	0.57	0.44	1.00	0.99	0.99	0.99	1.00	1.00	1.00
May	0.97	0.96	0.89	0.65	0.51	0.43	1.00	0.97	0.97	0.98	0.99	1.00	1.00
June	0.97	0.96	0.86	0.68	0.58	0.51	1.00	0.97	0.97	0.98	0.98	0.99	1.00
July	0.97	0.96	0.87	0.69	0.58	0.51	1.00	0.97	0.97	0.98	0.98	1.00	1.00
August	0.98	0.97	0.94	0.74	0.55	0.45	1.00	0.98	0.98	0.99	0.99	1.00	1.00
September	1.00	1.00	0.99	0.96	0.72	0.53	1.00	1.00	1.00	1.00	1.00	1.00	1.00
October	1.00	1.00	1.00	1.00	0.96	0.66	1.00	1.00	1.00	1.00	1.00	1.00	1.00
November	1.00	1.00	1.00	1.00	1.00	0.86	1.00	1.00	1.00	1.00	1.00	1.00	1.00
December	1.00	1.00	1.00	1.00	1.00	1.00	1.00	1.00	1.00	1.00	1.00	1.00	1.00

Table B.8: Shading reduction factor ($F_{sh,obst,m}$) for heat demand calculation for north facing surfaces (NEN, 2024)

B.2. Incident solar radiation

β	0°	30°						
γ	–	180°S	225°SW	270°W	315°NW	360°N	45°NE	90°E	135°SE
January	28,0	50,5	44,4	29,0	16,2	14,9	15,8	26,9	42,2
February	49,3	69,1	61,2	46,2	32,9	27,2	34,5	49,4	63,7
March	96,6	122,5	109,3	87,7	66,7	56,4	72,8	97,6	117,7
April	160,5	189,5	174,5	146,5	115,6	104,6	125,1	158,9	184,1
May	197,0	211,1	201,5	179,9	155,8	148,5	160,6	186,3	206,3
June	209,3	211,2	210,7	199,4	180,6	171,0	173,0	189,7	204,4
July	191,0	196,1	193,2	180,2	162,1	153,0	156,9	175,0	190,0
August	177,2	197,9	198,3	178,4	147,6	125,8	127,5	152,8	179,3
September	123,9	154,0	146,2	121,1	91,6	73,7	86,5	113,7	140,1
October	73,2	102,4	91,5	68,8	47,3	36,3	48,9	71,6	93,6
November	34,3	54,8	47,7	32,9	20,5	18,6	20,9	33,8	48,6
December	21,0	38,3	32,6	20,6	12,5	12,2	12,5	21,2	33,1

Table B.9: Monthly average total incident solar radiation, $I_{sol,m,i}$ averaged over all hours for inclination angles 0-30; ground reflection coefficient ρ = 0.2 (NEN, 2024)

β				45°				
γ	180°S	225°SW	270°W	315°NW	360°N	45°NE	90°E	135°SE
January	57,9	49,4	28,7	14,9	14,3	14,5	26,2	46,3
February	74,1	63,2	44,0	29,2	25,9	30,4	47,9	66,5
March	126,6	109,1	82,0	56,6	44,3	63,1	94,2	120,2
April	189,7	171,0	136,7	96,5	70,0	107,1	152,2	183,5
May	202,7	191,1	164,4	128,7	113,6	134,5	172,0	197,3
June	197,3	199,3	186,2	156,3	139,6	145,9	173,3	190,7
July	185,0	182,5	166,8	139,0	123,5	132,7	160,4	179,1
August	193,5	194,9	169,8	127,2	91,5	102,9	137,9	171,0
September	157,6	147,0	115,3	78,0	52,9	72,2	106,2	139,2
October	109,4	94,2	64,8	40,2	33,5	41,4	68,4	97,2
November	61,0	51,1	31,3	18,5	17,8	18,8	32,4	52,2
December	44,1	36,1	19,9	11,7	11,7	11,7	20,5	36,7

Table B.10: Monthly average total incident solar radiation, $I_{sol,m,i}$ averaged over all hours for inclination angles 45; ground reflection coefficient $\rho = 0.2$ (NEN, 2024)

β				60°				
γ	180°S	225°SW	270°W	315°NW	360°N	45°NE	90°E	135°SE
January	62,2	51,8	27,8	13,8	13,4	13,5	24,7	48,1
February	75,4	62,1	41,1	26,4	24,1	27,3	45,4	66,3
March	124,3	103,9	74,8	49,6	41,5	56,3	88,5	116,9
April	180,2	160,4	125,1	83,1	57,8	93,9	142,0	174,2
May	184,5	173,4	146,3	107,5	78,5	113,2	154,7	179,9
June	175,1	180,9	169,1	134,1	102,9	123,3	154,5	170,7
July	165,9	165,4	150,6	119,2	90,4	112,3	143,2	161,8
August	179,7	182,9	156,9	110,2	68,0	85,8	122,0	156,4
September	153,3	141,5	107,2	68,6	48,6	62,3	97,2	132,6
October	110,7	92,6	59,9	35,9	31,5	36,6	63,5	96,0
November	63,9	51,8	28,9	17,0	16,6	17,3	30,4	53,2
December	47,4	37,6	19,0	10,9	10,9	10,9	19,6	38,4

Table B.11: Monthly average total incident solar radiation, $I_{sol,m,i}$ averaged over all hours for inclination angles 60; ground reflection coefficient $\rho = 0.2$ (NEN, 2024)

β				90°				
γ	180°S	225°SW	270°W	315°NW	360°N	45°NE	90°E	135°SE
January	60,1	48,1	23,4	11,4	11,1	11,1	20,2	43,9
February	66,7	52,2	32,8	20,9	19,5	21,5	36,5	56,8
March	101,8	82,1	57,3	38,5	34,8	44,2	70,7	95,4
April	135,1	121,9	96,2	64,1	49,4	72,9	112,2	135,8
May	124,9	122,1	107,3	78,9	61,9	82,9	114,6	128,4
June	112,7	127,8	125,7	97,8	73,0	92,0	114,8	118,0
July	109,7	117,1	112,7	88,5	66,7	81,2	104,9	113,2
August	128,5	137,1	120,0	83,1	55,9	63,9	89,0	112,4
September	122,3	112,2	83,9	53,6	41,4	47,9	73,7	103,6
October	96,2	76,3	46,7	28,7	26,4	29,1	49,8	80,3
November	59,5	45,6	22,7	13,8	13,6	14,0	23,9	47,1
December	46,2	34,9	15,2	8,9	8,9	8,9	15,9	35,8

Table B.12: Monthly average total incident solar radiation, $I_{sol,m,i}$ averaged over all hours for inclination angles 90; ground reflection coefficient ρ = 0.2 (NEN, 2024)

β				135°					180°
γ	180°S	225°SW	270°W	315°NW	360°N	45°NE	90°E	135°SE	–
January	33,4	25,1	12,7	7,6	7,5	7,5	10,6	22,2	5,6
February	31,5	24,2	17,3	13,2	12,9	13,5	18,6	26,7	9,8
March	37,3	35,1	29,9	25,2	24,5	27,6	36,7	42,0	19,3
April	39,0	50,7	49,9	41,8	38,3	45,5	57,1	56,3	32,1
May	45,5	50,4	55,2	50,7	46,7	51,9	57,8	51,9	39,3
June	48,3	52,3	62,4	57,8	50,6	55,4	59,9	51,7	41,8
July	44,9	49,7	57,7	53,5	46,5	48,9	53,0	48,0	38,2
August	41,6	54,3	59,6	50,2	42,1	42,9	47,7	47,5	35,3
September	40,2	47,5	43,2	33,8	30,4	31,4	37,9	43,2	24,7
October	41,6	33,2	24,7	19,3	18,6	19,4	25,4	35,2	14,6
November	30,9	21,7	12,0	9,2	9,1	9,3	12,7	22,7	6,9
December	26,3	18,3	8,1	5,8	5,8	5,8	8,4	19,0	4,2

Table B.13: Monthly average total incident solar radiation, $I_{sol,m,i}$ averaged over all hours for inclination angles 135-180; ground reflection coefficient ρ = 0.2 (NEN, 2024)

C

Building data specification

Building ID	Year	Function	Typology	Perimeter	Cadastre units	Usable area
Pand ID 1742100000004574	1923	residential	VW	34.45	1	144 m^2
Pand ID 1742100000006518	1965	residential	TOEK	26.14	1	90 m^2

Table C.1: Building specification for the testing

Building ID	Element	U-value
Pand ID 1742100000004574	Ground Surface	2,33
Pand ID 1742100000004574	Wall Surface	1,67
Pand ID 1742100000004574	Roof Surface	0,97
Pand ID 1742100000004574	Windows	5.1
Pand ID 1742100000004574	Door	3,4
Pand ID 1742100000006518	Ground Surface	1.37
Pand ID 1742100000006518	Wall Surface	1.23
Pand ID 1742100000006518	Roof Surface	0.88
Pand ID 1742100000006518	Windows	2,82
Pand ID 1742100000006518	Door	3,34

Table C.2: Surface u-values attributes of the two test buildings

Building	Element	Attributes
1	Ventilation	Natural complete
1	Space Heating	HR107 boiler
2	Ventilation	Natural complete
2	Space Heating	HR107 boiler

Table C.3: Ventilation and heating system attributes of the two test buildings

Building	Surface	Lod2 Area	Azimuth	Inclination
NL.IMBAG.Pand.1742100000004574	GroundSurface	74	-1	180
NL.IMBAG.Pand.1742100000004574	WallSurface	48	88.6	90
NL.IMBAG.Pand.1742100000004574	WallSurface	32	358.5	90
NL.IMBAG.Pand.1742100000004574	WallSurface	33	178.5	90
NL.IMBAG.Pand.1742100000004574	WallSurface	48	268.6	90
NL.IMBAG.Pand.1742100000004574	RoofSurface	52	357.7	45
NL.IMBAG.Pand.1742100000004574	RoofSurface	52	178.1	45
NL.IMBAG.Pand.1742100000006518	GroundSurface	42	-1	180
NL.IMBAG.Pand.1742100000006518	WallSurface	34	195.7	90
NL.IMBAG.Pand.1742100000006518	WallSurface	49	285.7	90
NL.IMBAG.Pand.1742100000006518	WallSurface	49	105.7	90
NL.IMBAG.Pand.1742100000006518	WallSurface	32	15.7	90
NL.IMBAG.Pand.1742100000006518	RoofSurface	27	15.3	33.3
NL.IMBAG.Pand.1742100000006518	RoofSurface	23	194.2	33

Table C.4: Surface attributes of the two test buildings

Table C.5: Voorbeeldwoning heating system type per building typology and construction period

Element	Current condition	Period	Building type
Space heater	HR107 boiler	<1965	FW
Space heater	VR-boiler	1965 - 1974	FW
Space heater	HR107 boiler	1975 - 1991	FW
Space heater	HR107 boiler	1992 - 2005	FW
Space heater	HR107 boiler	2006 - 2014	FW
Space heater	HR107 boiler	2015 - 2018	FW
Space heater	HR107 boiler	<1965	GW
Space heater	VR-boiler	1965 - 1974	GW
Space heater	HR107 boiler	1975 - 1991	GW
Space heater	HR107 boiler	1992 - 2005	GW
Space heater	HR107 boiler	2006 - 2014	GW
Space heater	HR107 boiler	2015 - 2018	GW
Space heater	HR107 boiler	<1946	HW
Space heater	HR107 boiler	1946 - 1964	HW

Continued on next page

Table C.5 – continued from previous page

Element	Current condition	Period	Building type
Space heater	HR107 boiler	1965 - 1974	HW
Space heater	HR107 boiler	1975 - 1991	HW
Space heater	HR107 boiler	1992 - 2005	HW
Space heater	HR107 boiler	2006 - 2014	HW
Space heater	HR107 boiler	2015 - 2018	HW
Space heater	HR107 boiler	<1965	MW
Space heater	HR107 boiler	1965 - 1974	MW
Space heater	HR107 boiler	1975 - 1991	MW
Space heater	HR107 boiler	1992 - 2005	MW
Space heater	HR107 boiler	2006 - 2014	MW
Space heater	HR107 boiler	2015 - 2018	MW
Space heater	HR107 boiler	<1946	PW
Space heater	HR107 boiler	1946 - 1964	PW
Space heater	HR107 boiler	1965 - 1974	PW
Space heater	HR107 boiler	1975 - 1991	PW
Space heater	HR107 boiler	1992 - 2005	PW
Space heater	HR107 boiler	2006 - 2014	PW
Space heater	HR107 boiler	2015 - 2018	PW
Space heater	HR107 boiler	<1965	TOEK
Space heater	HR107 boiler	1965 - 1974	TOEK
Space heater	HR107 boiler	1975 - 1991	TOEK
Space heater	HR107 boiler	1992 - 2005	TOEK
Space heater	HR107 boiler	2006 - 2014	TOEK
Space heater	HR107 boiler	2015 - 2018	TOEK
Space heater	HR107 boiler	<1946	TW
Space heater	HR107 boiler	1946 - 1964	TW
Space heater	HR107 boiler	1965 - 1974	TW
Space heater	HR107 boiler	1975 - 1991	TW
Space heater	HR107 boiler	1992 - 2005	TW
Space heater	HR107 boiler	2006 - 2014	TW
Space heater	HR107 boiler	2015 - 2018	TW
Space heater	HR107 boiler	<1965	VW
Space heater	HR107 boiler	1965 - 1974	VW
Space heater	HR107 boiler	1975 - 1991	VW
Space heater	HR107 boiler	1992 - 2005	VW
Space heater	HR107 boiler	2006 - 2014	VW
Space heater	Electric heat pump	2015 - 2018	VW

Table C.6: Voorbeeldwoning 2022 thermal building attributes per building typology and construction period range (Ministerie van Binnenlandse Zaken en Koninkrijksrelaties, 2023)

Building type	Year min	Year max	Current condition	Element
FW	0	1965	1.82	WallSurface
FW	0	1965	3.34	Window
FW	0	1965	3.34	Door
FW	0	1965	1.05	GroundSurface
FW	0	1965	0.93	RoofSurface
FW	0	1965	volledig natuurlijk	ventilatietype
FW	0	1965	A1 standaard	ventilatievoorziening
FW	0	1965	geen warmteterugwinning	type warmteterugwinning
FW	0	1965	forfaitair	kierdichting (q;v10)
FW	0	1965	ketel HR107-ketel	Ruimteverwarming
FW	0	1965	individueel	type ruimteverwarming
FW	0	1965	ketel	toestel ruimteverwarming
FW	0	1965	HR107-ketel	ketel/luchtverwarming
FW	0	1965		lokale verwarming
FW	0	1965	radiatoren	Afgiftesysteem
FW	0	1965	90/70	temperatuurniveau
FW	0	1965	radiatoren	type afgiftesysteem
FW	0	1965	individueel gas combitoestel met gaskeur HR/CW	Warmtapwater
FW	0	1965	individueel	type tapwaterinstallatie
FW	0	1965	gas combitoestel met gaskeur HR/CW	type toestel individiueel
FW	0	1965	CW3	CW-klasse
FW	1965	1974	1.67	WallSurface
FW	1965	1974	2.92	Window
FW	1965	1974	3.27	Door
FW	1965	1974	2.33	GroundSurface
FW	1965	1974	0.9	RoofSurface
FW	1965	1974	natuurlijke toevoer, mechanische afvoer	ventilatietype
FW	1965	1974	C1 standaard	ventilatievoorziening
FW	1965	1974	geen warmteterugwinning	type warmteterugwinning
FW	1965	1974	forfaitair	kierdichting (q;v10)
FW	1965	1974	ketel VR-ketel	Ruimteverwarming
FW	1965	1974	collectief	type ruimteverwarming
FW	1965	1974	ketel	toestel ruimteverwarming
FW	1965	1974	VR-ketel	ketel/luchtverwarming
FW	1965	1974	radiatoren	Afgiftesysteem

Continued on next page

Table C.6 – continued from previous page

Building type	Year min	Year max	Current condition	Element
FW	1965	1974	90/70	temperatuurniveau
FW	1965	1974	radiatoren	type afgiftesysteem
FW	1965	1974	collectief	Warmtapwater
FW	1965	1974	collectief	type tapwaterinstallatie
FW	1965	1974	indirect verwarmd vat	type toestel met extern vat
FW	1965	1974	VR-ketel	type indirect verwarmd vat
FW	1975	1991	0.66	WallSurface
FW	1975	1991	2.95	Window
FW	1975	1991	3.31	Door
FW	1975	1991	0.88	GroundSurface
FW	1975	1991	0.63	RoofSurface
FW	1975	1991	natuurlijke toevoer, mechanische afvoer	ventilatietype
FW	1975	1991	C1 standaard	ventilatievoorziening
FW	1975	1991	geen warmteterugwinning	type warmteterugwinning
FW	1975	1991	forfaitair	kierdichting (q;v10)
FW	1975	1991	ketel HR107-ketel	Ruimteverwarming
FW	1975	1991	individueel	type ruimteverwarming
FW	1975	1991	ketel	toestel ruimteverwarming
FW	1975	1991	HR107-ketel	ketel/luchtverwarming
FW	1975	1991	radiatoren	Afgiftesysteem
FW	1975	1991	90/70	temperatuurniveau
FW	1975	1991	radiatoren	type afgiftesysteem
FW	1975	1991	individueel gas combitoestel met gaskeur HR/CW	Warmtapwater
FW	1975	1991	individueel	type tapwaterinstallatie
FW	1975	1991	gas combitoestel met gaskeur HR/CW	type toestel individiueel
FW	1975	1991	CW3	CW-klasse
FW	1992	2005	0.4	WallSurface
FW	1992	2005	2.37	Window
FW	1992	2005	3.3	Door
FW	1992	2005	0.36	GroundSurface
FW	1992	2005	0.37	RoofSurface
FW	1992	2005	natuurlijke toevoer, mechanische afvoer	ventilatietype
FW	1992	2005	C1 standaard	ventilatievoorziening
FW	1992	2005	geen warmteterugwinning	type warmteterugwinning
FW	1992	2005	forfaitair	kierdichting (q;v10)
FW	1992	2005	ketel HR107-ketel	Ruimteverwarming

Continued on next page

Table C.6 – continued from previous page

Building type	Year min	Year max	Current condition	Element
FW	1992	2005	individueel	type ruimteverwarming
FW	1992	2005	ketel	toestel ruimteverwarming
FW	1992	2005	HR107-ketel	ketel/luchtverwarming
FW	1992	2005	radiatoren	Afgiftesysteem
FW	1992	2005	90/70	temperatuurniveau
FW	1992	2005	radiatoren	type afgiftesysteem
FW	1992	2005	individueel gas combitoestel met gaskeur HR/CW	Warmtapwater
FW	1992	2005	individueel	type tapwaterinstallatie
FW	1992	2005	gas combitoestel met gaskeur HR/CW	type toestel individiueel
FW	1992	2005	CW3	CW-klasse
FW	2006	2014	0.36	WallSurface
FW	2006	2014	2.09	Window
FW	2006	2014	3.31	Door
FW	2006	2014	0.36	GroundSurface
FW	2006	2014	0.35	RoofSurface
FW	2006	2014	natuurlijke toevoer, mechanische afvoer	ventilatietype
FW	2006	2014	C1 standaard	ventilatievoorziening
FW	2006	2014	geen warmteterugwinning	type warmteterugwinning
FW	2006	2014	forfaitair	kierdichting (q;v10)
FW	2006	2014	ketel HR107-ketel	Ruimteverwarming
FW	2006	2014	individueel	type ruimteverwarming
FW	2006	2014	ketel	toestel ruimteverwarming
FW	2006	2014	HR107-ketel	ketel/luchtverwarming
FW	2006	2014	radiatoren	Afgiftesysteem
FW	2006	2014	90/70	temperatuurniveau
FW	2006	2014	radiatoren	type afgiftesysteem
FW	2006	2014	individueel gas combitoestel met gaskeur HR/CW	Warmtapwater
FW	2006	2014	individueel	type tapwaterinstallatie
FW	2006	2014	gas combitoestel met gaskeur HR/CW	type toestel individiueel
FW	2006	2014	CW3	CW-klasse
FW	2015	2018	0.21	WallSurface
FW	2015	2018	1.83	Window
FW	2015	2018	3.07	Door
FW	2015	2018	0.27	GroundSurface
FW	2015	2018	0.16	RoofSurface

Continued on next page

Table C.6 – continued from previous page

Building type	Year min	Year max	Current condition	Element
FW	2015	2018	natuurlijke toevoer, mechanische afvoer	ventilatietype
FW	2015	2018	C1 standaard	ventilatievoorziening
FW	2015	2018	geen warmteterugwinning	type warmteterugwinning
FW	2015	2018	forfaitair	kierdichting (q;v10)
FW	2015	2018	ketel HR107-ketel	Ruimteverwarming
FW	2015	2018	individueel	type ruimteverwarming
FW	2015	2018	ketel	toestel ruimteverwarming
FW	2015	2018	HR107-ketel	ketel/luchtverwarming
FW	2015	2018	vloer/wand/plafond	Afgiftesysteem
FW	2015	2018	45/40	temperatuurniveau
FW	2015	2018	vloer/wand/plafond	type afgiftesysteem
FW	2015	2018	individueel gas combitoestel met gaskeur HR/CW	Warmtapwater
FW	2015	2018	individueel	type tapwaterinstallatie
FW	2015	2018	gas combitoestel met gaskeur HR/CW	type toestel individiueel
FW	2015	2018	CW3	CW-klasse
GW	0	1965	1.56	WallSurface
GW	0	1965	2.89	Window
GW	0	1965	3.3	Door
GW	0	1965	1.72	GroundSurface
GW	0	1965	1.06	RoofSurface
GW	0	1965	volledig natuurlijk	ventilatietype
GW	0	1965	A1 standaard	ventilatievoorziening
GW	0	1965	geen warmteterugwinning	type warmteterugwinning
GW	0	1965	forfaitair	kierdichting (q;v10)
GW	0	1965	ketel HR107-ketel	Ruimteverwarming
GW	0	1965	individueel	type ruimteverwarming
GW	0	1965	ketel	toestel ruimteverwarming
GW	0	1965	HR107-ketel	ketel/luchtverwarming
GW	0	1965		lokale verwarming
GW	0	1965	radiatoren	Afgiftesysteem
GW	0	1965	90/70	temperatuurniveau
GW	0	1965	radiatoren	type afgiftesysteem
GW	0	1965	individueel gas combitoestel met gaskeur HR/CW	Warmtapwater
GW	0	1965	individueel	type tapwaterinstallatie
GW	0	1965	gas combitoestel met gaskeur HR/CW	type toestel individiueel

Continued on next page

Table C.6 – continued from previous page

Building type	Year min	Year max	Current condition	Element
GW	0	1965	CW3	CW-klasse
GW	1965	1974	1.49	WallSurface
GW	1965	1974	2.88	Window
GW	1965	1974	3.35	Door
GW	1965	1974	2.33	GroundSurface
GW	1965	1974	0.92	RoofSurface
GW	1965	1974	natuurlijke toevoer, mechanische afvoer	ventilatietype
GW	1965	1974	C1 standaard	ventilatievoorziening
GW	1965	1974	geen warmteterugwinning	type warmteterugwinning
GW	1965	1974	forfaitair	kierdichting (q;v10)
GW	1965	1974	ketel VR-ketel	Ruimteverwarming
GW	1965	1974	collectief	type ruimteverwarming
GW	1965	1974	ketel	toestel ruimteverwarming
GW	1965	1974	VR-ketel	ketel/luchtverwarming
GW	1965	1974	radiatoren	Afgiftesysteem
GW	1965	1974	90/70	temperatuurniveau
GW	1965	1974	radiatoren	type afgiftesysteem
GW	1965	1974	collectief	Warmtapwater
GW	1965	1974	collectief	type tapwaterinstallatie
GW	1965	1974	indirect verwarmd vat	type toestel met extern vat
GW	1965	1974	VR-ketel	type indirect verwarmd vat
GW	1975	1991	0.64	WallSurface
GW	1975	1991	3.08	Window
GW	1975	1991	3.33	Door
GW	1975	1991	1.02	GroundSurface
GW	1975	1991	0.58	RoofSurface
GW	1975	1991	natuurlijke toevoer, mechanische afvoer	ventilatietype
GW	1975	1991	C1 standaard	ventilatievoorziening
GW	1975	1991	geen warmteterugwinning	type warmteterugwinning
GW	1975	1991	forfaitair	kierdichting (q;v10)
GW	1975	1991	ketel HR107-ketel	Ruimteverwarming
GW	1975	1991	individueel	type ruimteverwarming
GW	1975	1991	ketel	toestel ruimteverwarming
GW	1975	1991	HR107-ketel	ketel/luchtverwarming
GW	1975	1991	radiatoren	Afgiftesysteem
GW	1975	1991	90/70	temperatuurniveau
GW	1975	1991	radiatoren	type afgiftesysteem

Continued on next page

Table C.6 – continued from previous page

Building type	Year min	Year max	Current condition	Element
GW	1975	1991	individueel gas combitoestel met gaskeur HR/CW	Warmtapwater
GW	1975	1991	individueel	type tapwaterinstallatie
GW	1975	1991	gas combitoestel met gaskeur HR/CW	type toestel individiueel
GW	1975	1991	CW3	CW-klasse
GW	1992	2005	0.4	WallSurface
GW	1992	2005	2.41	Window
GW	1992	2005	3.3	Door
GW	1992	2005	0.35	GroundSurface
GW	1992	2005	0.38	RoofSurface
GW	1992	2005	natuurlijke toevoer, mechanische afvoer	ventilatietype
GW	1992	2005	C1 standaard	ventilatievoorziening
GW	1992	2005	geen warmteterugwinning	type warmteterugwinning
GW	1992	2005	forfaitair	kierdichting (q;v10)
GW	1992	2005	ketel HR107-ketel	Ruimteverwarming
GW	1992	2005	individueel	type ruimteverwarming
GW	1992	2005	ketel	toestel ruimteverwarming
GW	1992	2005	HR107-ketel	ketel/luchtverwarming
GW	1992	2005	radiatoren	Afgiftesysteem
GW	1992	2005	90/70	temperatuurniveau
GW	1992	2005	radiatoren	type afgiftesysteem
GW	1992	2005	individueel gas combitoestel met gaskeur HR/CW	Warmtapwater
GW	1992	2005	individueel	type tapwaterinstallatie
GW	1992	2005	gas combitoestel met gaskeur HR/CW	type toestel individiueel
GW	1992	2005	CW3	CW-klasse
GW	2006	2014	0.37	WallSurface
GW	2006	2014	1.89	Window
GW	2006	2014	3.32	Door
GW	2006	2014	0.35	GroundSurface
GW	2006	2014	0.37	RoofSurface
GW	2006	2014	natuurlijke toevoer, mechanische afvoer	ventilatietype
GW	2006	2014	C1 standaard	ventilatievoorziening
GW	2006	2014	geen warmteterugwinning	type warmteterugwinning
GW	2006	2014	forfaitair	kierdichting (q;v10)
GW	2006	2014	ketel HR107-ketel	Ruimteverwarming

Continued on next page

Table C.6 – continued from previous page

Building type	Year min	Year max	Current condition	Element
GW	2006	2014	individueel	type ruimteverwarming
GW	2006	2014	ketel	toestel ruimteverwarming
GW	2006	2014	HR107-ketel	ketel/luchtverwarming
GW	2006	2014	radiatoren	Afgiftesysteem
GW	2006	2014	90/70	temperatuurniveau
GW	2006	2014	radiatoren	type afgiftesysteem
GW	2006	2014	individueel gas combitoestel met gaskeur HR/CW	Warmtapwater
GW	2006	2014	individueel	type tapwaterinstallatie
GW	2006	2014	gas combitoestel met gaskeur HR/CW	type toestel individiueel
GW	2006	2014	CW3	CW-klasse
GW	2015	2018	0.21	WallSurface
GW	2015	2018	1.77	Window
GW	2015	2018	3.4	Door
GW	2015	2018	0.27	GroundSurface
GW	2015	2018	0.16	RoofSurface
GW	2015	2018	volledig mechanisch	ventilatietype
GW	2015	2018	D1 standaard	ventilatievoorziening
GW	2015	2018	met warmteterugwinning	type warmteterugwinning
GW	2015	2018	forfaitair	kierdichting (q;v10)
GW	2015	2018	ketel HR107-ketel	Ruimteverwarming
GW	2015	2018	individueel	type ruimteverwarming
GW	2015	2018	ketel	toestel ruimteverwarming
GW	2015	2018	HR107-ketel	ketel/luchtverwarming
GW	2015	2018	vloer/wand/plafond	Afgiftesysteem
GW	2015	2018	45/40	temperatuurniveau
GW	2015	2018	vloer/wand/plafond	type afgiftesysteem
GW	2015	2018	individueel gas combitoestel met gaskeur HR/CW	Warmtapwater
GW	2015	2018	individueel	type tapwaterinstallatie
GW	2015	2018	gas combitoestel met gaskeur HR/CW	type toestel individiueel
GW	2015	2018	CW3	CW-klasse
HW	0	1946	1.67	GroundSurface
HW	0	1946	1.56	WallSurface
HW	0	1946	1.31	RoofSurface
HW	0	1946	3.23	Window
HW	0	1946	3.37	Door
HW	0	1946	volledig natuurlijk	ventilatietype
HW	0	1946	A1 standaard	ventilatievoorziening

Continued on next page

Table C.6 – continued from previous page

Building type	Year min	Year max	Current condition	Element
HW	0	1946	geen warmteterugwinning	type warmteterugwinning
HW	0	1946	forfaitair	kierdichting (q;v10)
HW	0	1946	ketel HR107-ketel	Ruimteverwarming
HW	0	1946	individueel	type ruimteverwarming
HW	0	1946	ketel	toestel ruimteverwarming
HW	0	1946	HR107-ketel	ketel/luchtverwarming
HW	0	1946		lokale verwarming
HW	0	1946	radiatoren	Afgiftesysteem
HW	0	1946	90/70	temperatuurniveau
HW	0	1946	radiatoren	type afgiftesysteem
HW	0	1946	individueel gas combitoestel met gaskeur HR/CW	Warmtapwater
HW	0	1946	individueel	type tapwaterinstallatie
HW	0	1946	gas combitoestel met gaskeur HR/CW	type toestel individiueel
HW	0	1946	CW4/5/6	CW-klasse
HW	1946	1964	1.79	GroundSurface
HW	1946	1964	1.23	WallSurface
HW	1946	1964	1.16	RoofSurface
HW	1946	1964	2.66	Window
HW	1946	1964	3.33	Door
HW	1946	1964	volledig natuurlijk	ventilatietype
HW	1946	1964	A1 standaard	ventilatievoorziening
HW	1946	1964	geen warmteterugwinning	type warmteterugwinning
HW	1946	1964	forfaitair	kierdichting (q;v10)
HW	1946	1964	ketel HR107-ketel	Ruimteverwarming
HW	1946	1964	individueel	type ruimteverwarming
HW	1946	1964	ketel	toestel ruimteverwarming
HW	1946	1964	HR107-ketel	ketel/luchtverwarming
HW	1946	1964		lokale verwarming
HW	1946	1964	radiatoren	Afgiftesysteem
HW	1946	1964	90/70	temperatuurniveau
HW	1946	1964	radiatoren	type afgiftesysteem
HW	1946	1964	individueel gas combitoestel met gaskeur HR/CW	Warmtapwater
HW	1946	1964	individueel	type tapwaterinstallatie
HW	1946	1964	gas combitoestel met gaskeur HR/CW	type toestel individiueel
HW	1946	1964	CW4/5/6	CW-klasse
HW	1965	1974	2	GroundSurface

Continued on next page

Table C.6 – continued from previous page

Building type	Year min	Year max	Current condition	Element
HW	1965	1974	1.11	WallSurface
HW	1965	1974	0.88	RoofSurface
HW	1965	1974	2.62	Window
HW	1965	1974	3.29	Door
HW	1965	1974	volledig natuurlijk	ventilatietype
HW	1965	1974	A1 standaard	ventilatievoorziening
HW	1965	1974	geen warmteterugwinning	type warmteterugwinning
HW	1965	1974	forfaitair	kierdichting (q;v10)
HW	1965	1974	ketel HR107-ketel	Ruimteverwarming
HW	1965	1974	individueel	type ruimteverwarming
HW	1965	1974	ketel	toestel ruimteverwarming
HW	1965	1974	HR107-ketel	ketel/luchtverwarming
HW	1965	1974	radiatoren	Afgiftesysteem
HW	1965	1974	90/70	temperatuurniveau
HW	1965	1974	radiatoren	type afgiftesysteem
HW	1965	1974	individueel gas combitoestel met gaskeur HR/CW	Warmtapwater
HW	1965	1974	individueel	type tapwaterinstallatie
HW	1965	1974	gas combitoestel met gaskeur HR/CW	type toestel individiueel
HW	1965	1974	CW4/5/6	CW-klasse
HW	1975	1991	0.91	GroundSurface
HW	1975	1991	0.63	WallSurface
HW	1975	1991	0.64	RoofSurface
HW	1975	1991	2.69	Window
HW	1975	1991	3.35	Door
HW	1975	1991	natuurlijke toevoer, mechanische afvoer	ventilatietype
HW	1975	1991	C1 standaard	ventilatievoorziening
HW	1975	1991	geen warmteterugwinning	type warmteterugwinning
HW	1975	1991	forfaitair	kierdichting (q;v10)
HW	1975	1991	ketel HR107-ketel	Ruimteverwarming
HW	1975	1991	individueel	type ruimteverwarming
HW	1975	1991	ketel	toestel ruimteverwarming
HW	1975	1991	HR107-ketel	ketel/luchtverwarming
HW	1975	1991	radiatoren	Afgiftesysteem
HW	1975	1991	90/70	temperatuurniveau
HW	1975	1991	radiatoren	type afgiftesysteem
HW	1975	1991	individueel gas combitoestel met gaskeur HR/CW	Warmtapwater

Continued on next page

Table C.6 – continued from previous page

Building type	Year min	Year max	Current condition	Element
HW	1975	1991	individueel	type tapwaterinstallatie
HW	1975	1991	gas combitoestel met gaskeur HR/CW	type toestel individiueel
HW	1975	1991	CW4/5/6	CW-klasse
HW	1992	2005	0.36	GroundSurface
HW	1992	2005	0.4	WallSurface
HW	1992	2005	0.37	RoofSurface
HW	1992	2005	2.42	Window
HW	1992	2005	3.32	Door
HW	1992	2005	natuurlijke toevoer, mechanische afvoer	ventilatietype
HW	1992	2005	C1 standaard	ventilatievoorziening
HW	1992	2005	geen warmteterugwinning	type warmteterugwinning
HW	1992	2005	forfaitair	kierdichting (q;v10)
HW	1992	2005	ketel HR107-ketel	Ruimteverwarming
HW	1992	2005	individueel	type ruimteverwarming
HW	1992	2005	ketel	toestel ruimteverwarming
HW	1992	2005	HR107-ketel	ketel/luchtverwarming
HW	1992	2005	radiatoren	Afgiftesysteem
HW	1992	2005	90/70	temperatuurniveau
HW	1992	2005	radiatoren	type afgiftesysteem
HW	1992	2005	individueel gas combitoestel met gaskeur HR/CW	Warmtapwater
HW	1992	2005	individueel	type tapwaterinstallatie
HW	1992	2005	gas combitoestel met gaskeur HR/CW	type toestel individiueel
HW	1992	2005	CW4/5/6	CW-klasse
HW	2006	2014	0.36	GroundSurface
HW	2006	2014	0.37	WallSurface
HW	2006	2014	0.37	RoofSurface
HW	2006	2014	1.83	Window
HW	2006	2014	3.21	Door
HW	2006	2014	natuurlijke toevoer, mechanische afvoer	ventilatietype
HW	2006	2014	C1 standaard	ventilatievoorziening
HW	2006	2014	geen warmteterugwinning	type warmteterugwinning
HW	2006	2014	forfaitair	kierdichting (q;v10)
HW	2006	2014	ketel HR107-ketel	Ruimteverwarming
HW	2006	2014	individueel	type ruimteverwarming
HW	2006	2014	ketel	toestel ruimteverwarming

Continued on next page

Table C.6 – continued from previous page

Building type	Year min	Year max	Current condition	Element
HW	2006	2014	HR107-ketel	ketel/luchtverwarming
HW	2006	2014	radiatoren	Afgiftesysteem
HW	2006	2014	90/70	temperatuurniveau
HW	2006	2014	radiatoren	type afgiftesysteem
HW	2006	2014	individueel gas combitoestel met gaskeur HR/CW	Warmtapwater
HW	2006	2014	individueel	type tapwaterinstallatie
HW	2006	2014	gas combitoestel met gaskeur HR/CW	type toestel individiueel
HW	2006	2014	CW4/5/6	CW-klasse
HW	2015	2018	0.27	GroundSurface
HW	2015	2018	0.21	WallSurface
HW	2015	2018	0.16	RoofSurface
HW	2015	2018	1.75	Window
HW	2015	2018	3.01	Door
HW	2015	2018	natuurlijke toevoer, mechanische afvoer	ventilatietype
HW	2015	2018	C1 standaard	ventilatievoorziening
HW	2015	2018	geen warmteterugwinning	type warmteterugwinning
HW	2015	2018	forfaitair	kierdichting (q;v10)
HW	2015	2018	ketel HR107-ketel	Ruimteverwarming
HW	2015	2018	individueel	type ruimteverwarming
HW	2015	2018	ketel	toestel ruimteverwarming
HW	2015	2018	HR107-ketel	ketel/luchtverwarming
HW	2015	2018	vloer/wand/plafond	Afgiftesysteem
HW	2015	2018	45/40	temperatuurniveau
HW	2015	2018	vloer/wand/plafond	type afgiftesysteem
HW	2015	2018	individueel gas combitoestel met gaskeur HR/CW	Warmtapwater
HW	2015	2018	individueel	type tapwaterinstallatie
HW	2015	2018	gas combitoestel met gaskeur HR/CW	type toestel individiueel
HW	2015	2018	CW4/5/6	CW-klasse
MW	0	1965	2.04	WallSurface
MW	0	1965	3.14	Window
MW	0	1965	3.36	Door
MW	0	1965	1.82	GroundSurface
MW	0	1965	1.56	RoofSurface
MW	0	1965	volledig natuurlijk	ventilatietype
MW	0	1965	A1 standaard	ventilatievoorziening

Continued on next page

Table C.6 – continued from previous page

Building type	Year min	Year max	Current condition	Element
MW	0	1965	geen warmteterugwinning	type warmteterugwinning
MW	0	1965	forfaitair	kierdichting (q;v10)
MW	0	1965	ketel HR107-ketel	Ruimteverwarming
MW	0	1965	individueel	type ruimteverwarming
MW	0	1965	ketel	toestel ruimteverwarming
MW	0	1965	HR107-ketel	ketel/luchtverwarming
MW	0	1965		lokale verwarming
MW	0	1965	radiatoren	Afgiftesysteem
MW	0	1965	90/70	temperatuurniveau
MW	0	1965	radiatoren	type afgiftesysteem
MW	0	1965	individueel gas combitoestel met gaskeur HR/CW	Warmtapwater
MW	0	1965	individueel	type tapwaterinstallatie
MW	0	1965	gas combitoestel met gaskeur HR/CW	type toestel individiueel
MW	0	1965	CW4/5/6	CW-klasse
MW	1965	1974	1.67	WallSurface
MW	1965	1974	2.83	Window
MW	1965	1974	3.04	Door
MW	1965	1974	2.33	GroundSurface
MW	1965	1974	0.97	RoofSurface
MW	1965	1974	volledig natuurlijk	ventilatietype
MW	1965	1974	A1 standaard	ventilatievoorziening
MW	1965	1974	geen warmteterugwinning	type warmteterugwinning
MW	1965	1974	forfaitair	kierdichting (q;v10)
MW	1965	1974	ketel HR107-ketel	Ruimteverwarming
MW	1965	1974	individueel	type ruimteverwarming
MW	1965	1974	ketel	toestel ruimteverwarming
MW	1965	1974	HR107-ketel	ketel/luchtverwarming
MW	1965	1974	radiatoren	Afgiftesysteem
MW	1965	1974	90/70	temperatuurniveau
MW	1965	1974	radiatoren	type afgiftesysteem
MW	1965	1974	individueel gas combitoestel met gaskeur HR/CW	Warmtapwater
MW	1965	1974	individueel	type tapwaterinstallatie
MW	1965	1974	gas combitoestel met gaskeur HR/CW	type toestel individiueel
MW	1965	1974	CW3	CW-klasse
MW	1975	1991	0.65	WallSurface
MW	1975	1991	3.05	Window

Continued on next page

Table C.6 – continued from previous page

Building type	Year min	Year max	Current condition	Element
MW	1975	1991	3.38	Door
MW	1975	1991	0.73	GroundSurface
MW	1975	1991	0.65	RoofSurface
MW	1975	1991	natuurlijke toevoer, mechanische afvoer	ventilatietype
MW	1975	1991	C1 standaard	ventilatievoorziening
MW	1975	1991	geen warmteterugwinning	type warmteterugwinning
MW	1975	1991	forfaitair	kierdichting (q;v10)
MW	1975	1991	ketel HR107-ketel	Ruimteverwarming
MW	1975	1991	individueel	type ruimteverwarming
MW	1975	1991	ketel	toestel ruimteverwarming
MW	1975	1991	HR107-ketel	ketel/luchtverwarming
MW	1975	1991	radiatoren	Afgiftesysteem
MW	1975	1991	90/70	temperatuurniveau
MW	1975	1991	radiatoren	type afgiftesysteem
MW	1975	1991	individueel gas combitoestel met gaskeur HR/CW	Warmtapwater
MW	1975	1991	individueel	type tapwaterinstallatie
MW	1975	1991	gas combitoestel met gaskeur HR/CW	type toestel individiueel
MW	1975	1991	CW3	CW-klasse
MW	1992	2005	0.39	WallSurface
MW	1992	2005	2.52	Window
MW	1992	2005	3.26	Door
MW	1992	2005	0.33	GroundSurface
MW	1992	2005	0.38	RoofSurface
MW	1992	2005	natuurlijke toevoer, mechanische afvoer	ventilatietype
MW	1992	2005	C1 standaard	ventilatievoorziening
MW	1992	2005	geen warmteterugwinning	type warmteterugwinning
MW	1992	2005	forfaitair	kierdichting (q;v10)
MW	1992	2005	ketel HR107-ketel	Ruimteverwarming
MW	1992	2005	individueel	type ruimteverwarming
MW	1992	2005	ketel	toestel ruimteverwarming
MW	1992	2005	HR107-ketel	ketel/luchtverwarming
MW	1992	2005	radiatoren	Afgiftesysteem
MW	1992	2005	90/70	temperatuurniveau
MW	1992	2005	radiatoren	type afgiftesysteem
MW	1992	2005	individueel gas combitoestel met gaskeur HR/CW	Warmtapwater

Continued on next page

Table C.6 – continued from previous page

Building type	Year min	Year max	Current condition	Element
MW	1992	2005	individueel	type tapwaterinstallatie
MW	1992	2005	gas combitoestel met gaskeur HR/CW	type toestel individiueel
MW	1992	2005	CW4/5/6	CW-klasse
MW	2006	2014	0.37	WallSurface
MW	2006	2014	1.78	Window
MW	2006	2014	3.29	Door
MW	2006	2014	0.38	GroundSurface
MW	2006	2014	0.37	RoofSurface
MW	2006	2014	volledig mechanisch	ventilatietype
MW	2006	2014	D1 standaard	ventilatievoorziening
MW	2006	2014	met warmteterugwinning	type warmteterugwinning
MW	2006	2014	forfaitair	kierdichting (q;v10)
MW	2006	2014	ketel HR107-ketel	Ruimteverwarming
MW	2006	2014	individueel	type ruimteverwarming
MW	2006	2014	ketel	toestel ruimteverwarming
MW	2006	2014	HR107-ketel	ketel/luchtverwarming
MW	2006	2014	radiatoren	Afgiftesysteem
MW	2006	2014	90/70	temperatuurniveau
MW	2006	2014	radiatoren	type afgiftesysteem
MW	2006	2014	individueel gas combitoestel met gaskeur HR/CW	Warmtapwater
MW	2006	2014	individueel	type tapwaterinstallatie
MW	2006	2014	gas combitoestel met gaskeur HR/CW	type toestel individiueel
MW	2006	2014	CW4/5/6	CW-klasse
MW	2015	2018	0.21	WallSurface
MW	2015	2018	1.78	Window
MW	2015	2018	3.29	Door
MW	2015	2018	0.27	GroundSurface
MW	2015	2018	0.16	RoofSurface
MW	2015	2018	volledig mechanisch	ventilatietype
MW	2015	2018	D1 standaard	ventilatievoorziening
MW	2015	2018	met warmteterugwinning	type warmteterugwinning
MW	2015	2018	forfaitair	kierdichting (q;v10)
MW	2015	2018	ketel HR107-ketel	Ruimteverwarming
MW	2015	2018	individueel	type ruimteverwarming
MW	2015	2018	ketel	toestel ruimteverwarming
MW	2015	2018	HR107-ketel	ketel/luchtverwarming
MW	2015	2018	radiatoren	Afgiftesysteem
MW	2015	2018	90/70	temperatuurniveau
MW	2015	2018	radiatoren	type afgiftesysteem

Continued on next page

Table C.6 – continued from previous page

Building type	Year min	Year max	Current condition	Element
MW	2015	2018	individueel gas combitoestel met gaskeur HR/CW	Warmtapwater
MW	2015	2018	individueel	type tapwaterinstallatie
MW	2015	2018	gas combitoestel met gaskeur HR/CW	type toestel individiueel
MW	2015	2018	CW4/5/6	CW-klasse
PW	0	1946	2.33	WallSurface
PW	0	1946	3.3	Window
PW	0	1946	3.32	Door
PW	0	1946	2.08	GroundSurface
PW	0	1946	1.69	RoofSurface
PW	0	1946	volledig natuurlijk	ventilatietype
PW	0	1946	A1 standaard	ventilatievoorziening
PW	0	1946	geen warmteterugwinning	type warmteterugwinning
PW	0	1946	forfaitair	kierdichting (q;v10)
PW	0	1946	ketel HR107-ketel	Ruimteverwarming
PW	0	1946	individueel	type ruimteverwarming
PW	0	1946	ketel	toestel ruimteverwarming
PW	0	1946	HR107-ketel	ketel/luchtverwarming
PW	0	1946		lokale verwarming
PW	0	1946	radiatoren	Afgiftesysteem
PW	0	1946	90/70	temperatuurniveau
PW	0	1946	radiatoren	type afgiftesysteem
PW	0	1946	individueel gas combitoestel met gaskeur HR/CW	Warmtapwater
PW	0	1946	individueel	type tapwaterinstallatie
PW	0	1946	gas combitoestel met gaskeur HR/CW	type toestel individiueel
PW	0	1946	CW3	CW-klasse
PW	1946	1964	1.82	WallSurface
PW	1946	1964	3.05	Window
PW	1946	1964	3.23	Door
PW	1946	1964	2.08	GroundSurface
PW	1946	1964	1.33	RoofSurface
PW	1946	1964	volledig natuurlijk	ventilatietype
PW	1946	1964	A1 standaard	ventilatievoorziening
PW	1946	1964	geen warmteterugwinning	type warmteterugwinning
PW	1946	1964	forfaitair	kierdichting (q;v10)
PW	1946	1964	ketel HR107-ketel	Ruimteverwarming
PW	1946	1964	individueel	type ruimteverwarming

Continued on next page

Table C.6 – continued from previous page

Building type	Year min	Year max	Current condition	Element
PW	1946	1964	ketel	toestel ruimteverwarming
PW	1946	1964	HR107-ketel	ketel/luchtverwarming
PW	1946	1964		lokale verwarming
PW	1946	1964	radiatoren	Afgiftesysteem
PW	1946	1964	90/70	temperatuurniveau
PW	1946	1964	radiatoren	type afgiftesysteem
PW	1946	1964	individueel gas combitoestel met gaskeur HR/CW	Warmtapwater
PW	1946	1964	individueel	type tapwaterinstallatie
PW	1946	1964	gas combitoestel met gaskeur HR/CW	type toestel individiueel
PW	1946	1964	CW3	CW-klasse
PW	1965	1974	1.52	WallSurface
PW	1965	1974	2.91	Window
PW	1965	1974	3.27	Door
PW	1965	1974	2.22	GroundSurface
PW	1965	1974	0.88	RoofSurface
PW	1965	1974	natuurlijke toevoer, mechanische afvoer	ventilatietype
PW	1965	1974	C1 standaard	ventilatievoorziening
PW	1965	1974	geen warmteterugwinning	type warmteterugwinning
PW	1965	1974	forfaitair	kierdichting (q;v10)
PW	1965	1974	ketel HR107-ketel	Ruimteverwarming
PW	1965	1974	individueel	type ruimteverwarming
PW	1965	1974	ketel	toestel ruimteverwarming
PW	1965	1974	HR107-ketel	ketel/luchtverwarming
PW	1965	1974	radiatoren	Afgiftesysteem
PW	1965	1974	90/70	temperatuurniveau
PW	1965	1974	radiatoren	type afgiftesysteem
PW	1965	1974	individueel gas combitoestel met gaskeur HR/CW	Warmtapwater
PW	1965	1974	individueel	type tapwaterinstallatie
PW	1965	1974	gas combitoestel met gaskeur HR/CW	type toestel individiueel
PW	1965	1974	CW3	CW-klasse
PW	1975	1991	0.67	WallSurface
PW	1975	1991	2.94	Window
PW	1975	1991	3.29	Door
PW	1975	1991	1.04	GroundSurface
PW	1975	1991	0.63	RoofSurface

Continued on next page

Table C.6 – continued from previous page

Building type	Year min	Year max	Current condition	Element
PW	1975	1991	natuurlijke toevoer, mechanische afvoer	ventilatietype
PW	1975	1991	C1 standaard	ventilatievoorziening
PW	1975	1991	geen warmteterugwinning	type warmteterugwinning
PW	1975	1991	forfaitair	kierdichting (q;v10)
PW	1975	1991	ketel HR107-ketel	Ruimteverwarming
PW	1975	1991	individueel	type ruimteverwarming
PW	1975	1991	ketel	toestel ruimteverwarming
PW	1975	1991	HR107-ketel	ketel/luchtverwarming
PW	1975	1991	radiatoren	Afgiftesysteem
PW	1975	1991	90/70	temperatuurniveau
PW	1975	1991	radiatoren	type afgiftesysteem
PW	1975	1991	individueel gas combitoestel met gaskeur HR/CW	Warmtapwater
PW	1975	1991	individueel	type tapwaterinstallatie
PW	1975	1991	gas combitoestel met gaskeur HR/CW	type toestel individiueel
PW	1975	1991	CW3	CW-klasse
PW	1992	2005	0.4	WallSurface
PW	1992	2005	2.65	Window
PW	1992	2005	3.3	Door
PW	1992	2005	0.38	GroundSurface
PW	1992	2005	0.38	RoofSurface
PW	1992	2005	natuurlijke toevoer, mechanische afvoer	ventilatietype
PW	1992	2005	C1 standaard	ventilatievoorziening
PW	1992	2005	geen warmteterugwinning	type warmteterugwinning
PW	1992	2005	forfaitair	kierdichting (q;v10)
PW	1992	2005	ketel HR107-ketel	Ruimteverwarming
PW	1992	2005	individueel	type ruimteverwarming
PW	1992	2005	ketel	toestel ruimteverwarming
PW	1992	2005	HR107-ketel	ketel/luchtverwarming
PW	1992	2005	radiatoren	Afgiftesysteem
PW	1992	2005	90/70	temperatuurniveau
PW	1992	2005	radiatoren	type afgiftesysteem
PW	1992	2005	individueel gas combitoestel met gaskeur HR/CW	Warmtapwater
PW	1992	2005	individueel	type tapwaterinstallatie
PW	1992	2005	gas combitoestel met gaskeur HR/CW	type toestel individiueel

Continued on next page

Table C.6 – continued from previous page

Building type	Year min	Year max	Current condition	Element
PW	1992	2005	CW3	CW-klasse
PW	2006	2014	0.37	WallSurface
PW	2006	2014	1.96	Window
PW	2006	2014	3.12	Door
PW	2006	2014	0.35	GroundSurface
PW	2006	2014	0.33	RoofSurface
PW	2006	2014	natuurlijke toevoer, mechanische afvoer	ventilatietype
PW	2006	2014	C1 standaard	ventilatievoorziening
PW	2006	2014	geen warmteterugwinning	type warmteterugwinning
PW	2006	2014	forfaitair	kierdichting (q;v10)
PW	2006	2014	ketel HR107-ketel	Ruimteverwarming
PW	2006	2014	individueel	type ruimteverwarming
PW	2006	2014	ketel	toestel ruimteverwarming
PW	2006	2014	HR107-ketel	ketel/luchtverwarming
PW	2006	2014	radiatoren	Afgiftesysteem
PW	2006	2014	90/70	temperatuurniveau
PW	2006	2014	radiatoren	type afgiftesysteem
PW	2006	2014	individueel gas combitoestel met gaskeur HR/CW	Warmtapwater
PW	2006	2014	individueel	type tapwaterinstallatie
PW	2006	2014	gas combitoestel met gaskeur HR/CW	type toestel individiueel
PW	2006	2014	CW3	CW-klasse
PW	2015	2018	0.21	WallSurface
PW	2015	2018	1.8	Window
PW	2015	2018	3.4	Door
PW	2015	2018	0.27	GroundSurface
PW	2015	2018	0.16	RoofSurface
PW	2015	2018	natuurlijke toevoer, mechanische afvoer	ventilatietype
PW	2015	2018	C1 standaard	ventilatievoorziening
PW	2015	2018	geen warmteterugwinning	type warmteterugwinning
PW	2015	2018	forfaitair	kierdichting (q;v10)
PW	2015	2018	ketel HR107-ketel	Ruimteverwarming
PW	2015	2018	individueel	type ruimteverwarming
PW	2015	2018	ketel	toestel ruimteverwarming
PW	2015	2018	HR107-ketel	ketel/luchtverwarming
PW	2015	2018	vloer/wand/plafond	Afgiftesysteem
PW	2015	2018	45/40	temperatuurniveau

Continued on next page

Table C.6 – continued from previous page

Building type	Year min	Year max	Current condition	Element
PW	2015	2018	vloer/wand/plafond	type afgiftesysteem
PW	2015	2018	individueel gas combitoestel met gaskeur HR/CW	Warmtapwater
PW	2015	2018	individueel	type tapwaterinstallatie
PW	2015	2018	gas combitoestel met gaskeur HR/CW	type toestel individiueel
PW	2015	2018	CW2	CW-klasse
TOEK	0	1965	1.54	GroundSurface
TOEK	0	1965	1.23	WallSurface
TOEK	0	1965	1.02	RoofSurface
TOEK	0	1965	2.91	Window
TOEK	0	1965	3.33	Door
TOEK	0	1965	volledig natuurlijk	ventilatietype
TOEK	0	1965	A1 standaard	ventilatievoorziening
TOEK	0	1965	geen warmteterugwinning	type warmteterugwinning
TOEK	0	1965	forfaitair	kierdichting (q;v10)
TOEK	0	1965	ketel HR107-ketel	Ruimteverwarming
TOEK	0	1965	individueel	type ruimteverwarming
TOEK	0	1965	ketel	toestel ruimteverwarming
TOEK	0	1965	HR107-ketel	ketel/luchtverwarming
TOEK	0	1965	radiatoren	Afgiftesysteem
TOEK	0	1965	90/70	temperatuurniveau
TOEK	0	1965	radiatoren	type afgiftesysteem
TOEK	0	1965	individueel gas combitoestel met gaskeur HR/CW	Warmtapwater
TOEK	0	1965	individueel	type tapwaterinstallatie
TOEK	0	1965	gas combitoestel met gaskeur HR/CW	type toestel individiueel
TOEK	0	1965	CW4/5/6	CW-klasse
TOEK	1965	1974	1.85	GroundSurface
TOEK	1965	1974	1.08	WallSurface
TOEK	1965	1974	0.81	RoofSurface
TOEK	1965	1974	2.61	Window
TOEK	1965	1974	3.35	Door
TOEK	1965	1974	volledig natuurlijk	ventilatietype
TOEK	1965	1974	A1 standaard	ventilatievoorziening
TOEK	1965	1974	geen warmteterugwinning	type warmteterugwinning
TOEK	1965	1974	forfaitair	kierdichting (q;v10)
TOEK	1965	1974	ketel HR107-ketel	Ruimteverwarming
TOEK	1965	1974	individueel	type ruimteverwarming

Continued on next page

Table C.6 – continued from previous page

Building type	Year min	Year max	Current condition	Element
TOEK	1965	1974	ketel	toestel ruimteverwarming
TOEK	1965	1974	HR107-ketel	ketel/luchtverwarming
TOEK	1965	1974	radiatoren	Afgiftesysteem
TOEK	1965	1974	90/70	temperatuurniveau
TOEK	1965	1974	radiatoren	type afgiftesysteem
TOEK	1965	1974	individueel gas combitoestel met gaskeur HR/CW	Warmtapwater
TOEK	1965	1974	individueel	type tapwaterinstallatie
TOEK	1965	1974	gas combitoestel met gaskeur HR/CW	type toestel individiueel
TOEK	1965	1974	CW4/5/6	CW-klasse
TOEK	1975	1991	0.88	GroundSurface
TOEK	1975	1991	0.63	WallSurface
TOEK	1975	1991	0.63	RoofSurface
TOEK	1975	1991	2.7	Window
TOEK	1975	1991	3.31	Door
TOEK	1975	1991	volledig natuurlijk	ventilatietype
TOEK	1975	1991	A1 standaard	ventilatievoorziening
TOEK	1975	1991	geen warmteterugwinning	type warmteterugwinning
TOEK	1975	1991	forfaitair	kierdichting (q;v10)
TOEK	1975	1991	ketel HR107-ketel	Ruimteverwarming
TOEK	1975	1991	individueel	type ruimteverwarming
TOEK	1975	1991	ketel	toestel ruimteverwarming
TOEK	1975	1991	HR107-ketel	ketel/luchtverwarming
TOEK	1975	1991	radiatoren	Afgiftesysteem
TOEK	1975	1991	90/70	temperatuurniveau
TOEK	1975	1991	radiatoren	type afgiftesysteem
TOEK	1975	1991	individueel gas combitoestel met gaskeur HR/CW	Warmtapwater
TOEK	1975	1991	individueel	type tapwaterinstallatie
TOEK	1975	1991	gas combitoestel met gaskeur HR/CW	type toestel individiueel
TOEK	1975	1991	CW4/5/6	CW-klasse
TOEK	1992	2005	0.37	GroundSurface
TOEK	1992	2005	0.4	WallSurface
TOEK	1992	2005	0.37	RoofSurface
TOEK	1992	2005	2.43	Window
TOEK	1992	2005	3.3	Door
TOEK	1992	2005	natuurlijke toevoer, mechanische afvoer	ventilatietype
TOEK	1992	2005	C1 standaard	ventilatievoorziening

Continued on next page

Table C.6 – continued from previous page

Building type	Year min	Year max	Current condition	Element
TOEK	1992	2005	geen warmteterugwinning	type warmteterugwinning
TOEK	1992	2005	forfaitair	kierdichting (q;v10)
TOEK	1992	2005	ketel HR107-ketel	Ruimteverwarming
TOEK	1992	2005	individueel	type ruimteverwarming
TOEK	1992	2005	ketel	toestel ruimteverwarming
TOEK	1992	2005	HR107-ketel	ketel/luchtverwarming
TOEK	1992	2005	radiatoren	Afgiftesysteem
TOEK	1992	2005	90/70	temperatuurniveau
TOEK	1992	2005	radiatoren	type afgiftesysteem
TOEK	1992	2005	individueel gas combitoestel met gaskeur HR/CW	Warmtapwater
TOEK	1992	2005	individueel	type tapwaterinstallatie
TOEK	1992	2005	gas combitoestel met gaskeur HR/CW	type toestel individiueel
TOEK	1992	2005	CW4/5/6	CW-klasse
TOEK	2006	2014	0.35	GroundSurface
TOEK	2006	2014	0.35	WallSurface
TOEK	2006	2014	0.36	RoofSurface
TOEK	2006	2014	1.94	Window
TOEK	2006	2014	3.28	Door
TOEK	2006	2014	natuurlijke toevoer, mechanische afvoer	ventilatietype
TOEK	2006	2014	C1 standaard	ventilatievoorziening
TOEK	2006	2014	geen warmteterugwinning	type warmteterugwinning
TOEK	2006	2014	forfaitair	kierdichting (q;v10)
TOEK	2006	2014	ketel HR107-ketel	Ruimteverwarming
TOEK	2006	2014	individueel	type ruimteverwarming
TOEK	2006	2014	ketel	toestel ruimteverwarming
TOEK	2006	2014	HR107-ketel	ketel/luchtverwarming
TOEK	2006	2014	radiatoren	Afgiftesysteem
TOEK	2006	2014	90/70	temperatuurniveau
TOEK	2006	2014	radiatoren	type afgiftesysteem
TOEK	2006	2014	individueel gas combitoestel met gaskeur HR/CW	Warmtapwater
TOEK	2006	2014	individueel	type tapwaterinstallatie
TOEK	2006	2014	gas combitoestel met gaskeur HR/CW	type toestel individiueel
TOEK	2006	2014	CW4/5/6	CW-klasse
TOEK	2015	2018	0.27	GroundSurface
TOEK	2015	2018	0.21	WallSurface

Continued on next page

Table C.6 – continued from previous page

Building type	Year min	Year max	Current condition	Element
TOEK	2015	2018	0.16	RoofSurface
TOEK	2015	2018	1.8	Window
TOEK	2015	2018	2.69	Door
TOEK	2015	2018	natuurlijke toevoer, mechanische afvoer	ventilatietype
TOEK	2015	2018	C1 standaard	ventilatievoorziening
TOEK	2015	2018	geen warmteterugwinning	type warmteterugwinning
TOEK	2015	2018	forfaitair	kierdichting (q;v10)
TOEK	2015	2018	ketel HR107-ketel	Ruimteverwarming
TOEK	2015	2018	individueel	type ruimteverwarming
TOEK	2015	2018	ketel	toestel ruimteverwarming
TOEK	2015	2018	HR107-ketel	ketel/luchtverwarming
TOEK	2015	2018	vloer/wand/plafond	Afgiftesysteem
TOEK	2015	2018	45/40	temperatuurniveau
TOEK	2015	2018	vloer/wand/plafond	type afgiftesysteem
TOEK	2015	2018	individueel gas combitoestel met gaskeur HR/CW	Warmtapwater
TOEK	2015	2018	individueel	type tapwaterinstallatie
TOEK	2015	2018	gas combitoestel met gaskeur HR/CW	type toestel individiueel
TOEK	2015	2018	CW4/5/6	CW-klasse
TW	0	1946	1.72	GroundSurface
TW	0	1946	1.72	WallSurface
TW	0	1946	1.08	RoofSurface
TW	0	1946	3.03	Window
TW	0	1946	3.37	Door
TW	0	1946	volledig natuurlijk	ventilatietype
TW	0	1946	A1 standaard	ventilatievoorziening
TW	0	1946	geen warmteterugwinning	type warmteterugwinning
TW	0	1946	forfaitair	kierdichting (q;v10)
TW	0	1946	ketel HR107-ketel	Ruimteverwarming
TW	0	1946	individueel	type ruimteverwarming
TW	0	1946	ketel	toestel ruimteverwarming
TW	0	1946	HR107-ketel	ketel/luchtverwarming
TW	0	1946		lokale verwarming
TW	0	1946	radiatoren	Afgiftesysteem
TW	0	1946	90/70	temperatuurniveau
TW	0	1946	radiatoren	type afgiftesysteem
TW	0	1946	individueel gas combitoestel met gaskeur HR/CW	Warmtapwater

Continued on next page

Table C.6 – continued from previous page

Building type	Year min	Year max	Current condition	Element
TW	0	1946	individueel	type tapwaterinstallatie
TW	0	1946	gas combitoestel met gaskeur HR/CW	type toestel individiueel
TW	0	1946	CW4/5/6	CW-klasse
TW	1946	1964	2	GroundSurface
TW	1946	1964	1.49	WallSurface
TW	1946	1964	1.1	RoofSurface
TW	1946	1964	3.03	Window
TW	1946	1964	3.35	Door
TW	1946	1964	volledig natuurlijk	ventilatietype
TW	1946	1964	A1 standaard	ventilatievoorziening
TW	1946	1964	geen warmteterugwinning	type warmteterugwinning
TW	1946	1964	forfaitair	kierdichting (q;v10)
TW	1946	1964	ketel HR107-ketel	Ruimteverwarming
TW	1946	1964	individueel	type ruimteverwarming
TW	1946	1964	ketel	toestel ruimteverwarming
TW	1946	1964	HR107-ketel	ketel/luchtverwarming
TW	1946	1964		lokale verwarming
TW	1946	1964	radiatoren	Afgiftesysteem
TW	1946	1964	90/70	temperatuurniveau
TW	1946	1964	radiatoren	type afgiftesysteem
TW	1946	1964	individueel gas combitoestel met gaskeur HR/CW	Warmtapwater
TW	1946	1964	individueel	type tapwaterinstallatie
TW	1946	1964	gas combitoestel met gaskeur HR/CW	type toestel individiueel
TW	1946	1964	CW3	CW-klasse
TW	1965	1974	2	GroundSurface
TW	1965	1974	1.27	WallSurface
TW	1965	1974	0.84	RoofSurface
TW	1965	1974	2.71	Window
TW	1965	1974	3.28	Door
TW	1965	1974	volledig natuurlijk	ventilatietype
TW	1965	1974	A1 standaard	ventilatievoorziening
TW	1965	1974	geen warmteterugwinning	type warmteterugwinning
TW	1965	1974	forfaitair	kierdichting (q;v10)
TW	1965	1974	ketel HR107-ketel	Ruimteverwarming
TW	1965	1974	individueel	type ruimteverwarming
TW	1965	1974	ketel	toestel ruimteverwarming
TW	1965	1974	HR107-ketel	ketel/luchtverwarming

Continued on next page

Table C.6 – continued from previous page

Building type	Year min	Year max	Current condition	Element
TW	1965	1974	radiatoren	Afgiftesysteem
TW	1965	1974	90/70	temperatuurniveau
TW	1965	1974	radiatoren	type afgiftesysteem
TW	1965	1974	individueel gas combitoestel met gaskeur HR/CW	Warmtapwater
TW	1965	1974	individueel	type tapwaterinstallatie
TW	1965	1974	gas combitoestel met gaskeur HR/CW	type toestel individiueel
TW	1965	1974	CW4/5/6	CW-klasse
TW	1975	1991	0.93	GroundSurface
TW	1975	1991	0.64	WallSurface
TW	1975	1991	0.65	RoofSurface
TW	1975	1991	2.83	Window
TW	1975	1991	3.33	Door
TW	1975	1991	natuurlijke toevoer, mechanische afvoer	ventilatietype
TW	1975	1991	C1 standaard	ventilatievoorziening
TW	1975	1991	geen warmteterugwinning	type warmteterugwinning
TW	1975	1991	forfaitair	kierdichting (q;v10)
TW	1975	1991	ketel HR107-ketel	Ruimteverwarming
TW	1975	1991	individueel	type ruimteverwarming
TW	1975	1991	ketel	toestel ruimteverwarming
TW	1975	1991	HR107-ketel	ketel/luchtverwarming
TW	1975	1991	radiatoren	Afgiftesysteem
TW	1975	1991	90/70	temperatuurniveau
TW	1975	1991	radiatoren	type afgiftesysteem
TW	1975	1991	individueel gas combitoestel met gaskeur HR/CW	Warmtapwater
TW	1975	1991	individueel	type tapwaterinstallatie
TW	1975	1991	gas combitoestel met gaskeur HR/CW	type toestel individiueel
TW	1975	1991	CW4/5/6	CW-klasse
TW	1992	2005	0.36	GroundSurface
TW	1992	2005	0.39	WallSurface
TW	1992	2005	0.37	RoofSurface
TW	1992	2005	2.32	Window
TW	1992	2005	3.32	Door
TW	1992	2005	natuurlijke toevoer, mechanische afvoer	ventilatietype
TW	1992	2005	C1 standaard	ventilatievoorziening

Continued on next page

Table C.6 – continued from previous page

Building type	Year min	Year max	Current condition	Element
TW	1992	2005	geen warmteterugwinning	type warmteterugwinning
TW	1992	2005	forfaitair	kierdichting (q;v10)
TW	1992	2005	ketel HR107-ketel	Ruimteverwarming
TW	1992	2005	individueel	type ruimteverwarming
TW	1992	2005	ketel	toestel ruimteverwarming
TW	1992	2005	HR107-ketel	ketel/luchtverwarming
TW	1992	2005	radiatoren	Afgiftesysteem
TW	1992	2005	90/70	temperatuurniveau
TW	1992	2005	radiatoren	type afgiftesysteem
TW	1992	2005	individueel gas combitoestel met gaskeur HR/CW	Warmtapwater
TW	1992	2005	individueel	type tapwaterinstallatie
TW	1992	2005	gas combitoestel met gaskeur HR/CW	type toestel individiueel
TW	1992	2005	CW4/5/6	CW-klasse
TW	2006	2014	0.36	GroundSurface
TW	2006	2014	0.37	WallSurface
TW	2006	2014	0.37	RoofSurface
TW	2006	2014	1.87	Window
TW	2006	2014	3.18	Door
TW	2006	2014	natuurlijke toevoer, mechanische afvoer	ventilatietype
TW	2006	2014	C1 standaard	ventilatievoorziening
TW	2006	2014	geen warmteterugwinning	type warmteterugwinning
TW	2006	2014	forfaitair	kierdichting (q;v10)
TW	2006	2014	ketel HR107-ketel	Ruimteverwarming
TW	2006	2014	individueel	type ruimteverwarming
TW	2006	2014	ketel	toestel ruimteverwarming
TW	2006	2014	HR107-ketel	ketel/luchtverwarming
TW	2006	2014	vloer/wand/plafond	Afgiftesysteem
TW	2006	2014	45/40	temperatuurniveau
TW	2006	2014	vloer/wand/plafond	type afgiftesysteem
TW	2006	2014	individueel gas combitoestel met gaskeur HR/CW	Warmtapwater
TW	2006	2014	individueel	type tapwaterinstallatie
TW	2006	2014	gas combitoestel met gaskeur HR/CW	type toestel individiueel
TW	2006	2014	CW4/5/6	CW-klasse
TW	2015	2018	0.27	GroundSurface
TW	2015	2018	0.21	WallSurface

Continued on next page

Table C.6 – continued from previous page

Building type	Year min	Year max	Current condition	Element
TW	2015	2018	0.16	RoofSurface
TW	2015	2018	1.77	Window
TW	2015	2018	3.27	Door
TW	2015	2018	natuurlijke toevoer, mechanische afvoer	ventilatietype
TW	2015	2018	C1 standaard	ventilatievoorziening
TW	2015	2018	geen warmteterugwinning	type warmteterugwinning
TW	2015	2018	forfaitair	kierdichting (q;v10)
TW	2015	2018	ketel HR107-ketel	Ruimteverwarming
TW	2015	2018	individueel	type ruimteverwarming
TW	2015	2018	ketel	toestel ruimteverwarming
TW	2015	2018	HR107-ketel	ketel/luchtverwarming
TW	2015	2018	vloer/wand/plafond	Afgiftesysteem
TW	2015	2018	45/40	temperatuurniveau
TW	2015	2018	vloer/wand/plafond	type afgiftesysteem
TW	2015	2018	individueel gas combitoestel met gaskeur HR/CW	Warmtapwater
TW	2015	2018	individueel	type tapwaterinstallatie
TW	2015	2018	gas combitoestel met gaskeur HR/CW	type toestel individiueel
TW	2015	2018	CW4/5/6	CW-klasse
VW	0	1965	1.37	GroundSurface
VW	0	1965	1.23	WallSurface
VW	0	1965	0.88	RoofSurface
VW	0	1965	2.82	Window
VW	0	1965	3.34	Door
VW	0	1965	volledig natuurlijk	ventilatietype
VW	0	1965	A1 standaard	ventilatievoorziening
VW	0	1965	geen warmteterugwinning	type warmteterugwinning
VW	0	1965	forfaitair	kierdichting (q;v10)
VW	0	1965	ketel HR107-ketel	Ruimteverwarming
VW	0	1965	individueel	type ruimteverwarming
VW	0	1965	ketel	toestel ruimteverwarming
VW	0	1965	HR107-ketel	ketel/luchtverwarming
VW	0	1965	radiatoren	Afgiftesysteem
VW	0	1965	90/70	temperatuurniveau
VW	0	1965	radiatoren	type afgiftesysteem
VW	0	1965	individueel gas combitoestel met gaskeur HR/CW	Warmtapwater
VW	0	1965	individueel	type tapwaterinstallatie

Continued on next page

Table C.6 – continued from previous page

Building type	Year min	Year max	Current condition	Element
VW	0	1965	gas combitoestel met gaskeur HR/CW	type toestel individiueel
VW	0	1965	CW4/5/6	CW-klasse
VW	1965	1974	1.96	GroundSurface
VW	1965	1974	1.02	WallSurface
VW	1965	1974	0.78	RoofSurface
VW	1965	1974	2.72	Window
VW	1965	1974	3.3	Door
VW	1965	1974	volledig natuurlijk	ventilatietype
VW	1965	1974	A1 standaard	ventilatievoorziening
VW	1965	1974	geen warmteterugwinning	type warmteterugwinning
VW	1965	1974	forfaitair	kierdichting (q;v10)
VW	1965	1974	ketel HR107-ketel	Ruimteverwarming
VW	1965	1974	individueel	type ruimteverwarming
VW	1965	1974	ketel	toestel ruimteverwarming
VW	1965	1974	HR107-ketel	ketel/luchtverwarming
VW	1965	1974	radiatoren	Afgiftesysteem
VW	1965	1974	90/70	temperatuurniveau
VW	1965	1974	radiatoren	type afgiftesysteem
VW	1965	1974	individueel gas combitoestel met gaskeur HR/CW	Warmtapwater
VW	1965	1974	individueel	type tapwaterinstallatie
VW	1965	1974	gas combitoestel met gaskeur HR/CW	type toestel individiueel
VW	1965	1974	CW4/5/6	CW-klasse
VW	1975	1991	0.88	GroundSurface
VW	1975	1991	0.6	WallSurface
VW	1975	1991	0.59	RoofSurface
VW	1975	1991	2.73	Window
VW	1975	1991	3.29	Door
VW	1975	1991	volledig natuurlijk	ventilatietype
VW	1975	1991	A1 standaard	ventilatievoorziening
VW	1975	1991	geen warmteterugwinning	type warmteterugwinning
VW	1975	1991	forfaitair	kierdichting (q;v10)
VW	1975	1991	ketel HR107-ketel	Ruimteverwarming
VW	1975	1991	individueel	type ruimteverwarming
VW	1975	1991	ketel	toestel ruimteverwarming
VW	1975	1991	HR107-ketel	ketel/luchtverwarming
VW	1975	1991	radiatoren	Afgiftesysteem
VW	1975	1991	90/70	temperatuurniveau

Continued on next page

Table C.6 – continued from previous page

Building type	Year min	Year max	Current condition	Element
VW	1975	1991	radiatoren	type afgiftesysteem
VW	1975	1991	individueel gas combitoestel met gaskeur HR/CW	Warmtapwater
VW	1975	1991	individueel	type tapwaterinstallatie
VW	1975	1991	gas combitoestel met gaskeur HR/CW	type toestel individiueel
VW	1975	1991	CW4/5/6	CW-klasse
VW	1992	2005	0.37	GroundSurface
VW	1992	2005	0.4	WallSurface
VW	1992	2005	0.37	RoofSurface
VW	1992	2005	2.38	Window
VW	1992	2005	3.23	Door
VW	1992	2005	natuurlijke toevoer, mechanische afvoer	ventilatietype
VW	1992	2005	C1 standaard	ventilatievoorziening
VW	1992	2005	geen warmteterugwinning	type warmteterugwinning
VW	1992	2005	forfaitair	kierdichting (q;v10)
VW	1992	2005	ketel HR107-ketel	Ruimteverwarming
VW	1992	2005	individueel	type ruimteverwarming
VW	1992	2005	ketel	toestel ruimteverwarming
VW	1992	2005	HR107-ketel	ketel/luchtverwarming
VW	1992	2005	radiatoren	Afgiftesysteem
VW	1992	2005	90/70	temperatuurniveau
VW	1992	2005	radiatoren	type afgiftesysteem
VW	1992	2005	individueel gas combitoestel met gaskeur HR/CW	Warmtapwater
VW	1992	2005	individueel	type tapwaterinstallatie
VW	1992	2005	gas combitoestel met gaskeur HR/CW	type toestel individiueel
VW	1992	2005	CW4/5/6	CW-klasse
VW	2006	2014	0.36	GroundSurface
VW	2006	2014	0.35	WallSurface
VW	2006	2014	0.35	RoofSurface
VW	2006	2014	1.84	Window
VW	2006	2014	3.21	Door
VW	2006	2014	natuurlijke toevoer, mechanische afvoer	ventilatietype
VW	2006	2014	C1 standaard	ventilatievoorziening
VW	2006	2014	geen warmteterugwinning	type warmteterugwinning
VW	2006	2014	forfaitair	kierdichting (q;v10)

Continued on next page

Table C.6 – continued from previous page

Building type	Year min	Year max	Current condition	Element
VW	2006	2014	ketel HR107-ketel	Ruimteverwarming
VW	2006	2014	individueel	type ruimteverwarming
VW	2006	2014	ketel	toestel ruimteverwarming
VW	2006	2014	HR107-ketel	ketel/luchtverwarming
VW	2006	2014	vloer/wand/plafond	Afgiftesysteem
VW	2006	2014	45/40	temperatuurniveau
VW	2006	2014	vloer/wand/plafond	type afgiftesysteem
VW	2006	2014	individueel gas combitoestel met gaskeur HR/CW	Warmtapwater
VW	2006	2014	individueel	type tapwaterinstallatie
VW	2006	2014	gas combitoestel met gaskeur HR/CW	type toestel individiueel
VW	2006	2014	CW4/5/6	CW-klasse
VW	2015	2018	0.27	GroundSurface
VW	2015	2018	0.21	WallSurface
VW	2015	2018	0.16	RoofSurface
VW	2015	2018	1.76	Window
VW	2015	2018	2.88	Door
VW	2015	2018	natuurlijke toevoer, mechanische afvoer	ventilatietype
VW	2015	2018	C1 standaard	ventilatievoorziening
VW	2015	2018	geen warmteterugwinning	type warmteterugwinning
VW	2015	2018	forfaitair	kierdichting (q;v10)
VW	2015	2018	elektrische warmtepomp	Ruimteverwarming
VW	2015	2018	individueel	type ruimteverwarming
VW	2015	2018	elektrische warmtepomp	toestel ruimteverwarming
VW	2015	2018		ketel/luchtverwarming
VW	2015	2018	vloer/wand/plafond	Afgiftesysteem
VW	2015	2018	45/40	temperatuurniveau
VW	2015	2018	vloer/wand/plafond	type afgiftesysteem
VW	2015	2018	individueel combi warmtepomp	Warmtapwater
VW	2015	2018	individueel	type tapwaterinstallatie
VW	2015	2018	combi warmtepomp	type toestel individiueel
VW	2015	2018	CW4/5/6	CW-klasse